CO_2 Photoreduction

DOI: 10.1002/anie.201207199

Photocatalytic Reduction of CO_2 on TiO_2 and Other Semiconductors

Severin N. Habisreutinger, Lukas Schmidt-Mende, and Jacek K. Stolarczyk**

Keywords:
CO_2 reduction · photocatalysis · nanoparticles · solar fuel · titanium dioxide

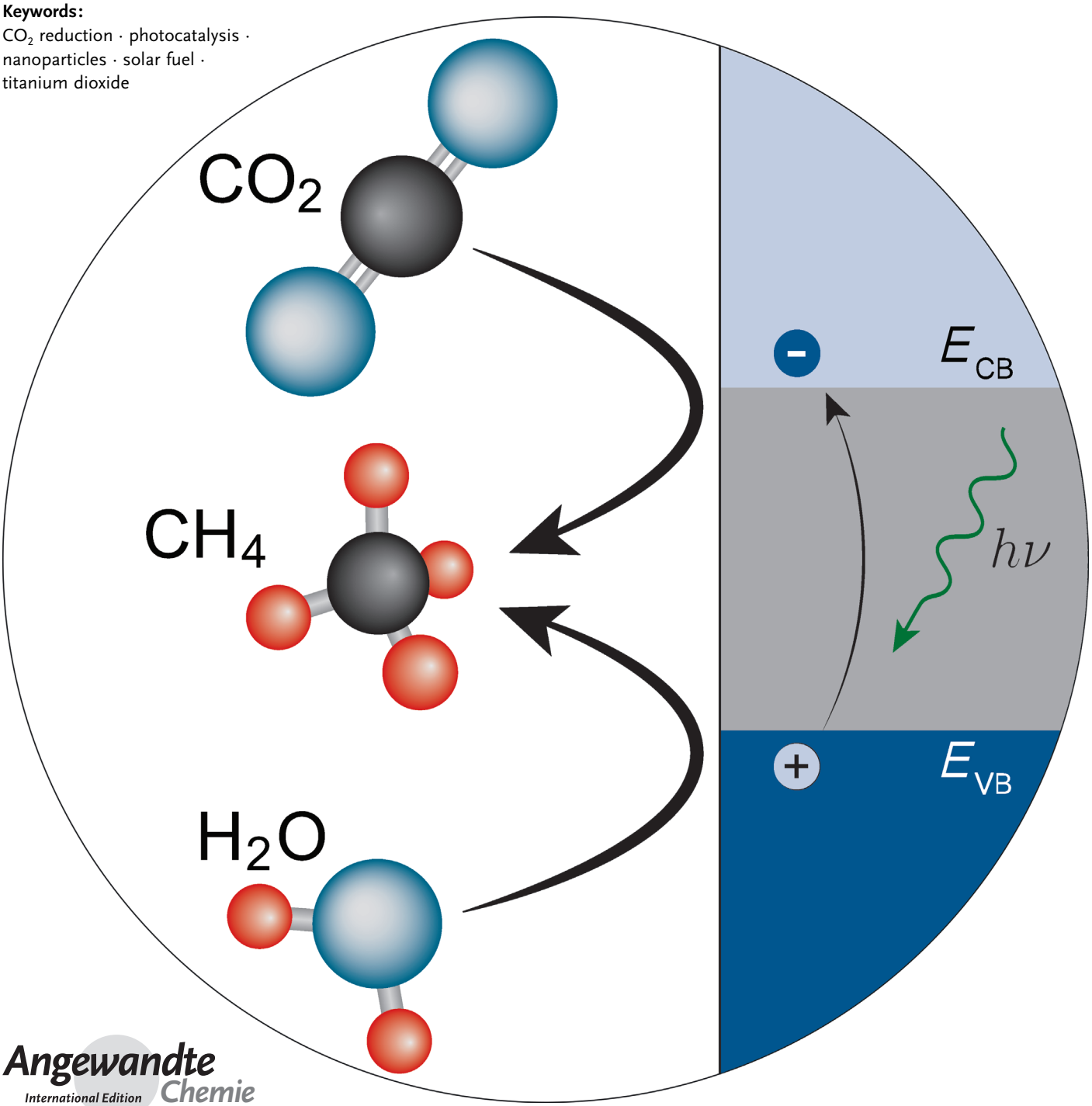

Rising atmospheric levels of carbon dioxide and the depletion of fossil fuel reserves raise serious concerns about the ensuing effects on the global climate and future energy supply. Utilizing the abundant solar energy to convert CO_2 into fuels such as methane or methanol could address both problems simultaneously as well as provide a convenient means of energy storage. In this Review, current approaches for the heterogeneous photocatalytic reduction of CO_2 on TiO_2 and other metal oxide, oxynitride, sulfide, and phosphide semiconductors are presented. Research in this field is focused primarily on the development of novel nanostructured photocatalytic materials and on the investigation of the mechanism of the process, from light absorption through charge separation and transport to CO_2 reduction pathways. The measures used to quantify the efficiency of the process are also discussed in detail.

From the Contents

1. Introduction

Harvesting the energy of solar light and its subsequent storage in the form of chemical fuels hold promise to address the current and future demand of energy supply. The rate of global energy consumption averaged 15–17 TW in 2010[1] and is projected to increase to 25–27 TW by 2050.[2] In 2011, 81 % of the energy needs were met by fossil fuels, while renewable sources accounted for 13 %.[3] The share of the latter is set to increase, but it is estimated that only up to 20 TW can by extracted from wind, tides, biomass, and geothermal sources.[4] In contrast, solar radiation provides a seemingly infinite source of energy. The solar light energy reaching Earth in one hour corresponds roughly to the annual global consumption of energy.[2] In other words, converting about 10 % of the solar energy on 0.3 % of the land surface of the planet would suffice to exceed the projected energy needs in 2050.

The heavy reliance on fossil fuels for the production of energy results in emissions of 30.4 Gt of carbon dioxide into the atmosphere.[3] All human activities currently generate about 37 Gt of CO_2 emissions.[5] This number will likely increase to 36–43 Gt by 2035, depending on the policies governing emissions and energy use, even if renewable sources increase their share.[3] Considering that the natural cycle of CO_2 emission and uptake (fixation by terrestrial plants and microorganisms, plus underground inorganication) involves about 90 Gt,[6] it is not unexpected that the anthropogenic emissions significantly disturb the balance. The atmospheric level of CO_2 rose from $\delta = 270$ ppm in the preindustrial era[6] to almost $\delta = 395$ ppm in 2012.[7] The current CO_2 concentration far exceeds its natural fluctuation ($\delta = 180$–300 ppm) over the past 800 000 years,[7a] and is probably the highest in about 15 million years based on boron isotope ratios in planktonic shells.[8] The greenhouse gas effect is considered to be a factor for anthropogenic climate change, and therefore the steady rise in the CO_2 level is a great cause for concern.[5,9] Mitigating the effect of increasing CO_2 emissions through its sequestration has been studied intensively. However, the process generally requires a substantial input of energy and careful prevention of leakage of CO_2 back into the atmosphere.[10]

In this context, the use of solar energy to chemically reduce CO_2 to higher energy compounds such as methanol or methane offers a way to address this problem. Solar fuels, as these compounds are often referred to,[11] can then be combusted or used in fuel cells, thus releasing the CO_2. This closes the carbon cycle, since the external addition of CO_2 from fossil fuels is no longer part of the cycle. The term "methanol economy" was suggested for such a cycle involving methanol obtained from CO_2.[12] An additional benefit of such an approach is that the existing energy production and transport infrastructure could be used with little alteration.

Another important aspect of the conversion of CO_2 into liquid or gaseous fuels is the high-density storage of solar energy in the form of chemical bonds, mainly C–H. Renewable sources generally provide only an intermittent and unreliable supply of energy; therefore, the energy storage capacity of solar fuels is an attractive solution. Apart from the applications as fuel, some of the products of CO_2 conversion may also be conveniently utilized in chemical synthesis. Thus, instead of being an undesired waste, potentially damaging the planet, CO_2 may become a valuable and cheap carbon feedstock that also replaces fossil fuels in this role.[6,13] Approaches which combine the chemical conversion of CO_2 (e.g. synthesis of urea) with a change in the reduction state of carbon have also been proposed.[14]

Several methods to reduce CO_2 by using solar energy are being pursued. In the first example, photovoltaic cells are used to convert the incident irradiation into electricity, which

[*] S. N. Habisreutinger,[+] Prof. L. Schmidt-Mende, Dr. J. K. Stolarczyk
Department für Physik und Center for Nanoscience (CeNS)
Ludwig-Maximilians-Universität (LMU) München
Amalienstrasse 54, 80799 München (Germany)
E-mail: jacek.stolarczyk@physik.uni-muenchen.de
S. N. Habisreutinger,[+] Prof. L. Schmidt-Mende
Fachbereich Physik, Universität Konstanz
Universitätsstrasse 10, 78457 Konstanz (Germany)
E-mail: Lukas.Schmidt-Mende@uni-konstanz.de
[+] Present address: Clarendon Laboratory
Department of Physics, Oxford University
Parks Road, Oxford, OX1 3PU (Great Britain)

is then used to electrochemically reduce CO_2 on metal electrodes;[15] the use of an electro-bioreactor containing lithoautotrophic microorganisms is also possible.[16] In the second example of photoelectrochemical cells, these two functions are not separated but combined into one device, although the catalytic reduction process requires an external electrical potential bias to proceed.[17] In the third option, water is photocatalytically split and the produced hydrogen is used to catalytically hydrogenate CO_2 to produce useful chemicals for use in further synthesis or as fuels.[18] This approach takes advantage of the recent developments in the photocatalytic generation of H_2 and avoids problems associated with hydrogen storage.[19] In another option, CO_2 is directly reduced photocatalytically by using molecular catalysts.[15b,20] This homogeneous process is usually catalyzed by metal complexes which act as both light antennas and catalysts. The disadvantage of this approach is that it relies primarily on rare and expensive metals such as ruthenium or rhenium.[21]

In this Review, an alternative process for the direct photocatalytic reduction of CO_2 on semiconductors is described. In contrast to the homogeneous process mentioned above, the reaction takes place at either a solid–liquid or a solid–gas interface. In this heterogeneous process, the photocatalyst is usually a hybrid material which absorbs light, separates the photogenerated charges, transports them to the surface, and provides active sites for the catalytic reaction.[22] The main component is a semiconductor such as TiO_2, ZnS, or $InTaO_4$, which is responsible for the first three functions, although a separate material, a sensitizing agent, is sometimes used to enhance the absorption of light, especially in the visible range. The actual catalytic process is usually more efficient on the surface of a co-catalyst, although it may also proceed on the surface of the semiconductor. Typically, metal (Pt, Pd, Cu, Ni, etc.) or metal oxide (NiO, RuO_2) nanoparticles (NPs) which form a composite structure with the semiconductor are employed as the co-catalyst. In recent years, emphasis has been placed on nanostructuring and/or dispersing the semiconductor to improve its charge-separation and transport properties as well as increase the available surface area.[23]

The photocatalytic reduction of CO_2 requires multiple electron transfers and can lead to the formation of many different products depending on the specific reaction pathway taken and the number of electrons transferred, which determines the final oxidation state of the carbon atom. Carbon monoxide, formic acid, formaldehyde, methanol, methane, ethane, and ethene have been observed in many experiments, but oxalic acid, acetaldehyde, ethanol, higher alcohols, and higher hydrocarbons were also detected in some systems. Clearly, the process follows a rather complex mechanism, with potentially branching pathways leading to different products at the same time. This has inspired many studies focused on understanding the mechanism and the control of its selectivity.

The reduction half-reaction consumes only the photogenerated electrons. In an ideal case, the oxidation half-reaction would lead to the generation of oxygen or hydrogen peroxide through the oxidation of water. However, this process is difficult to accomplish, as attested by the extensive research on water splitting.[19,24] Very few systems have been shown to simultaneously reduce CO_2 and oxidize water.

Severin Habisreutinger studied physics at the Ludwig-Maximilians University in Munich where he received his BSc in 2009 and his MSc in 2011 in the group of Prof. L. Schmidt-Mende. His current research interests include photocatalytic reactions on metal-doped TiO_2 particles in aqueous solutions. He is currently pursuing his PhD in physics at the University of Oxford under the supervision of Prof. Robin J. Nicholas.

Lukas Schmidt-Mende carried out his PhD under the supervision of Prof. Sir Richard Friend at the University of Cambridge, UK. Afterwards he joined the group of Prof. Michael Grätzel for postdoctoral research at the École Polytechnique Fédérale de Lausanne, Switzerland, where he investigated solid-state dye-sensitized solar cells. He returned to Cambridge to the Department of Materials Science, where he worked as a Marie Curie Fellow before taking up a University Research Fellowship from the Royal Society. In autumn 2007 he became Associate Professorship at the Ludwig-Maximilians University, Munich, and in 2011 he moved to the University of Konstanz for a full professorship. He leads the "Hybrid Nanostructures" group in the Department of Physics.

Jacek Stolarczyk studied chemistry and computer science at the Silesian University of Technology in Gliwice, Poland, where he also received his PhD in chemistry in 2003. He then carried out postdoctoral research at University College Dublin and Dublin City University in Ireland and finally at LMU in the group of Prof. Schmidt-Mende. He is currently a senior researcher in the Photonics and Optoelectronics Group at Dept. of Physics, LMU. His research interests include self-assembly and controlled aggregation of nanostructures, modeling of their interactions, as well as studies of photocatalysis on semiconductor nanoparticles.

Therefore, the focus of the research on CO_2 conversion remains on the reduction, whilst the oxidation is achieved by a surrogate reaction involving sacrificial electron donors.

By definition, a catalytic reaction has a negative difference in the Gibbs free energy, $\Delta G^0 < 0$, where the function of the catalyst is to lower the kinetic barrier of the reaction without it being damaged, used-up, or inactivated.[25] In this strict sense, the photocatalytic reduction of CO_2 is not a catalytic process, because it is an uphill reaction, that is, it requires a significant energy input, $\Delta G^0 > 0$, which is provided by the incident photons. Nonetheless, this inconsistency is commonly ignored, and the process is referred to as being photocatalytic. It is argued, however, that the process instead represents an example of (artificial) photosynthesis.[26] Even though the former term may be less precise from a chemical point of view, we adopted the broader definition of photocatalysis throughout this Review to comply with the vast majority of publications on the subject.

Despite nearly 40 years of research on the photocatalytic reduction of CO_2, the scientific community is still a long way from efficient and commercially viable devices. The highest rates of product formation generally do not exceed tens of μmol of product (e.g. methane) per hour of illumination per gram of photocatalyst. It is a complex process with plenty of unresolved questions concerning its mechanism and the effect of the photocatalyst composition, architecture, and other parameters. The initial report by Inoue et al.[27] on the successful reduction of CO_2 on several semiconductors upon illumination with UV light generated much excitement and encouraged many studies. These efforts did not translate immediately into significant improvements in the efficiency, and over time interest in the topic decreased slightly. However, faced with an inexorable rise in the atmospheric CO_2 level and the need for alternative energy sources, there has been renewed interest in the field over recent years, with improved synthetic methods being used to prepare nanostructured semiconductors and with better computational capabilities. The number of reports has grown exponentially over the last few years, with many bringing exciting new developments. It can be expected that they will lead to the development of much more efficient photocatalysts in the years to come.

This Review is organized as follows. The second section is focused on the mechanism of photocatalysis on semiconductors, the electrochemical potentials of CO_2 reduction, and possible chemical pathways leading to the formation of methane and methanol. This is followed in the third section by a discussion of the methods to quantify the efficiency of the heterogeneous photocatalytic process. We attempt to address several misconceptions which make a comparison of experimental results very difficult and thereby hinder progress in the field. The longest, fourth, section provides a snapshot of the current developments in the photocatalytic reduction of CO_2 on TiO_2 and other semiconductors, especially other oxides, sulfides, and phosphides. The last section summarizes this Review.

2. Mechanism

2.1. Semiconductors as Photocatalysts

Semiconductors are an attractive type of materials for light-harvesting applications because of their energy band gap—an energy interval void of any normally available electronic states—which has an energy range similar to that of visible light.[28] The energy states of the valence band (VB) lie below the gap and are occupied by electrons in the ground state, whereas the states above the gap form the conduction band (CB) and are unoccupied at $T = 0$ K. At higher temperatures, some electrons are thermally excited to the CB and the resulting electron-density distribution is characterized by the Fermi level of the semiconductor. Upon absorption of a photon with energy equal to or higher than the band gap, an electron is excited from the VB into the CB, thereby leaving behind an empty state that constitutes a quasiparticle that is referred to as a hole. This means that the populations of both charge carriers, that is, electrons and holes, in an illuminated semiconductor are larger than in the equilibrium, with the new steady state described by quasi-Fermi levels. The carriers, once spatially separated, may migrate to the surface of the photocatalyst and eventually transfer to the adsorbed acceptor molecules, thereby initiating the corresponding reduction or oxidation process.[22a] The actual reaction sites may be located either directly on the surface of the semiconductor within which the photoexcitation took place, or indirectly across the interface at the surface of another semiconductor or metal nanoparticle, which is usually referred to as the co-catalyst.[29] Accordingly, the primary role of the semiconductor in photocatalysis is to absorb an incident photon, generate an electron–hole pair, and facilitate its separation and transport, whereas catalysis of the reaction is an additional function which is usually performed by a different material.

The band-gap excitation and formation of free charge carriers—an electron and a hole—is followed by several pathways of de-excitation (Scheme 1). The successful dona-

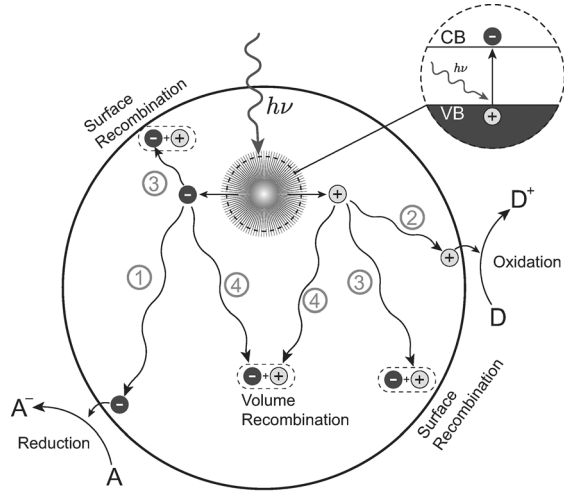

Scheme 1. Photoinduced formation of an electron–hole pair in a semiconductor with possible decay paths. A = electron acceptor, D = electron donor. Adapted from Ref. [22a].

tion of the carrier to the acceptor molecules at the surface, which leads to the desired redox reactions (pathways 1 and 2), competes with a number of recombination processes.[30] The carriers can recombine with their counterparts of opposite charge trapped on the surface (pathway 3), or the recombination of two carriers can occur in the bulk of the semiconductor (pathway 4). The latter process is called volume recombination.

Both recombination processes are detrimental to the efficiency of the photocatalytic reaction. There are various factors which determine the recombination rates, such as mobility and trapping of charge carriers, defect density in the semiconductor lattice,[22b,25a,31] or the presence of an interface with a secondary material which acts as an electron or a hole sink.[29,32] In the case of metal nanoparticles supported on the semiconductor, the photogenerated electrons are accepted by the metal because the available states of its Fermi level lie energetically below the CB states of the semiconductor.[33] This effect shifts the Fermi level of the semiconductor–metal composite upwards, so that its potential becomes more negative.[29] Thus, the electrons can be shuttled to the adsorbate and be discharged more easily than by the semiconductor itself, that is, the composite is more reductive. This path is illustrated in Scheme 2. This can lead to the formation

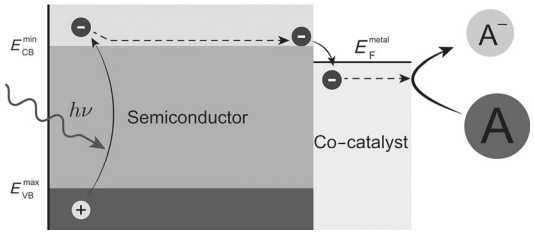

Scheme 2. Transfer of a photogenerated electron from a semiconductor to the acceptor molecule via the metal co-catalyst.

of a Schottky barrier at the semiconductor–metal interface, thus promoting the separation of the charge carriers by accumulation of the electrons in the metal, while the holes remain in the semiconductor.[34] Improved separation translates into slower recombination rates and an increase in the efficiency of the process. The presence of platinum particles supported on the surface of TiO_2 was also associated with a shift of the band edges, which accelerates the migration of electrons.[35]

Another process (not illustrated) that is able to further decrease the photocatalytic efficiency is a back-transfer of charge carriers from the adsorbed molecules to the semiconductor. The average distance which a carrier can migrate before recombining is the diffusion length, which is a material-dependent parameter. Nanostructured materials and nanoparticles in particular are, therefore, highly effective because they exhibit very high surface-to-volume ratios. This means that, as a consequence of the short distances to the surface, the photogenerated charges have a much higher probability of reaching the interface without recombination. Additionally, these materials possess a large reactive surface for interactions with adsorbate molecules.[23]

The tendency of the molecular orbital of the adsorbed species to accept/donate electrons manifests itself in its reduction/oxidation potential, respectively. According to thermodynamics, the ability of a semiconductor to transfer photogenerated charge carriers to adsorbed molecules is governed by the alignment of the quasi-Fermi levels of the electrons and holes with this redox potential.[36] However, it is usually assumed that these levels are located very near the conduction and valence band edges, respectively, which is a good approximation, especially for n-type semiconductors such as TiO_2. Therefore, the reaction conditions are typically expressed in terms of the position of the band edges: for reduction processes, the conduction band edge must lie above the lowest unoccupied molecular orbital (LUMO) of the acceptor molecule. In other words, since the scale of the redox potential goes from positive to negative with increasing energy, the potential level of the conduction band has to be more negative than the reduction potential of the acceptor (Scheme 3). Even electrons excited by highly energetic

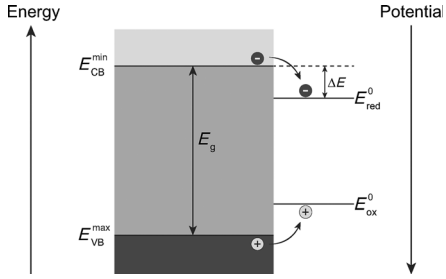

Scheme 3. Thermodynamic constraints on the transfer of charge carriers to the adsorbed molecules. ΔE represents the kinetic overpotential of the reduction process.

photons (hot electrons) relax on a femtosecond time scale to lower states in the conduction band or intraband trap states before they reach the surface, so they do not provide a higher reduction potential.[37] Analogously, the transfer of a photogenerated hole from the semiconductor to an adsorbed molecule, equivalent to the transfer of an electron in the opposite direction, requires the energy level of the highest occupied molecular orbital (HOMO) of the oxidized molecule to lie above the valence band or—in terms of redox potentials—it has to be more negative than the potential of the valence band.

These thermodynamic considerations mean that the choice of a suitable photocatalyst needs to be a compromise between two opposing aspects. On one hand, for reasons of efficiency, it is highly beneficial to absorb light in the visible range. This condition requires the semiconductor to have a comparably small band gap. On the other hand, as discussed above, the band gap has to span the range of the reduction and oxidation potentials relevant to the photocatalyzed reaction.

From a kinetics point of view, it is in fact critical to provide an overpotential for each process, that is, the range of potentials should not only be spanned, but there should be substantial margins on each side, such as that shown for the

reduction process and designated as ΔE in Scheme 3. Without an overpotential, even a good catalyst would not ensure a high rate of reaction. Thus, the band gap should be as wide as possible. These limitations in the width of the band gap mean that the exact positions of its edges play an important role in determining the applicability of each semiconductor to the photocatalytic process in question. The consequences of this limition, along with possible approaches to address it through sensitization or band-gap engineering, are discussed in detail in Section 4.

2.2. Chemical Pathways

The transfer of an electron to the adsorbed molecule initiates a cascade of chemical reactions which eventually determine the outcome and the efficiency of the photocatalytic process. In the case of carbon dioxide, the multistep reduction involves up to eight electrons and protons, cleavage of C–O bonds, formation of C–H bonds, and may lead to several different products depending on the specific pathway taken. In this context, achieving substantial improvements in the photocatalytic reduction of CO_2 relies on an in-depth understanding of its underlying chemical mechanism. The potential benefits can be considered on two levels. Firstly, knowledge of the mechanism may enable an increase in the overall conversion rate of CO_2 through minimization of the relevant thermodynamic or kinetic barriers of the intermediate reactions. Secondly, as a consequence of the large number of possible products, it is crucial that the selectivity of the process is controlled so that the process can be directed towards the desired products, for example, methane or methanol. Since the reduction of CO_2 usually proceeds in the presence of water (vapor or liquid phase), it is also important to suppress the concurrent generation of hydrogen which competes with carbon species for the photogenerated electrons.

The exact mechanism of CO_2 photoreduction on semiconductors still remains to be unravelled. There are still many open questions concerning the exact reaction pathway, the effects of the reaction conditions, as well as the selectivity and efficiency of the entire process. Nonetheless, more information is steadily being gathered, as the mechanism has been the subject of intense scrutiny in recent years. Numerous experimental methods have been employed in these studies. Gas[38] and ion-exchange[39] chromatography, often in conjunction with mass spectrometry, are routinely used to identify and quantify the intermediate and final products. The former technique is applied mostly to volatile molecules through headspace or liquid-phase measurements, while the latter is suitable for nonvolatile, ionic species such as formate or oxalate. The chromatographic methods are supplemented by IR,[40] EPR,[41] Auger electron, and X-ray photoelectron spectroscopy.[42]

The reduction of CO_2 is thought to proceed through several radical intermediates. These largely unstable molecules have an unpaired electron and hence are paramagnetic. Therefore, EPR is an important tool in elucidating the mechanism. Other methods include transient absorption measurements,[41c] scanning tunneling microscopy,[43] and many surface-oriented studies.[22b,25a] The methods for analyzing semiconductor excitation, charge-carrier lifetimes, mobility, and separation are generally the same as for photovoltaic approaches, and have been comprehensively reviewed elsewhere.[32,44] Important information is also obtained from kinetic analysis of the process[45] and from studies on the electrochemical reduction of CO_2.[15b,46] Computational methods provide critical information regarding the adsorption of the reagents on the photocatalyst surface as well as the structure and energetics of the putative intermediate products and transition states.[15a,41d,43,47]

Carbon dioxide molecules are stable and chemically inert with a closed-shell electronic configuration, linear geometry, and $D_{\infty h}$ symmetry.[49] The addition of a single electron causes a bending of the molecular structure because of repulsion between the newly acquired electron situated on the electrophilic carbon atom and the free electron pairs on the oxygen atoms. The loss of symmetry and the increased repulsion between these free electron pairs in the bent structure with a C_{2v} symmetry contribute to the high energy of the LUMO of CO_2 and thus the very low electron affinity of the molecule. The single-electron reduction of CO_2 to an anion radical $CO_2^{\bullet-}$ [Eq. (1)] has, therefore, a strongly negative electrochemical potential of -1.9 V versus the normal hydrogen electrode (NHE).[50] In effect, virtually no semiconductor provides sufficient potential to transfer a single photogenerated electron to a free CO_2 molecule (Scheme 4), thus making this step highly improbable. Although the transfer of a single electron to CO_2 has a very unfavorable energy

$$CO_2 + e^- \rightarrow CO_2^{\bullet-} \qquad E^0_{redox} = -1.90\ V \qquad (1)$$

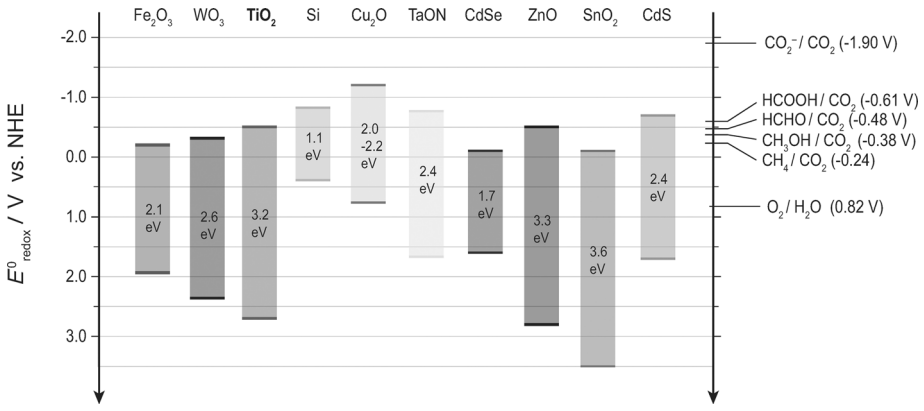

Scheme 4. Conduction band, valence band potentials, and band gap energies of various semiconductor photocatalysts relative to the redox potentials at pH 7 of compounds involved in CO_2 reduction. Adapted from Ref. [48].

balance, the situation is better for a proton-assisted transfer of multiple electrons. Equations (2)–(6) list the electrochemical CO_2 reduction potentials versus the NHE at pH 7 to formic acid, carbon monoxide, formaldehyde, methanol and methane, respectively. The reactions require the transfer of two to eight electrons and a corresponding number of protons.[41b,49b] The values are comparable to proton reduction itself [Eq. (7)], although the latter is a one-electron process. Importantly, the potentials are less negative than the conduction band of many semiconductors (Scheme 4), so that it appears that these reactions are feasible. Unfortunately, there is little evidence in the literature of such concerted multi-electron transfer processes.[29] This means that the reaction is likely to proceed through a series of one-electron steps and that the first electron transfer remains a severe obstacle to the photoreduction of CO_2, and likely constitutes a strongly limiting step.[40a,51]

$$CO_2 + 2H^+ + 2e^- \rightarrow HCOOH \qquad E^0_{redox} = -0.61\ V \tag{2}$$

$$CO_2 + 2H^+ + 2e^- \rightarrow CO + H_2O \qquad E^0_{redox} = -0.53\ V \tag{3}$$

$$CO_2 + 4H^+ + 4e^- \rightarrow HCHO + H_2O \qquad E^0_{redox} = -0.48\ V \tag{4}$$

$$CO_2 + 6H^+ + 6e^- \rightarrow CH_3OH + H_2O \qquad E^0_{redox} = -0.38\ V \tag{5}$$

$$CO_2 + 8H^+ + 8e^- \rightarrow CH_4 + 2H_2O \qquad E^0_{redox} = -0.24\ V \tag{6}$$

$$2H^+ + 2e^- \rightarrow H_2 \qquad E^0_{redox} = -0.41\ V \tag{7}$$

The adsorption of CO_2 on a semiconductor surface offers one way of activating the otherwise inert molecule for reduction. It is understood that adsorption leads to the formation of a partially charged species $CO_2^{\delta\bullet-}$ through interactions with surface atoms.[49b] This adsorbate no longer has the linear symmetry of the free CO_2 molecule and thus has a lower barrier for accepting an electron because the LUMO level of CO_2 decreases as the molecule bends.[49a] Computational studies of the adsorption of CO_2 on anatase TiO_2 suggest that these interactions are not strong enough with stoichiometric, defect-free surfaces to sufficiently lower the barrier and enable transfer of conduction-band electrons.[47b] The interactions are much stronger at oxygen vacancy sites where a foreign oxygen atom can fill the vacancy. This may lead to the dissociation of CO_2 upon electron transfer and subsequent release of carbon monoxide.[43,52] The oxygen atom of the CO_2 molecule is left in place to heal the vacancy. In another possible binding mode, the $CO_2^{\bullet-}$ species bridges two Ti surface atoms, thereby forming a bidentate configuration with its oxygen atoms. In the absence of an oxygen atom between the Ti atoms, this configuration is a plausible intermediate step in the reduction process.[47b]

The activation of CO_2 is more efficiently performed on semiconductors decorated with a co-catalyst, usually noble-metal nanoparticles. The formation of the bent anion radical $CO_2^{\bullet-}$ was first reported on a Rh/TiO_2 composite and was attributed to the transfer of an electron from the metal d orbital to the (C-O) π^* orbital.[40a] Tanaka et al. concluded that step sites on Pt are active sites of CO_2 dissociation to CO. This was accompanied by the appearance of bidentate carbonate species on the TiO_2 support.[42,53] As discussed earlier, metal NPs enhance charge separation at the metal–semiconductor interface, but their role in the chemical mechanism of CO_2 reduction is not limited to the activation of CO_2. They catalyze the subsequent steps of CO_2 reduction and play an important role in determining the selectivity of the process.[15a]

The activation barrier was found by Dimitrijevic et al. to be lower in an aqueous dispersion of the photocatalyst because of stabilization of the surface charge of the anion radical $CO_2^{\bullet-}$ by dipolar interactions with water molecules.[41b] However, in an aqueous environment, the pH value of the solution is an important parameter.[36] The conduction band becomes more reductive in alkaline solutions according to Equation (8).[54]

$$E^0 = E^0(\text{pH } 0) - 0.06\,\text{pH} \tag{8}$$

It should be noted that the electrochemical reduction potentials [Eqs. (2)–(6)] are also affected in a similar manner, according to the Nernst Equation. Moreover, the pH value determines the solubility and chemical form of the CO_2. The reason for this is that the solubility of CO_2 is low, but it partially hydrates in water to carbonic acid, which then dissociates at a higher pH value to bicarbonate HCO_3^- and carbonate CO_3^{2-} ions. Equations (9) and (10) give the corresponding equilibria.[51]

$$CO_2 + H_2O \rightleftharpoons (H_2CO_3) \rightleftharpoons H^+ + HCO_3^- \qquad pK_a = 6.4 \tag{9}$$

$$HCO_3^- \rightleftharpoons H^+ + CO_3^{2-} \qquad pK_a = 10.3 \tag{10}$$

This means that a different form dominates, depending on the pH value of the solution. Importantly, these forms of CO_2 possess different adsorption characteristics on semiconducting materials which may result in different reduction pathways. In non-aqueous solvents, the conduction-band potential also depends on the adsorption/desorption equilibrium of protons. Therefore, in protic solvents such as methanol or ethanol the E_{CB} value is significantly more positive than in aprotic solvents such as acetonitrile or DMF.[55]

In contrast to research on water splitting, where both half-reactions—reduction and oxidation—receive approximately equal attention, in CO_2 photoreduction studies the focus lies mostly on the reduction side, which involves electrons. This reflects the fact that CO_2 reduction is a more complex and difficult process to realize than the generation of hydrogen from water. However, the fate of the concomitantly photogenerated holes, which also migrate to the surface (often faster than the electrons),[56] cannot be ignored. At the surface they may react with adsorbed water or hydroxide ions OH^-_{ads} to generate oxygen. Thermodynamically, this is a feasible process, because the valence band of most semiconductors is located well below the oxidation potential of water [Eqs. (11) and (12) give values versus the NHE at pH 7 (h^+ = hole)], but there are only a few reports where this has been achieved.[19,24] These problems are attributed to the need for four holes per oxygen molecule and difficulties in desorbing the products. An alternative to the production of oxygen is the formation of strongly oxidizing hydroxyl radicals $^\bullet OH$. The oxidative

environment can affect the mechanism of CO_2 reduction because some intermediate products might be more readily oxidized than reduced, thereby halting the process before the six- or eight-electron reduction products are obtained.[57]

$$2\,H_2O + 4\,h^+ \rightarrow O_2 + 4\,H^+ \qquad E^0_{redox} = 0.82\,V \tag{11}$$

$$H_2O + h^+ \rightarrow {}^{\bullet}OH + H^+ \qquad E^0_{redox} = 2.32\,V \tag{12}$$

Additionally, the accumulation of holes would lead to an increase in surface recombination. Moreover, some semiconductors such as sulfides are unstable under these conditions. Thus, many studies employ additives referred to as hole scavengers to prevent these phenomena. These additives are usually organic or inorganic reducing agents. Their function is to donate electrons, but the products of their oxidation are considered to be an undesired side product of the photocatalytic process. In this context, they are also commonly referred to as sacrificial electron donors. Tertiary amines, especially triethanolamine (TEOA)[58] and triethylamine (TEA),[59] and alcohols, such as methanol,[40b,60] ethanol,[44b,61] and propan-2-ol,[60b,62] are typically used for this purpose. The application of methanol confirms the concerns that it might be easily oxidized on an illuminated semiconductor surface. Other suggested hole scavengers include ascorbic acid,[63] EDTA,[58a] Na_2SO_3,[64] and NaOH.[65] Bicarbonate and carbonate anions were also suggested to act in this role in solution.[41b] The tertiary amines appear to be particularly efficient, most likely through formation of a charge-transfer complex involving the radical anion $CO_2^{\bullet-}$ and the radical cation $TEA^{\bullet+}$, which activates the CO_2 molecule and enables transfer of one α-carbon hydrogen atom to CO_2.[66] These observations led to the design of a cyclic tertiary amine which could be easily recycled from its oxidized state with hydrogen generated from water splitting. In effect, there is no sacrificial agent used in the process.[67]

The detection of methane or CO following illumination in the presence of a photocatalyst and CO_2 is usually considered as proof of CO_2 reduction. However, the isotope labeling studies performed by Yang et al. showed that ^{12}CO was generated even when $^{13}CO_2$ was used as a carbon source.[40d] This prompted the authors to ask whether the CO_2 photoreduction is fact or fiction. Similar findings regarding the formation of $^{12}CH_4$ were reported by Yui et al.[38b] In both cases the authors attributed the formation of ^{12}C species to the presence of carbon residue in the photocatalyst, left over from its preparation. This was confirmed by the observation of ^{13}C products when care was taken to remove any residue. These results suggest that great caution should be exercised in interpreting the finding of certain products and underline the need for isotope labeling experiments to confirm the actual reduction of CO_2.

2.2.1. Reduction Pathways on a Semiconductor Surface

Most detailed studies on the mechanism of CO_2 reduction on semiconductors have been carried out on TiO_2, although the results should also be applicable to other materials. In a typical system, TiO_2 NPs are dispersed in water and illuminated with UV light. In an ideal case, the solvent acts as both the electron and proton donor, but the difficulty with this arrangement lies in the inability to separate the reduction and oxidation half-reactions which happen on similar or neighboring sites on the surface of the NPs.[41c] This increases the risk of back reactions or surface-charge recombination. Nonetheless, it is the simplest setup with the lowest number of different molecules in the system and thus a relatively convenient subject of study.

After the activation of CO_2 by a one-electron transfer and formation of surface-bound $CO_2^{\bullet-}$, the reduction proceeds though a series of elementary steps which involve the transfer of an electron, a proton, or hydrogen radical ($H^{\bullet}$), as well as breaking C–O bonds and creating new C–H bonds. Several of the intermediates are radical species, whose recombination at different stages partially accounts for the number of possible pathways and final products. The exact order and mechanistic details of each subsequent step have not been fully elucidated, but three full pathways detailing the conversion of CO_2 into methane have been proposed in the literature. In the following, they are referred to as 1) the formaldehyde pathway, 2) the carbene pathway, and 3) the glyoxal pathway on account of their unique intermediate.

The differences between the pathways start with the binding mode of $CO_2^{\bullet-}$ to the surface of the TiO_2. Monodentate binding through one of the oxygen atoms to a titanium atom or binding through the carbon atom to a surface-bridging O atom generally favors the formation of the carboxyl (hydroxyformyl) radical $^{\bullet}COOH$.[51] On the other hand, bidentate binding of the CO_2 through both oxygen atoms to two Ti atoms results in the preferential attachment of a hydrogen atom to the carbon atom, which leads to the formation of a formate anion bound in a bidentate mode.[47a] The free hydrogen atom (radical) originates from the reduction of a proton by a conduction-band electron.

According to the first mechanism, the carboxyl radical recombines with a hydrogen radical $H^{\bullet}$ to form formic acid.[68] This is the favored reaction in a medium with a high dielectric constant such as water. The full pathway is presented in Scheme 5. In the next step, formic acid accepts a further $H^{\bullet}$ to form a dihydroxymethyl radical, which dehydrates upon attachment of another $H^{\bullet}$ to formaldehyde. Two more reduction steps lead to methanol, which is further reduced in another two steps to methane. There are two important observations about this pathway. The first one is that formaldehyde and methanol are intermediate steps in the process, not side products. The second one is that cleaving C–O bonds occurs very late in the process. This mechanism has not been verified experimentally. Formaldehyde and methanol were reported as products in some setups, but the specific radical intermediates were not detected. Early formation of, for example, methanol before the production of methane would also be expected, but this phenomenon was also not observed. Additionally, Koči et al. evaluated their experimental data on CO_2 photoreduction with respect to a kinetic model of the formaldehyde pathway.[45b] Their study concluded that the concentration profiles for the formation of methane and methanol did not correspond with the consecutive formation according to this mechanism.

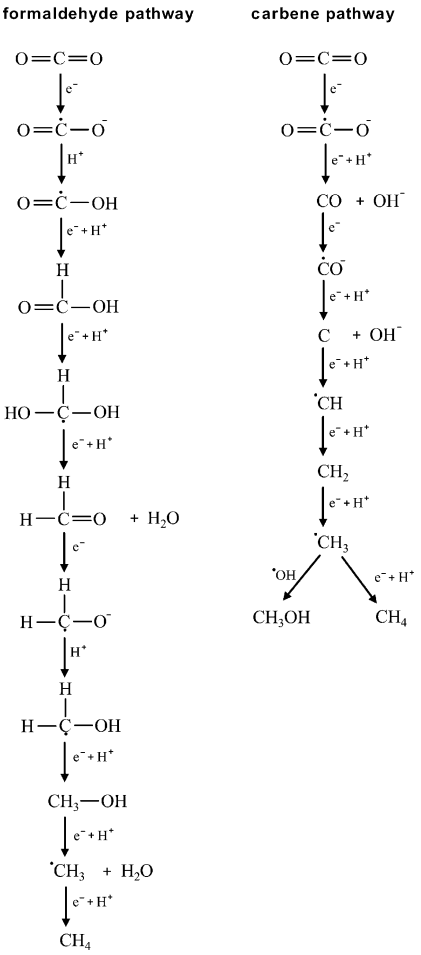

Scheme 5. Two proposed mechanisms for the reduction of CO_2 to methane: formaldehyde and carbene pathways.

In the carbene pathway, the attachment of $H^{\cdot}$ to the oxygen atom of an adsorbed radical $CO_2^{\bullet-}$ leads to an immediate cleavage of the bond between this oxygen atom and the carbon atom.[41a,45] Such a mechanism is favored if $CO_2^{\bullet-}$ is bound to the semiconductor through the carbon atom. A carbon monoxide molecule is left adsorbed and can accept two additional electrons, thereby leading to carbon residue on the surface. Signals corresponding to the carbon radicals have been detected by ESR spectroscopy.[41a] These radicals can subsequently combine with up to four $H^{\bullet}$ radicals, thereby forming a $CH^{\bullet}$ radical, carbene, a methyl radical, and eventually methane. If the methyl radical instead recombines with a hydroxyl radical, then methanol is produced. This means that methanol is a side product, not an intermediate in this pathway, while formaldehyde is not formed at all. It is worth noting that the combination of CO with methanol and/or methane is a rather common set of products, which are observed in many experiments.[41a,69] Some reports indeed imply that methanol and methane are formed competitively from methyl radicals, with one of the products being favored depending on the hydrophilicity of the semiconductor and the relative amount of water in the system.[70] Additionally, Tan et al. and Koči et al. were able to fit their experimental results of methanol and methane production to the kinetic model of this mechanism.[45] In view of these results, the carbene pathway appears to be more plausible than the formaldehyde pathway.

The carbene pathway was also suggested in the context of CO_2 photoreduction on isolated tetrahedrally coordinated Ti^{4+} centers embedded in silica matrices (zeolites), which have some unique characteristics.[71] As a result of quantum confinement effects in these spatially separated "single-site photocatalysts", the absorption of UV light results in the formation of a charge-transfer excited state, usually denoted as $(Ti^{3+}\text{-}O^{-})^*$, in which the photogenerated electron and hole are localized on neighboring atoms. This is closer than in the bulk semiconductors, where the charge carriers are free to diffuse off, which results in a larger separation. The centers in the mesoporous structure of the matrix are easily accessible to water and CO_2 molecules. A specific feature of the $(Ti^{3+}\text{-}O^{-})^*$ photocatalysts is that methanol is often the predominant or one of the major products of the reaction, especially if a metal co-catalyst is not used. This is because water molecules are usually present in sufficient quantities to favor the recombination of methyl radicals with hydroxyl radicals, thus leading to the formation of methanol instead of methane. The addition of Pt NPs modifies the hydrophilicity of the surface, so that methane is formed preferentially.

Shkrob et al. have recently performed an EPR study of CO_2 reduction intermediates in an aqueous dispersion of anatase TiO_2 NPs.[41d,57] Of particular interest was the tendency of possible intermediates, especially formic acid, formaldehyde, and methanol, towards reduction versus oxidation in the presence of both photogenerated electrons and holes. This is an important—and often ignored—aspect of the mechanism in view of the strongly oxidative nature of the holes on TiO_2 and many other semiconductors. As described earlier, the initial steps of the process were calculated to involve a $CO_2^{\bullet-}$ molecule bound to two Ti atoms in a bidentate mode. This radical anion presumably accepts a hydrogen radical $H^{\bullet}$ at the carbon site so quickly that it cannot be detected by EPR spectroscopy. The bidentate formate is then able to bind a proton to form a formic acid molecule adsorbed in a monodentate mode.[47a] However, formic acid was found to oxidize rather easily to form stable $CO_2^{\bullet-}$ bound in a monodentate mode. The authors concluded that the only way for the CO_2 reduction to progress beyond formic acid is a concerted process in which a CB electron transfer to the acid is coupled to the transfer of an oxygen atom from a hydroxy group to the metal (Ti) atom on the surface (Scheme 6). The energy gain from the formation of the bond between the metal and the oxygen atom offsets the energy needed for the electron transfer.[41d] The reaction leads to the release of a free formyl radical $HC^{\bullet}O$, traceable by EPR spectroscopy. This observation corroborates other findings that this radical is a likely intermediate in the photoreduction of CO_2.[72]

Another crucial observation in this EPR study was that, under the same experimental conditions, formaldehyde and methanol were more readily oxidized than reduced, at least when single-electron or -hole processes were compared.[57] The initial products of the oxidation were formyl and hydroxymethyl radicals, respectively. This effectively means

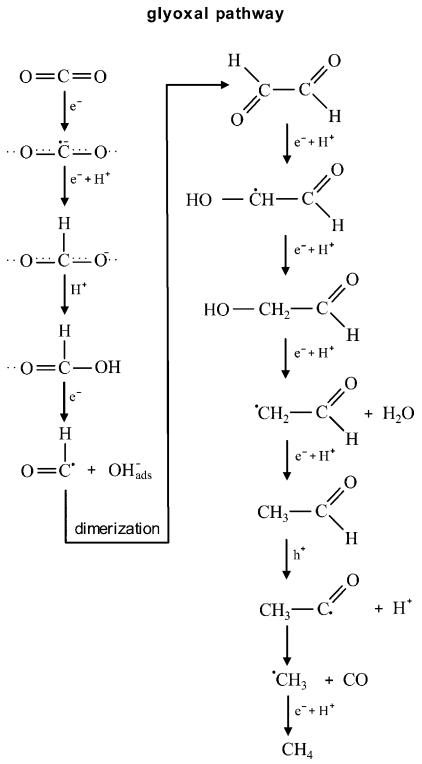

Scheme 6. The third proposed mechanism for the conversion of CO_2 into methane: the glyoxal pathway.

that the pathway of CO_2 reduction cannot pass through either formaldehyde or methanol. Shkrob et al. postulated an alternative mechanism involving a number of C_2 compounds in a complex sequence of reactions, which includes both reduction and oxidation steps. A simplified version of this pathway is presented in Scheme 6. Specifically, the authors suggested that the formyl radicals recombine (dimerize) to yield glyoxal. This C_2 compound has a considerable electron affinity because of its π conjugation, and therefore can be easily reduced, first to *trans*-ethane-1,2-semidione and then to glycolaldehyde. The latter can be reduced to the vinoxyl radical $^{\bullet}CH_2CHO$ accompanied by the elimination of a hydroxide ion. The vinoxyl radical is in turn a known precursor of acetaldehyde, which was also observed among the products of CO_2 reduction.[73] Acetaldehyde is further oxidized to an unstable acetyl radical, which undergoes decarbonylation to a methyl radical. Similar to other pathways, the recombination of the methyl radical with a hydrogen atom leads to the formation of methane. Carbon monoxide, eliminated from the aldehyde, is a by-product commonly observed in CO_2 reduction. Methyl radicals can also be formed from acetaldehyde along a different pathway if the aldehyde is oxidized to acetic acid. The acid can be further oxidized in a photo-Kolbe reaction, in which methyl radicals are obtained through decarboxylation of the acid.[74] In this reaction, one molecule of CO_2 is formed as a by-product and can be recycled back to the beginning of the pathway. Shkrob et al. investigated a number of other potential C_2 intermediates such as oxalic acid, glyoxylic acid, and glycolic acid. They concluded, however, that these compounds could not plausibly lead to the formation of methyl radicals because of their predisposition for oxidation. The proposed complex pathway avoids intermediates which would block the process before reaching methane, while the intertwined reduction and oxidation steps, as well as the recycling of CO_2, partially account for the poor quantum efficiency of the CO_2 reduction process. The glyoxal pathway appears to be an important step in understanding the mechanism of the reaction.

2.2.2. *Reduction Pathways on a Co-Catalyst Surface*

Coupling semiconductors with metal NPs has been shown to be beneficial for the performance of photocatalysts because of, among other factors, improved charge separation, facilitated CO_2 activation, and the provision of active catalytic sites for the reduction process.[29,40a,42] In a typical realization of this concept, the often nanostructured semiconductor is surface-decorated or wet impregnated with metal or metal oxide NPs. This architecture is utilized in almost all of the most efficient photocatalytic systems. Nonetheless, even more insights into the chemical mechanism of the CO_2 photoreduction on the metal surface can be gathered from electrochemical studies when the reaction proceeds on a metal electrode that acts as an electrocatalyst. It is a convenient setup which allows the catalytic process to be isolated from the light-harvesting and charge-separation functions of the photocatalyst. It should be noted though that the pathways which include reduction and oxidation steps, such as the glyoxal pathway, are not possible in the absence of holes at the cathode.

Early studies by Hori et al. have shown that the selectivity of the CO_2 photoreduction is determined by the chemical composition of the electrocatalyst.[75] Hydrocarbons were preferentially formed on copper and to a lesser extent on nickel and palladium, while CO was formed on gold and silver electrodes. The rate of the competing process of hydrogen generation on platinum or nickel surfaces was much higher than the rate of CO_2 reduction. Understandably, most of the research focused on electrochemical reduction on copper electrodes, although applying a potential of -0.8 V is required for the onset of CH_4 production from CO_2. That is a significant overpotential against the standard reduction potential of CO_2 to methane [see Eq. (6)]. The developments in the field were reviewed, for example, by Gattrell et al.[51] Combined DFT calculations and electrochemical measurements suggest that, in the initial step, the radical anion $CO_2^{\bullet-}$ adsorbed on the copper surface through its C atom binds a proton to form a carboxyl radical $^{\bullet}COOH$.[46b] Upon interaction with $H^{\bullet}$, this carboxyl radical dehydrates to carbon monoxide, still bound to the surface through the C atom. According to the calculations, the key and rate-limiting step of the process is the hydrogenation of CO to the adsorbed formyl radical $^{\bullet}CHO$. This step is even less favorable on platinum, and the hydrogen radicals instead recombine to form H_2. On the other hand, on surfaces such as gold or silver, where CO is not bound as strongly, it desorbs and is the main reduction product.[15a] Alternatively, the $^{\bullet}CHO$ radical is further hydrogenated, firstly to formaldehyde which is weakly bound to the copper electrode. In the following step, formaldehyde is

hydrogenized to a methoxyl radical $^{\bullet}OCH_3$, which is oriented perpendicular to the surface with the methyl group pointing away. Up to this step, the pathway is essentially a combination of the formaldehyde and carbene pathways, but the methoxyl radical is a unique intermediate of the mechanism on copper electrodes; other proposed pathways involve methyl radicals. Additionally, reduction pathways very similar to the carbene pathway were also proposed.[51] Attachment of a proton from the solution to the methoxyl radical produces methane, while the oxygen atom on the surface is subsequently protonated to eventually form a water molecule. It was also speculated that the orientation of the methoxy group influences the selectivity of the process.[46b] Specifically, in an electrochemical setting, the proton approaches the methoxy group from the solution, so that it interacts with the carbon atom of the moiety. This path of approach favors the formation of methane. In gas-phase experiments the proton is more likely to be adsorbed on the surface of the catalyst, which allows it to easily interact with the surface-bound oxygen atom. Under these circumstances, methanol is preferentially formed.[71]

Ethene is the other major product of CO_2 photoreduction on copper electrodes.[75a] The C_2 product was attributed to the dimerization of two CO molecules adsorbed on neighboring Cu sites. The pathway to ethene then proceeds through the formation of adsorbed enediol.[38a] This means that the C–C bond is formed very early in the reduction process.

3. Measures of Efficiency

The photocatalytic reduction of CO_2 is a complex, multistep process that combines different aspects of light harvesting, charge separation and transfer, heterogeneous (photo)catalysis, electrocatalysis, and surface science. Each step, namely photon absorption, electron and hole transport to surface reaction sites, adsorption of reactants, catalytic reactions, and desorption of the products, contributes to its overall efficiency. This field has attracted great interest from many scientific disciplines such as chemistry, physics, and material science for several years. Nevertheless, at present there is no single measure of the efficiency of photocatalytic systems that encompasses their complexity and—crucially—allows unambiguous comparison of their performance. Instead, there are two types of measures which relate to either the amount of the catalyst or to the strength of the illumination. To some extent this division reflects the varied background of the researchers (e.g. catalysis, photovoltaics, etc.), but it is also used to highlight a specific scientific or economic merit of the investigated system. It is noteworthy that none of the commonly used measures takes into account the amount of the main reactant, that is, carbon dioxide. This is because CO_2 is usually used in large excess and its availability is not thought to be a limiting factor.

The terminology used to define the efficiency of the photocatalytic reduction of CO_2 is generally the same as for other heterogeneous photocatalytic processes,[76] such as the generation of hydrogen from water. At the same time, there is a strong emphasis on the efficient utilization of the full solar spectrum to drive the reaction, such as in solar-cell technologies. The similarities bring together the terminologies of the two approaches to light harvesting. In most cases these two independent backgrounds (catalysis and photovoltaics) only result in complementary measures of efficiency. Unfortunately, there are also some conflicting definitions, which will be discussed in detail below.

3.1. Catalyst-Based Measures

The most often used measure of the catalytic performance of a material is the rate of formation of a product. For a cumulative process, such as CO_2 photoreduction, it is generally expressed as the amount of product divided by the time it took to accumulate and by the amount of catalyst [Eq. (13)]. Accordingly, a common unit of R is mol of product per hour of illumination per gram of catalyst, although the product is also often given in smaller molar units (μmol) or in concentration (ppm). Despite its popularity and simplicity, each term of Equation (13) requires additional clarification in the context of the photocatalytic reduction of CO_2:

$$R = \frac{[\text{Product}]}{\text{Time}[\text{Catalyst}]} \tag{13}$$

1) The complex mechanism involving a cascade of reactions, as described in the previous section, leads to a multitude of products, some of which are unstable or difficult to detect and quantify. Neglecting them would lead to the overall performance of the catalyst being seemingly decreased. Hence the formation rates of all the relevant products are needed to properly assess the catalyst. Alternatively, these may be expressed as selectivities of the process towards specific products, for example, methanol or methane. It is not always apparent how to classify certain products. This particularly concerns H_2, formation of which often accompanies CO_2 reduction in aqueous environments. When considering the light-harvesting or charge-separation and transfer qualities of the catalyst, it may be rightly considered as one of the products. However, from a point of view of CO_2 conversion, it is clearly a product of a competing reaction that decreases the efficiency of the process in question, and should not be included.

2) The product evolution tends not to proceed linearly with illumination time. In fact, it is usually a saturation curve, especially when sacrificial hole scavengers are employed. Therefore, the point in time when the measurement is taken has a strong impact on the evaluation of the catalyst. There is no general agreement in the literature in regard to a standard starting time and duration of the experiment. The former typically coincides with the start of the illumination. However, in some cases, an early burst of product (e.g. methane) formation is observed, which is attributed to originate from carbon residue on the photocatalyst.[38b,40d] The actual measurement should then start once the initial burst is over and the catalyst is free of any contaminants which affect the rate of product formation. The length of the experiment depends on the stability of the catalyst, that is, how long it is able to

sustain an approximately constant formation rate before a saturation regime is reached. To compare different catalytic materials, it would be preferable to have a common specific period of time over which the catalytic activity is measured, for example 24 h, as recently suggested by Maschmeyer and Che.[77]

3) The photocatalyst is often a composite material in which the light absorption, charge transport, and catalytic functions are separated and performed by different materials, for example, CdSe, TiO_2, and Pt.[78] Usually the total mass is used in the denominator of Equation (13). This approach neglects the fact that the noble-metal co-catalyst, present only as a fraction of a percent of the total mass, can determine both the number of catalytically active sites and the overall cost of the catalyst. Thus, from the mechanistic and the economic perspectives, it would also be sensible to define the formation rate in relation to this component. Additionally, the formation rate increases linearly with catalyst concentration only up to a certain value, when a saturation level is reached. The plateau is associated with a reduced light penetration depth and increased scattering by the concentrated catalyst. It has been suggested that the measurements should be taken in the linear regime or at the onset of the plateau, where these limiting factors are less relevant.[79]

4) Perhaps the most important factor, the formation rate is independent of the incident photon flux (rate of incident photons), at least for low light intensities. Until the light saturation regime is reached, the formation rate may therefore be increased by simply increasing the intensity of the incident irradiation. There are wide implications on the ability to compare the results reported in different publications, especially those coming from different laboratories. It is almost impossible to rank the performance of the respective photocatalysts in terms of production rate because the illumination sources of different spectra and more importantly of different intensities, as well as different reactor designs, are very often employed.

Another group of measures, called turnovers, relate the amount of product to the number of active catalytic sites. Turnover frequency (TOF) is defined as the number of photoinduced transformations N (i.e. number of evolved product molecules) per catalytic site per time period[76a] [Eq. (14)]. Here, N_a is the number of catalytically active

$$\mathrm{TOF} = \frac{1}{N_a} \cdot \frac{dN}{dt} \tag{14}$$

sites. The notion of active sites is poorly defined in heterogeneous photocatalysis because the sites may be temporarily or permanently inactivated or made otherwise unavailable, new ones may be created, or specific sites may participate only in part of the CO_2 reduction cascade.[80] In effect, this number is usually unknown. The surface area of the catalyst, determined by Brunauer–Emmett–Teller (BET) measurements, is recommended to be used instead of N_a,[76a,77] thus giving the unit of TOF as $s^{-1}m^{-2}$. However, the surface area may not accurately describe the amount of available catalyst because of internal shading, which means that not all the surface is illuminated uniformly at all times. Additionally, the agglomeration and clustering of photocatalytic material may, particularly in dispersions, lead to a further decrease in the number of effective catalytic sites or exposed area. These restrictions severely limit the applicability of the TOF in measuring the efficiency of CO_2 photoreduction. The term turnover rate (TOR) is usually, although not always, used interchangeably with TOF.[80]

The turnover number (TON) is a related, dimensionless measure that expresses how many times a site participates in the catalytic cycle over the course of the illumination. Notwithstanding the problems with determining the number of sites, it is a useful method for assessing whether a process is indeed catalytic ($\mathrm{TON} \gg 1$) or only stoichiometric ($\mathrm{TON} \approx 1$).[25b] TON is sometimes erroneously expressed per unit time and consequently considered equivalent to TOF/TOR. All turnovers are independent of the photon flux, and hence suffer from the same problems as the rate of formation when they are used to compare different photocatalyst systems.

3.2. Light-Based Measures

An alternative and complementary approach to quantify the performance of a photocatalyst is to measure how efficiently an impinging photon is converted into an electron–hole pair, which is subsequently used to drive the desired photocatalytic event. The latter notion refers to a single-electron (hole) redox process along the formation pathway to the final product. For example, the reduction of one molecule of CO_2 to methane requires eight electrons, and so it involves eight photocatalytic events. On the basis of the premise that a photon must be absorbed to be effective, quantum efficiency is typically defined in photocatalysis as the ratio of the rate of photocatalytic events to the absorbed photons flux within the specified wavelength range[76a] [Eq. (15)] The photocatalytic

$$\phi = \frac{\dot{N}_{\text{photocat. events}}}{\dot{N}_{\text{absorbed photons}}} \tag{15}$$

events have to be summed over the (molar) amounts of all the products, $N = \Sigma_i n_i M_i$, where n_i is the number of electrons (holes) required to obtain one molecule of product M_i. The definition in Equation (15) is adopted from homogeneous photocatalysis, where a precise measurement of the absorption by the sample is not problematic. It can be construed as analogous to the internal quantum efficiency (IQE) used for solar cells.[81] In practice, it is very difficult in heterogeneous photocatalysis to determine the actual number of absorbed photons at any wavelength because of reflection and scattering of light, whereas the incident photon flux can be measured much more reliably inside the reaction vessel by actinometry or by using reference solar cells.

The absorption of light is a critical phase in the generation of solar fuel, so it is important not to omit this part from the assessment of the process efficiency. In fact Equation (15) is used in only about every second literature report on the subject.[41b,69b,76b,82] Others define quantum efficiency as a ratio of the rate of photocatalytic events to the incident photon

flux.[11a,17b,20c,58b,83] This quantity is called photonic efficiency ξ, according to recent IUPAC recommendation,[76a] and corresponds to the external quantum efficiency (EQE), known also as incident photon to current conversion efficiency (IPCE), in solar cells.[44a,84] The lack of consistency in the literature is certainly confusing and unhelpful. There appears to be an agreement, however, that the measure relating to incident flux, referred to as either photonic or quantum efficiency, is the most convenient in heterogeneous catalysis, provided that the actual photon flux inside the reactor is taken into account.[79b] This eliminates the issues associated with the reflection and scattering by the walls of the reaction vessel. Some publications use the terms efficiency and yield interchangeably, but the latter should only refer to monochromatic irradiation.[76a] In the context of solar applications, the term efficiency thus seems to be more suitable.

Neither photonic nor quantum efficiency by either definition incorporates the amount of catalyst involved in the reaction, and generally it can be increased by increasing the catalyst concentration. Moreover, there is a saturation regime when the quantum efficiency decreases with increasing light intensity, as additional photons cannot be absorbed by the limited amount of catalyst.[82c,83b] Hence, a simple strategy for increasing the efficiency would be to use a light source with low intensity and a narrow spectral band in a reactor setting which allows the maximum amount of the photocatalyst to be exposed to the photon flux. Although the values might improve, they would not reflect an actual improvement in the performance of the photocatalyst.

It appears that quantum efficiencies can only be reliably compared between different systems if a light source with the same spectrum and intensity is used and the amounts of the catalyst and reactants are the same. This is illustrated by two publications from the same research group who reported a quantum efficiency value of 6.06 % for a Cu (1.0 wt %)/TiO_2 catalyst[65b] and a value of 0.00074 % for the same catalyst[85] in a different setting. A disparity of four orders of magnitude between two systems using the same material clearly indicates that variables beyond the intrinsic properties of the photocatalyst are determining factors of the quantum efficiency. The major differences were in the light sources: while an 8 W Hg lamp with a maximum light intensity at 254 nm was used in one, in the other a 150 W high-pressure Hg lamp was used. A liquid-phase slurry reactor was used in the first experiment, while a gas-phase optical fiber reactor was used in the second.

The power conversion efficiency η is a related measure defined as a ratio between the energy stored in the chemical bonds of the products to the energy supplied by the incident photon flux.[11a,86] For multiple possible products of CO_2, the efficiency η can be calculated from the molar heats of combustion ΔH^0_c and rates of formation r of each product, as well as the power of the photon flux P [Eq. (16)]. It is clear

$$\eta = \frac{\sum_i \Delta H^0_{c,i} \cdot r_i}{P} \tag{16}$$

that an ideal measure of the efficiency of a photocatalyst would depend solely on its intrinsic properties. None of the measures presented above meet this criterion, because they depend on either irradiation intensity and spectrum or the amount of catalyst. This means that a direct comparison of different photocatalytic materials tested in different setups is almost impossible. Consequently, any ranking of the materials should be treated with caution. In this Review we quote the efficiency values only in the context of similar setups and use relative values to highlight the effect of a specific investigated aspect.

Clearly, the ability to directly compare the performances of photocatalysts would be highly beneficial for the field of solar-fuel generation. We believe that substantial progress could be made if standard conditions of temperature (25 °C), pressure (1 bar), and irradiation were commonly used in a nondiffusion-limited regime.[77] In terms of future implementation in real-world applications based on solar irradiation, it seems reasonable to use the standard solar intensity of (AM 1.5 global (AM: air mass)) and the corresponding solar spectrum.

Additionally, it would be important that at least one efficiency measure from each of the two families is reported, for example, rate of formation or photonic efficiency. While the two are interdependent, it would still help in the assessment of the photocatalyst. As discussed previously, one measure can be improved at the expense of the other, but an improvement in both would be highly significant. An alternative approach would be to devise a new measure of efficiency that incorporates both the amount of catalyst and the photonic flux; however, the discussion of the merits of such an exercise is beyond the scope of this Review.

4. Photoreduction of CO_2 on Semiconductors

The efficient utilization of solar energy requires the use of materials with a small band gap so that a large part of the visible light spectrum can be absorbed. Unfortunately, many promising semiconductors, especially oxides, have a wide band gap, which results in an onset of the absorption below 400 nm. A red-shift of this onset to the visible range is achieved by either sensitizing the semiconductor or engineering its band gap. In the former technique, the absorption region of the photocatalyst is enhanced by the introduction of a secondary material which absorbs visible light. Typically, nanoparticulate narrow-band semiconductors (quantum dots) or visible-light-active molecules (dyes) are used as sensitizing agents (Scheme 7). To this end, coupled semiconductors, for example, CdS and TiO_2, or CdSe and ZnO, have been shown to enhance the efficiency through extension of the absorption range and improvement in the charge separation.[87] When the band gap edges match, an electron is preferentially transferred to the semiconductor with the lower CB edge (TiO_2), while a hole moves in the opposite direction to a higher VB level (CdS), thereby contributing to the decrease in the recombination rate. Sensitization with dyes is a commonly used technique in solar cells, where a large number of inorganic (especially ruthenium-based) or organic dyes have been tested.[44a] The LUMO of the dye has to be higher in energy than the conduction band edge of the semiconductor for the electron transfer to occur, but its rate also depends on

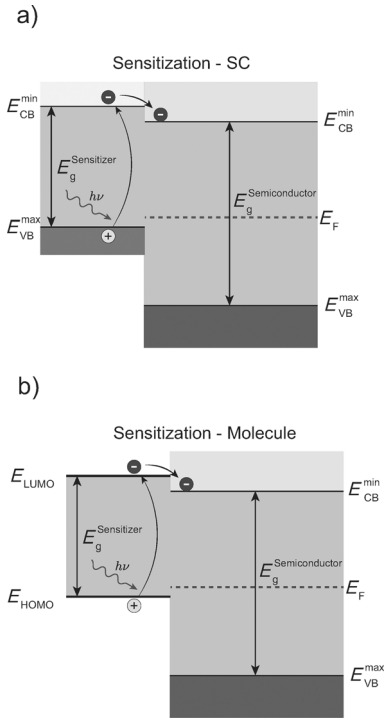

Scheme 7. Sensitization of a wide band gap semiconductor with a) a narrow band gap with aligned conduction band minima or b) a dye that absorbs in the visible region.

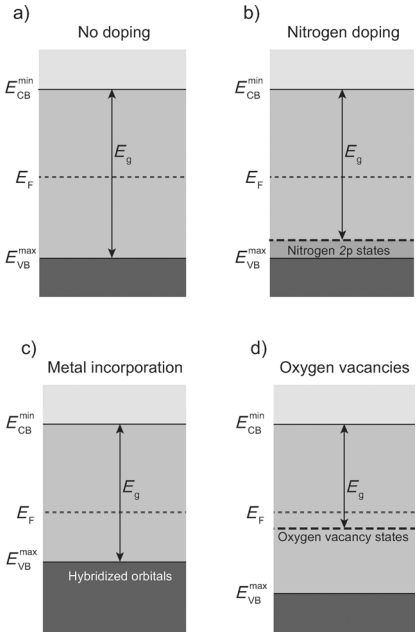

Scheme 8. a) Semiconductor with a wide band gap and approaches to decrease its width: b) creation of dopant states above the VB level, c) hybridization with other orbitals to raise the VB, d) creation of impurity states, for example, from oxygen vacancies, below the Fermi level.

a number of parameters such as the orientation and distance of the light absorbing unit with respect to the surface or size and flexibility of the anchoring unit.[88] Similar to sensitization with quantum dots, the added benefit is the improved charge separation, because the opposite charge is associated with the oxidized dye.

The weakly reductive conduction band of many semiconductors, for example, TiO_2, does not leave much room to minimize the band gap by lowering its energy. In contrast, there is plenty of distance between the energy levels in the valence band (often constituted by 2p orbitals of the O atoms) and the water oxidation potential [1.23 V at pH 0; see Eq. (11)]. Therefore, aside from sensitization, two main strategies have been employed to shift the onset of absorption towards longer wavelengths: doping to create intraband states above the valence band (Scheme 8b) and raising the valence band by forming a solid solution of two or more semiconductors (Scheme 8c).[89] Another possibility is the creation of intraband impurity states, for example, oxygen vacancy states, below the Fermi level (Scheme 8d)[90] or additional states arising from the aggregation of semiconductor NPs.[91] Examples of each strategy are given later in this section.

In the following, the photocatalytic properties of TiO_2 are first discussed in detail and then an extensive overview of experimental approaches for the photoreduction of CO_2 on TiO_2, other oxides, and various sulfides and phosphides is given. Apart from the strategies to improve the absorption properties highlighted above, special emphasis is placed on the effects of employing a co-catalyst as well as the role of the nanostructure and crystallographic properties of the photocatalyst.

4.1. Photocatalytic Properties of TiO_2

The prerequisite for photocatalysts having a sufficiently wide band gap is met by titanium dioxide, which has a band gap exceeding 3.0 eV. TiO_2 is by far the most common semiconductor in photocatalysis, and is used in pollutant degradation, dye bleaching, and water cleaning. Early studies by Fujishima, Honda et al. have shown its applicability to the photocatalytic splitting of water[92] and reduction of CO_2[27] upon irradiation with UV light. Together with its applications as a photoanode in inorganic and hybrid solar cells[44a,84,93] as well as in photo- and electrochromic devices,[94] TiO_2 has attracted enormous interest in terms of studies on its crystal lattice, surface, charge transport, and other relevant properties.[25a,49b,95]

The preponderance of TiO_2 as a semiconductor of choice can be attributed to a variety of reasons. It is cheap, nontoxic, made up of abundant elements, and resistant to photocorrosion.[95a] Its band structure (Scheme 4) allows for both water reduction and oxidation to occur simultaneously.[82a] To this end, the CB edge is located at around −0.16 V versus the NHE at pH 0,[54,96] so that the reduction of protons ($E_{NHE}(H^+/H_2) = 0.0$ V at pH 0) is possible. The low position of the valence band means that the oxidation of water ($E_{NHE}(O_2/H_2O) = 1.23$ V at pH 0) is also thermodynamically favorable. Herein lies the above-mentioned resistance to photocorrosion, which is induced by photogenerated charge carriers

initiating redox reactions which eventually lead to a disintegration of the material.[82a] In an aqueous environment, however, TiO_2 is not prone to this damaging process because the oxidation of water is thermodynamically more favorable than the formation of oxygen molecules from oxide anions. Since this stability extends over a wide range of pH values, TiO_2 is a very convenient semiconductor material for use in suspension-based photocatalytic systems.

TiO_2 exists mainly in four different polymorphs (crystallographic phases): rutile (tetragonal), anatase (tetragonal), brookite (orthorhombic), and TiO_2(B) (monoclinic).[95a] However, from the viewpoint of photocatalysis, the main body of research has been carried out on the first two. The structures of these two polymorphs can be characterized as chains of elongated TiO_6 octahedra,[22a,95b] with each Ti^{4+} ion surrounded by six O^{2-} ions. In the rutile configuration, this octahedron exhibits a slight orthorhombic distortion. The distortion of the anatase octahedron is much more significant, and so it shows a lower symmetry. This fact is also reflected by different distances between the titanium and oxygen atoms in the two phases. While the Ti–Ti distances are larger in anatase than in rutile, the Ti–O distances are smaller. The anatase unit cell can be regarded as octahedra connected by their vertices. In contrast, the unit cell of rutile is built up of octahedra connected on their edges, which means each octahedron is in contact with ten neighboring octahedra.

Generally, TiO_2 is an n-type semiconductor, a property which is attributed to a small number of oxygen vacancies which are then compensated by the presence of Ti^{3+} centers. The valence band is formed by the overlap of 2p orbitals of the oxygen atoms. The lower part of the conduction band is formed by 3d states of titanium Ti^{4+} ions with t_{2g} symmetry. The differences in the crystal structures are responsible for the different band gaps of anatase (3.2 eV) and rutile (3.0 eV). The minimum energy of photons required to initiate an interband transition lies, therefore, in the UV range, with 389 nm for anatase and 413 nm for rutile. It has been shown that the difference between anatase and rutile is mainly due to the position of the CB edge, which lies 0.2 eV higher for anatase.[54] The crystal symmetry of TiO_2 in its natural configuration allows only indirect interband transitions.[95a] This means that photoexciting an electron from the valence band into the conduction band requires the simultaneous presence of a photon to provide the energy and a phonon to provide a change in momentum. This decreases the photonic efficiency, as the rate of absorption events that yield available charge carriers is limited. Additionally, the rate of recombination of the photogenerated charge-carrier pairs can reach up to 90% within a period of 10 ns after their generation,[95a,97] thereby significantly limiting the number of charge carriers available for surface reactions.

According to thermodynamic calculations based on calorimetric data, rutile is the most stable polymorph at all temperatures and pressures up to 6 kbar. The Gibbs free energy of formation of anatase is 15 kJ mol^{-1} lower than that of rutile, but it can be considered stable at ambient conditions. Annealing anatase at temperatures above 400 °C promotes the transformation to rutile. It has been demonstrated that the surface crystallinity of TiO_2 plays a crucial role in determining the efficiency of the photocatalyst, with anatase found to possess particularly good adsorption affinity for organic compounds. Anatase has received much attention by researchers because it also exhibits recombination rates up ten times lower than rutile. Grela and Colussi observed a factor of ten increase in the quantum yield of the photodegradation of nitrophenol with highly crystallized TiO_2 relative to poorly crystallized TiO_2.[98] This may be connected to the observation that the carrier lifetime increases with improved crystallinity. High crystallinity is also assumed to lead to a greater efficiency in the electronic coupling between orbitals of adsorbed dyes and CB states in TiO_2. For example, it has been shown that the observed rates of electron transfer between anthracene carboxylic acid dyes and TiO_2 NPs are much faster in crystalline than in amorphous TiO_2.[99] The correlation of higher crystallinity with improved photocatalytic performance is attributed to fewer dangling bonds and lattice distortions, which can constitute both trapping and recombination sites.[22b] There has been extensive effort to determine which of the two phases of TiO_2 is the more beneficial for photocatalytic applications, and has been reviewed by Henderson.[22b] It has been found, in fact, that mixed-phase TiO_2 shows particularly interesting photocatalytic properties, such as enhanced photocatalytic efficiencies, that are not found in either of the phases separately.[100]

The standard material in the field of photocatalysis is P-25 from Evonik (formerly Degussa), a TiO_2 powder, which is a composite made of about 80% anatase and 20% rutile. The particle size usually ranges from 20 to 80 nm in diameter (with an average of about 25 nm in diameter). Its effective surface area (BET) is considered to be extremely large, at about 49–56 m^2 g^{-1}. Numerous studies have been carried out on P-25 powder.[101] It has also served as a benchmark system in experiments focused on new materials and systems. The high activity of P-25 is attributed to complementary effects of the two constituting TiO_2 phases.[102] There is still much debate about the exact nature of those effects, especially because it is challenging to clearly determine the distribution of rutile and anatase in the mixed-phase powder. There is, however, a general agreement that the interfaces between the phases could play a key role.[103] The first explanation is based on the different positions of their electronic bands (the CB of anatase is about 0.2 V higher), which leads to the formation of a heterojunction. In this configuration, it is energetically preferential for photogenerated electrons to transfer from anatase to rutile, while the concomitant holes stay in the anatase VB, thereby improving the charge-carrier separation (Scheme 9). This model, however, is challenged by various research groups, who argue that the data used to support this explanation is too ambiguous.[101c] An alternative explanation is based on the presence of trapping sites in anatase which are up to 0.8 eV lower in energy than the CB edge.[104] This would suggest that electrons may actually transfer in the opposite direction than previously proposed, with the anatase trap states acting as a sink for electrons generated in the rutile phase. These trap states are considered to be more stable in anatase than in rutile, which results in a stabilization of the charge separation, thus allowing both charge carriers to contribute to the photocatalytic reactions on the surface.

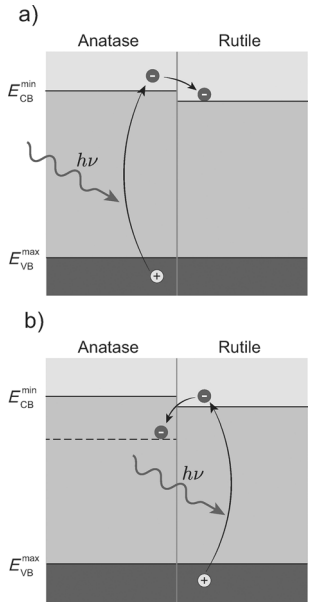

Scheme 9. Two possible mechanisms responsible for the high performance of mixed-phase TiO_2: a) the offset of the two conduction band edges of 0.2 eV is the cause for the improved separation of the charge carriers through electron transfer from anatase to rutile; b) trap states located 0.8 eV below the CB edge of anatase are populated by electrons from rutile, thus facilitating charge separation.

Finally, the interface region between anatase and rutile itself may act as a site for charge-carrier trapping, thus facilitating charge separation.[105]

In terms of the generation of solar fuel, the wide band gap of TiO_2 has a considerable drawback, because it limits the absorption of light to the UV range. Only about 10% of the power of the incident solar photon flux can thus be absorbed.[22a] The two types of modifications mentioned earlier are commonly used to overcome this limitation and shift the onset of the absorption from the UV to the visible region: sensitization and doping.[95a] Examples of both approaches will be given below, the results are also summarized in Table 1.

4.2. Reduction of CO_2 on TiO_2

The TiO_2 band structure has several specific implications for the photocatalytic reduction of CO_2. Perhaps most importantly, the single-electron reduction potential of CO_2 to the radical anion $CO_2^{\bullet-}$ at -1.9 V versus the NHE is much more negative than the conduction band of TiO_2, so that a direct electron transfer from TiO_2 to CO_2 is thermodynamically prohibited. The reduction process may proceed only through adsorbed CO_2 species on TiO_2[43,52,106] or on selected metal catalysts,[40a,46b] and even then the overpotential is very low.[15a] Proton reduction is more favorable [cf. Eq. (7)] and, therefore, competes with CO_2 for electrons. To avoid decreasing the efficiency, the catalyst would have to suppress the H_2 generation process. It should be noted that the multielectron reduction of CO_2 to formic acid, methanol, or methane is less negative than the conduction band of TiO_2 [cf. Eqs. (2)–(6)], although the mechanisms of such reactions remain to be elucidated and proven.[29]

Furthermore, the hole in the valence band has a highly positive potential of about $+2.94$ V (versus the NHE), thereby creating a very strongly oxidizing environment through surface trapped holes and $OH^{\bullet}$ radicals ($E^0(OH^{\bullet}/H_2O) = 2.27$ V versus the NHE). This is why most photocatalytic applications of TiO_2 are oxidation reactions of various organic substances.[95c,107] As discussed in Section 2.2.1, there is a possibility that the products of CO_2 reduction, such as formates or methanol, could be easily oxidized back to CO_2, especially in the presence of a cocatalyst.[108] In some studies, sacrificial hole scavengers are employed to prevent the re-oxidation from taking place. Despite these constraints, TiO_2 remains an attractive semiconductor that has been shown to be capable of photocatalytically converting CO_2 into valuable hydrocarbons at ambient temperatures and pressures,[71] even with a simple system composed of a photocatalyst (TiO_2), water, and a UV light source.

4.2.1. Solid–Liquid Interface Photoreactions

A very straightforward implementation of such a system is a dispersion of TiO_2 NPs in a CO_2-saturated aqueous solution.[104] Both liquid- (formic acid, formaldehyde, and methanol) and gas-phase (methane) products were detected under ambient conditions. Various approaches have been investigated to improve the efficiency of bare TiO_2 in liquid suspensions. For example, an increase in the CO_2 pressure brought an increase in the yield of the liquid-phase products (up to a certain amount) and of gaseous products such as methane, ethane, and ethene.[109] The addition of electrolytes increased the overall yield under ambient as well as high-pressure conditions, and also resulted in the formation of C_2 products such as ethanol and acetaldehyde. One of the rate-limiting factors was considered to be the lack of electron donors. The addition of propan-2-ol as a hole scavenger was shown to enhance the rate of formation of methane under higher pressure conditions,[62a] yet none of the previously observed C_2 compounds were reported in the presence of propan-2-ol. A similar trend was also reported under ambient pressure.[73] Additionally, the formation of CO was observed.

When carbonate anions rather than gaseous CO_2 were used as the carbon source in an aqueous suspension, the formation of methanol and methane was improved at lower pH values.[110] The optimal concentration of P-25 NPs was determined to be 1.0 $g\,L^{-1}$ (Figure 1). It was argued that the overall efficiency decreased at higher concentrations because of the limited penetration by the UV light, although it should be noted that this optimal concentration relates to a specific intensity of 12.64 $W\,m^{-2}$. It was also shown that, compared to other sizes, anatase NPs with a diameter of 14 nm gave the highest yields of methanol and methane.[111] The decreased performance with larger particles may be due to smaller surface areas and longer electron migration paths. The decrease in activity with smaller particles was associated with changes in the optical and electronic properties, espe-

Table 1: TiO_2-based photocatalytic systems for CO_2 reduction.

Category	Best system	Co-catalyst		Major product	R_{max}[a]	Minor products	Traces	Ref.
TiO_2 (P-25) in suspension	TiO_2 (P-25) particles	–	–	CH_3OH	3.4[b]	CH_4		[110]
TiO_2 anatase particles with a crystallite diameter ranging from 4.5 to 29 nm	14 nm anatase particles	–	–	CH_4	0.4	CH_3OH	H_2, CO	[111]
TiO_2 powder (P-25) in 2-propanol	P-25 particles	–	–	HCOOH	1.2	HCOOH		[62a]
TiO_2 (anatase) powders in liquid CO_2	anatase particles	–	–	HCOOH	1.2			[112]
TiO_2 powder in supercritical fluid CO_2	anatase particles	–	–	CH_4	1.8			[60b]
TiO_2 powder (P-25) coated glass pellets	P-25 particles	–	–	CH_4	4.11	CO, C_2H_6		[256]
TiO_2 (anatase, 325 mesh) in aqueous suspension with propan-2-ol	anatase particles	–	–	CO	15.3[c]	CH_4, H_2		[73b]
sputtered TiO_2 films	mixed-phase TiO_2	–	–	CH_4	0.032		CH_3OH	[141]
TiO_2 coated onto sapphire disks	anatase particles	–	–	CH_4	7	H_2	C_2H_6	[140]
immobilized TiO_2 particles	JRC-TiO-4 particles	–	–	CH_4	93		C_2H_6, C_2H_4	[150]
immobilized TiO_2 particles	JRC-TiO-4 particles	–	–	CH_4	0.020		C_2H_4, C_2H_6, O_2	[41a]
sensitized TiO_2 particles in suspension	Ag/TiO_2 particles	Ag	7.0 wt%	CH_4	9	H_2, CH_3OH,CO		[127]
sensitized TiO_2 particles in suspension	Ag/TiO_2 particles	Ag	5.2 wt%	$CH_4 + CH_3OH$	10.5			[128]
sensitized TiO_2 particles in suspension	Cu/TiO_2 particles	Cu	2.0 wt%	CH_3OH	19.8			[65b]
sensitized TiO_2 particles in suspension	Cu/TiO_2 particles	Cu	2.0 wt%	CH_3OH	17			[118]
sensitized TiO_2 particles in suspension	Cu/TiO_2 particles	Cu	2.0 wt%	CH_3OH	20			[65a]
sensitized TiO_2 particles in suspension	Cu/TiO_2 (P-25) particles	Cu	3.0 wt%	CH_3OH	443			[119]
sensitized TiO2/SBA-15 composite in suspension	(Cu/TiO_2) 45 wt%/SBA-15	Cu	2.0 wt%	CH_3OH	627			[121]
sensitized TiO_2 particles in suspension	Cu-Ce/TiO_2 particles	Cu/Ce	2.0 wt%	CH_3OH	11.3			[120]
sensitized TiO_2 particles in suspension	CuO/TiO_2 particles	CuO	1.0 wt%	$HCOOCH_3$	1602			[60a]
sensitized TiO_2 particles in suspension	enzyme/TiO_2 (P-25)	Enzyme		CO	300			[132]
sensitized TiO_2 supported on zeolite	Fe-TiO_2/HZSM-5	Fe	10.0 wt%	CH_4N_2O	18[d]			[122]
sensitized TiO_2 particles in suspension		Pd		$HCOO^-$	2.22[e]			[124]
sensitized TiO_2 particles in suspension	Pd/TiO_2 particles	Pd	2.0 wt%	CH_4	0.6	CO	C_2H_6	[38b]
sensitized TiO_2 particles in suspension	Pd/TiO_2 particles	Pd	2.0 wt%	CH_4	0.3	C_2H_6	CH_3OH, HCOOH, CH_3CO_2H	[123]
TiO_2 anchored on Vycor glass	TiO_2 particles	–	–	CH_4	0.11	CH_3OH	C_2H_4, C_2H_6, CO, O_2	[138]
TiO_2 powder	JRC-TIO-4 (anatase) particles	–	–	CH_4	0.02	CH_3OH, CO	C_2H_4, C_2H_6, O_2	[41a]
quartz wool immersed in P-25 suspension	TiO_2 (P-25) particles	–	–	CH_4	0.1	CO, H_2		[139]
TiO_2 pellets (made of P-25)	TiO_2 pellets	–	–	CH_4	0.22[e]	H_2	CO	[257]
immobilized TiO_2 (P-25) powder	TiO_2 (P-25) particles	–	–	CH_4	135[f]			[170]
two types of Ti-β-zeolites: Ti-β(OH) and Ti-β(F)	Ti-beta(OH)	–	–	CH_4	5.8	CH_3OH	CO, C_2H_4, O_2	[70a]
Ti-containing porous silica (PS) films	Ti-PS (hexagonal, Si/Ti = 50)	–	–	CH_4	7.1	CH_3OH		[69b]
Ti-MCM-41; Ti-MCM-48; Ti-SBA-15	Ti-SBA-15	–	–	CH_4	106	CH_3OH	C_2H_4, C_2H_6, CO, O_2	[146]
optical fiber coated with sensitized TiO_2	sensitized TiO_2 on glass fiber	Ag	1.0 wt%	CH_3OH	4.1			[153]
sensitized TiO_2 films	anatase films	Au		CH_4	15[g]	C_2H_6; HCHO; CH_3OH		[169]
optical fiber coated with sensitized TiO_2	sensitized TiO_2 on glass fiber	Cu	1.2 wt%	CH_3OH	0.5			[151]
glass wool supported sensitized TiO_2-SiO_2 composite	porous TiO_2-SiO_2	Cu	0.5 wt%	CO	60	CH_4		[156]
glass wool supported sensitized TiO_2-SiO_2 composite	TiO_2 (2 mol%)-SiO_2 composite particles	Cu	0.01 mol%	CO	17.5			[157]
optical fiber coated with sensitized TiO_2 on SiO_2 support	sensitized TiO_2 on glass fiber	Cu-Fe	0.5wt%–0.5wt%	CH_4; C_2H_4	1.86; 0.56		CH_3OH, C2H6	[154]
optical fiber coated with sensitized TiO_2	sensitized TiO_2 on glass fiber	Cu-Fe	0.5 wt%–0.5 wt%	CH_4; C_2H_4	0.91; 0.58		CH_3OH, C_2H_6	[85]

Table 1: (Continued)

Category	Best system	Co-catalyst		Major product	R_{max}[a]	Minor products	Traces	Ref.
optical fiber coated with sensitized TiO_2	sensitized TiO_2 on glass fiber	Cu-Fe, N3	0.5 wt%–0.5 wt%	CH_4; C_2H_4	0.85; 0.56			[155]
sensitized TiO_2 films	TiO_2 on glass beads	Pt	0.25 wt%	CH_4	0.3			[162a]
sensitized anatase-type TiO_2 nanorods	TiO_2/Pt nanorods	Pt	1.0 wt%	CH_4	6			[160]
titanium oxide species anchored within the Y-zeolite cavities	Pt/ex-Ti-oxide/Y-zeolite	Pt	1.0 wt%	CH_4	6.7	CH_3OH	C_2H_4, C_2H_6, CO, O_2	[143]
mesoporous titania zeolites (Ti-MCM-41, Ti-MCM-48, TS-1)	Pt/Ti-MCM-48	Pt		CH_4	12.3	CH_3OH	C_2H_4, C_2H_6, CO, O_2	[145]
immobilized TiO_2 particles	JRC-TiO-4 particles	Rh	4.0 wt%	CO	5.1	CH_4		[168a]

[a] Maximum formation rate reported for the major product(s), in $\mu mol\,g^{-1}\,h^{-1}$, unless stated otherwise. [b] In $mg\,L^{-1}\,h^{-1}$. [c] In μL. [d] In $ppm\,g^{-1}\,h^{-1}$. [e] $\mu mol\,h^{-1}$. [f] In ppm. [g] In $\mu mol\,m^{-2}\,h^{-1}$.

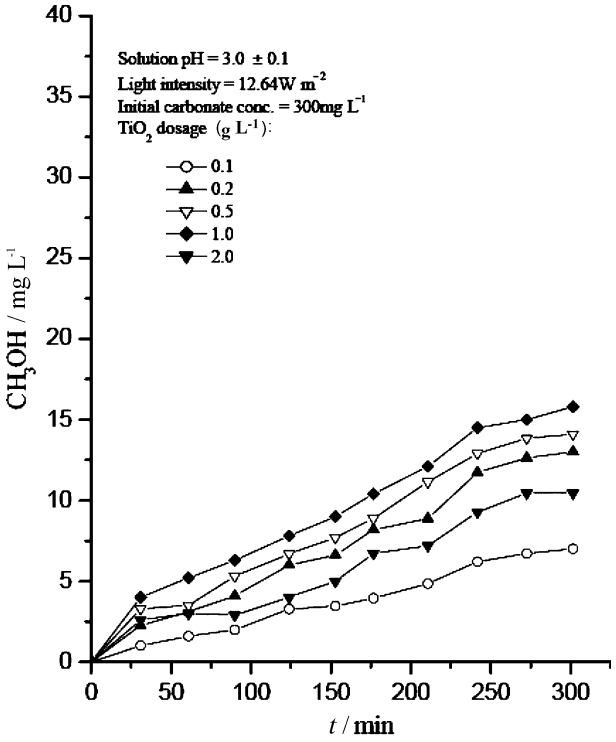

Figure 1. Evolution of methanol for different concentrations of P-25 nanoparticles in aqueous dispersion. Reproduced from Ref. [110] with permission.

cially with a widening of the band gap and associated blue-shift of the onset of absorption.[87b]

The solubility of carbon dioxide in water is rather low, and at the same time, as mentioned before, water reduction occurs competitively with the CO_2 reduction. Therefore, the effect of replacing water by supercritical liquid CO_2 was investigated.[60b,112] Washing the suspended TiO_2 powder with water after exposure to light yielded formic acid. This result indicates that the illumination of TiO_2 in liquid CO_2 resulted in the formation of $CO_2^{\bullet-}$ radicals, which were subsequently protonated. This is underlined by the fact that washing the TiO_2 with acidic solutions instead of pure water gave larger yields of formic acid.

TiO_2 microcrystals embedded in SiO_2 matrices (Q-TiO_2/SiO_2) were shown to exhibit improved photocatalytic properties compared to bulk TiO_2/SiO_2 powders.[113] These composites were dispersed in water mixed with propan-2-ol as a hole scavenger. The added CO_2 was photocatalytically converted into formate, methane, and ethene. A decrease in the the Ti/Si ratio led to an increase in the efficiency of the product formation. The fact that the observed product spectrum differed from what had been reported previously was ascribed to the use of propan-2-ol as the electron donor. In further studies of the role of solvents, TiO_2 NPs embedded in SiO_2 were spin-coated onto a quartz plate, which was then illuminated upon immersion in a suspension containing propan-2-ol and solvents with different dielectric constants ε.[114] The two detected CO_2 reduction products were formate and CO. The ratio of formate to CO increased with an increase in the dielectric constant of the employed solvent. It was shown by using isotopically labeled $^{13}CO_2$ that both were products of the CO_2 reduction process and did not originate from the decomposition of either the solvent or the hole scavenger. A comparison of the Q-TiO_2/SiO_2 with bulk P-25 TiO_2 powder illustrated the superior performance of the composite structure. The formation of methanol was observed when Q-TiO_2 was immobilized in a poly(vinylpyrrolidone) film. This finding suggests that the matrix used for the immobilization of TiO_2 also influences the reduction pathway of CO_2. Ammonia and urea appeared in the products, together with formate and CO, when lithium nitrate was present in the solution.[115] In this case an increase in the dielectric constant led to larger amounts of ammonia and urea, while the amounts of formate and CO both decreased.

The improved efficiency of the TiO_2/SiO_2 systems was attributed to enhanced charge separation through the presence of bridging Ti-O-Si bonds. This conjecture was verified by doping the composite with ruthenium by a solid-state dispersion method.[68b] Loading pure anatase NPs with 0.5 wt% Ru by wet impregnation had been previously shown to improve their photocatalytic activity because of the formation of a Schottky barrier and improved charge separation. In contrast, doping the composite with Ru led to a decrease in activity. This detrimental effect was associated with the formation of the Ti-O-Si bonds being inhibited.

A composite system of TiO_2 and kaolinite was examined for the photoreduction of CO_2 by Kočí et al. and compared with pure P-25 TiO_2 particles in an aqueous solution of 0.2 M NaOH under UV illumination.[116] The rates of formation of

methane and methanol increased, but the rate of formation of CO, although generally small, was smaller for the TiO_2/kaolinite system than for P-25. Various factors were proposed to explain the enhanced performance of the composite photocatalyst. These include a larger effective surface area because of a weaker agglomeration of the particles, a reduced recombination rate of the photogenerated charges, a modified acidity of the surface of the composite system, and a smaller size of the anatase crystallites.

In a study focused on finding photocatalysts able to form C_2 and possibly C_3 compounds from CO_2, TiO_2 catalysts were supported on amphiphilic materials.[68a] The dependence of the selectivity for specific photocatalytic products on the nature of the catalytic support shows its importance for the process. The highest yields and best selectivity was obtained for a 10 wt% TiO_2/Pd/Al_2O_3 system, which produced acetone and ethanol as major products, and ethane and methane as minor products from a CO_2-saturated aqueous solution.

Electrochemical studies have shown that various metals such as copper, platinum, and palladium were able to catalyze the electrochemical reduction of CO_2;[15,46] therefore, metal doping was used in an analogous way in photocatalytic systems. In early studies, Hirano et al. added Cu NPs to a TiO_2 slurry. This system produced mainly methanol and showed no activity in the absence of copper.[117] It was assumed in this case that the role of the copper was not only as a catalyst but also as a hole scavenger. Copper-loaded TiO_2 particles prepared in a sol–gel procedure were examined in an alkaline suspension to determine the optimal copper loading for CO_2 reduction (Figure 2).[65] It was found that the largest methanol

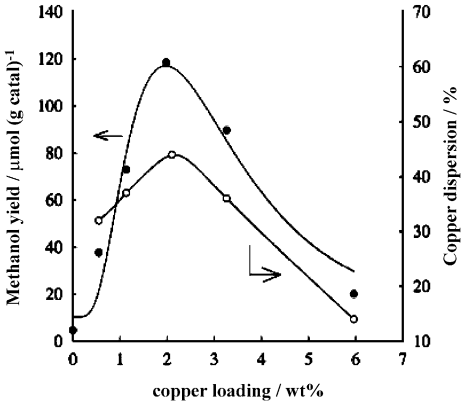

Figure 2. Effect of the copper loading concentration on the rate of methanol formation (○) and copper dispersion (●). Reproduced from Ref. [65b] with permission.

yield could be achieved with a Cu loading of 2 wt%. The use of copper-loaded particles resulted in a strong increase in the yield of methanol compared to non-doped TiO_2. The active state of the Cu for the photoreduction was assumed to be highly dispersed Cu^I on the basis of a decrease in the photoactivity on reduction of Cu^I to Cu^0 or aggregation upon reduction with H_2.[118] The generally positive effect of copper loading on the photocatalytic reaction is ascribed to the ability of the metal to trap electrons and thus reduce recombination losses of the photogenerated charges without affecting the mobility of the electrons. In another study, a loading of 3 wt% CuO on P-25 was determined to be optimal for the formation of methanol in an aqueous suspension.[119] A higher surface loading was associated with shading effects, which reduced the overall absorption capacity of the TiO_2 particles. It was also claimed that CuO is the most active copper species compared to Cu and Cu_2O. In another approach, TiO_2-CuO composites were synthesized by using cetyl trimethylammonium bromide (CTAB) as a dispersant.[60a] In this case, the highest photocatalytic activity was observed with 1.0 wt% CuO. Annealing the catalyst at 450 °C also improved the performance, possibly because of the high crystallinity which enabled rapid electron transfer. In this study, the reaction was carried out in methanol to increase the solubility of CO_2 and to provide an additional hole scavenger. The main product was methyl formate, resulting from the dimerization of formaldehyde, itself an oxidation product of methanol. Simultaneous doping of TiO_2 with Cu and Ce was also shown to be very beneficial for the formation of methanol from CO_2 in an alkaline suspension,[120] with an optimal Cu loading of 2 wt%. According to calculations, the cerium atoms were inserted into the TiO_2 crystal lattice, thereby creating distortions and facilitating the formation of catalytically active adsorbed CO_2 and H_2O species. The effect of Ce appeared to be stronger than that of Cu doping.

In another study, a two-way approach was chosen to improve the photocatalytic activity of TiO_2 by dispersing TiO_2 nanocrystallites in the channels of a mesoporous silicate (SBA-15) and loading this composite structure with copper.[121] Irradiation of the photocatalyst in an aqueous solution of 0.1 N NaOH saturated with CO_2 led to the formation of methanol. The highest photocatalytic activity was observed for a structure of highly dispersed anatase NPs loaded with 2 wt% Cu embedded in SBA-15. The superior performance was attributed to the highly dispersed state of TiO_2 because of the mesoporous structure of SBA-15, on the one hand, and to the catalytic properties of copper, on the other hand.

The molecular sieve 5A was investigated as another mesoporous support for dispersed Cu-loaded TiO_2 NPs.[122] The photocatalytic reduction of CO_2 bubbled through an aqueous 0.2 M NaOH solution resulted in the formation of mainly oxalic acid, through dimerization of $^{\bullet}$COOH radicals, as well as smaller amounts of acetic acid and methanol. The highest formation rate of oxalic acid in alkaline conditions (65.6 $\mu g\,g^{-1}\,h^{-1}$) was obtained for a sieve with 10 wt% P-25 TiO_2 loaded with 2 wt% Cu. Under neutral conditions, however, P-25 particles without Cu outperformed the other composite structures.

Copper is particularly appealing compared to other metals such as platinum, rhodium, palladium, gold, and ruthenium because it is inexpensive and abundant. However, all of these metals are known for their outstanding catalytic properties. In an early study by Ishitani et al., palladium led to the largest increase in the rate of formation of methane when P-25 particles were loaded with 2 wt% of the metals.[123] Other reported products included ethene, formic acid, acetic acid, and traces of methanol. Isotope labeling with $^{13}CO_2$

proved that CO_2 indeed served as the carbon source for the formation of methane. Additionally, a much smaller amount of methane was detected and production ceased after about 4–5 h under N_2. It was concluded that, in this case, methane formed from the carbonate dissolved in the water. XPS measurements showed the presence of partly oxidized Pd species after the illumination. Oxidation and deactivation of the catalyst explains the decrease in the formation rate after 8 h and eventual termination of the process. This proposal was confirmed by the fact that methane was formed at a much lower rate after degassing the reactor and reintroduction of CO_2 after 24 h.

Palladium loading of TiO_2 colloids in aqueous suspension had previously been reported to lead to the photoreduction of carbonates to formates.[124] This finding was corroborated by another study in which TiO_2 particles were doped with palladium and ruthenium oxide (RuO_2).[125] The deposited Pd was assumed to catalyze the conversion of CO_2 into formate, whilst RuO_2 was a catalyst for the oxidation reaction. Surface photovoltage spectrum (SPS) measurements showed a strong response by the metal-doped particles in the near IR region, which could be correlated with an increased photocatalytic activity.

Other metals such as gold and silver can, in addition to their catalytic function and acting as an electron sink, also extend the light-absorption range of the photocatalyst through plasmonic excitations. These excitations in metal NPs are known to enhance photocatalytic oxidation processes on TiO_2.[126] Accordingly, Kočí et al. reported that loading TiO_2 NPs with 1–7 wt% Ag indeed improved the rate of formation of methane and methanol.[127] The increase in the rate was correlated with the amount of silver. Although the effective surface appeared to increase because of silver doping, it was not the decisive effect in explaining the increase in product yields. Instead two different causes were proposed: 1) doping with up to 5 wt% Ag led to a noticeable shift of the absorption towards visible wavelengths and 2) the silver atoms formed metal clusters, which led to the formation of Schottky barriers at the metal–semiconductor interface. This phenomenon is known to enhance the charge-carrier separation.[29] In a separate study, an improvement in the product yield with metal loading was observed for illumination at 254 nm, but not at 365 nm.[128]

Coating P-25 TiO_2 NPs with Nafion (a perfluorinated polymer with sulfonate groups) membranes was shown to improve the photoconversion of CO_2 into methane and ethane because the polymer is an excellent proton-conducting medium, it stabilizes the reaction intermediates, and is itself inert to photoinduced redox processes.[129] The combination of a Nafion layer with silver loading further improved the photoconversion. In this case, however, the main products were methanol and formaldehyde, whose formation rates increased with the amount of silver.[130]

In the most common approach to sensitization, dye molecules are chemisorbed on the TiO_2 surface. If the LUMO of the dye lies above the conduction band edge of TiO_2 then, after the absorption of a photon, the excited electron can be injected into the semiconductor. In this context, TiO_2 NPs with diameters of 20 nm were synthesized by a sol–gel method by using a homogeneous hydrolysis technique and with a cobalt phthalocyanine dye (TiO_2-CoPc) used as a sensitizer.[64] This electron transfer to TiO_2 separates the electron from the hole, and thus improves the overall photocatalytic activity. This was demonstrated by a larger total yield of the photoreduction products from CO_2 bubbled through an aqueous 0.15 N NaOH solution containing Na_2SO_3 as a hole scavenger when a TiO_2-CoPc system was used compared to pure TiO_2. The formation rates of formic acid and formaldehyde strongly increased, but at the same time a small decrease in the formation rates of CO and methane was noted. The presence of sacrificial electron donors (Na_2SO_3 and OH^- groups) improved the photocatalytic performance of the system.

A different approach to a suspension-based system was proposed by Woolerton et al.[131,132] P-25 TiO_2 particles were sensitized with a ruthenium dye ($[Ru^{II}(bpy)_2(4,4'\text{-}(PO_3H_2)_2\text{-}bpy)]Br_2$ (bpy = 2,2'-bipyridine), referred to as RuP, to increase the absorption of light in the visible range. Instead of using a metal catalyst for the catalytic reduction of CO_2, an enzyme *Ch* CODH I from the anaerobic microbe *Carboxydothermus hydrogenoformans* was attached to the TiO_2 particles (Scheme 10). This enzyme is known to catalyze

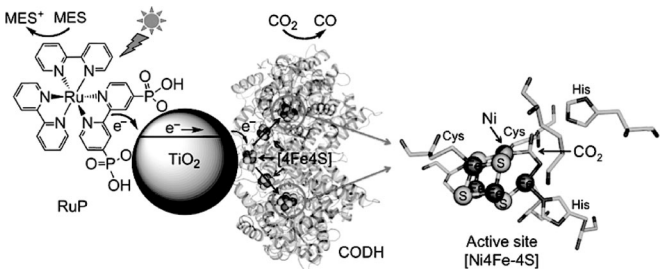

Scheme 10. A CO_2 reduction system composed of TiO_2 nanoparticles, a RuP sensitizer, and *Ch* CODH I enzyme. MES = 2-(*N*-morpholino)ethanesulfonic acid. Reproduced from Ref. [131] with permission.

a two-electron reduction of CO_2 to yield CO.[133] In such a system, the RuP sensitizer absorbs visible light and subsequently injects an excited electron into the conduction band of the TiO_2 particles. After migrating through the conduction band of TiO_2, the electron is transferred into the enzyme and its active sites, and CO_2 is reduced to CO. The addition of EDTA as an additional electron donor increased the rate of formation of CO by up to 40%, which led to the conclusion that the limiting factor was the regeneration of the ruthenium sensitizer.

Silver bromide (AgBr), known to be highly sensitive to light, was also used as a sensitizing agent.[134] The system with the highest yields was found to consist of 23.2 wt% AgBr coupled with P-25 TiO_2 NPs, which performed best at pH 8.5. The system was tested in an aqueous suspension with 0.2 N $KHCO_3$ and illuminated by visible light. The detected reduction products were methane, methanol, CO, and ethanol. The system exhibited a high stability and almost no deterioration in performance over repeated reduction cycles under visible light.

Chemically bonded nanocomposites of TiO_2 (P-25) and graphene are promising photocatalysts because of their good adsorptivity of dyes, extended light-absorption range, and efficient charge separation through the graphene sheet.[136] Such composite structures were also tested for the photocatalytic reduction of CO_2, with particular focus on the enhancement of the performance as a consequence of the carbon structure and the effect of defects in graphene on the photocatalytic reaction.[135] For this purpose, two types of graphene with different defect densities were synthesized and coupled to P-25 TiO_2 particles to form a composite thin film. Photoreduction of CO_2 in the presence of water was then attempted under UV-A (365 nm) and visible light and compared to the results obtained for a pure TiO_2 film. Both hybrid systems resulted in an enhanced photocatalytic rate of formation of methane under visible light. However, the catalyst with fewer defects (SEG-TiO_2) was more than three times better than the graphene/TiO_2 (SRGO-TiO_2) structure containing more defects. The same trend was apparent under UV illumination, where only SEG-TiO_2 enhanced the photocatalytic yield. Defect sites are usually considered to be highly reactive; however, they appear to be rather detrimental to the photoreduction of CO_2. This was assumed to be related to the decreased electron mobility because of charge carrier scattering events. In contrast, the better performance of the composite with fewer defects was linked to the high electron mobility, which translates into a longer mean free diffusion path (Scheme 11). This ensures rapid separation of photogenerated charges, thus reducing the recombination rate and increasing the chances of an electron reaching and interacting with an adsorbed reactant. Moreover, the electronic coupling between SEG and TiO_2 appears to be stronger, hence facilitating electron injections from one structure to the other. Lastly, the absorption range of TiO_2 is shown to be extended into the visible region by coupling to graphene, which was the assumed reason for the composites performing significantly better than the pure TiO_2 film under visible illumination.

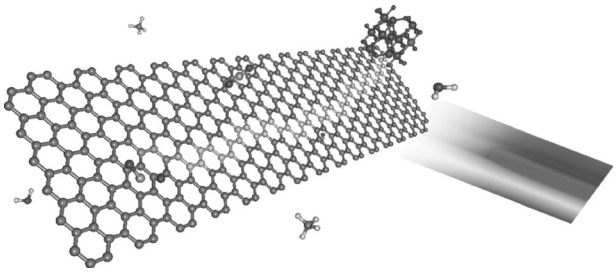

Scheme 11. Proposed photocatalytic mechanism for graphene–TiO_2 nanocomposites. Upon illumination, the photoexcited electron is injected into the graphene nanoplatelet, leaving behind a TiO_2-confined hole. As a consequence of its lower density of defects, electrons in the SEG are able to diffuse farther, thus sampling a larger surface area for adsorbed CO_2. Reproduced from Ref. [135] with permission.

Another approach that combines nonstoichiometric $Ti_{0.91}O_2$ and graphene to a composite photocatalyst was to stack nanosheets of each material to form robust hollow spheres.[137] The increased yield of CO and CH_4 from CO_2 compared to with P-25 TiO_2 was attributed to the thin nature of the nanosheets, which enabled a very rapid transport of the photogenerated electrons to the surface, where the reaction could occur. Additionally, the electron transfer from $Ti_{0.91}O_2$ to graphene was argued to enhance the lifetime of the charge carriers. It was also speculated that the hollow spheres might be able to enhance the absorption of light through multiscattering of incident photons.

4.2.2. Photoreactions at the Solid–Gas Interface

The photocatalytic reduction of CO_2 at the liquid–solid interface is most commonly done by preparing an aqueous dispersion of a nanoparticulate photocatalyst. In contrast, the photocatalyst has to be immobilized for reactions at the gas–solid interface. Although this may decrease the accessible area for both photons and reactants, this approach significantly facilitates the separation of products, reactants, and photocatalytic material.[71] In this case, both the structure of the photocatalyst and of its substrate affects the overall efficiency of the process. Another drawback of aqueous suspensions is the low solubility of CO_2, which can be overcome in gaseous mixtures of CO_2 and H_2O. In addition, the ratio of H_2O to CO_2, easily tunable in the gas phase, was found to play a significant role in determining the reaction rate.[138] For example, in a system of TiO_2 NPs immobilized on Vycor glass, the rate of formation of methane increased as the ratio of the H_2O vapor to CO_2 increased. The other major product, methanol, was formed at the highest rate with a H_2O/CO_2 ratio of 5:1.

In contrast, methane and CO were the only detected CO_2 reduction products when P-25 TiO_2 NPs were immobilized on glass wool.[139] The same compounds were obtained for P-25 TiO_2 pellets illuminated with UV light in the presence of water vapor and CO_2. These pellets were more effective than photocatalysts immobilized by thin-film or anchoring techniques. A UV-C light source (253.7 nm) gave, as expected, a significantly higher yield than illumination with UV-A (365 nm).

Ethane was detected among the products of CO_2 reduction on P-25 and anatase NPs coated onto sapphire glass.[140] In this setup, the effect of temperature on the reaction rate was also investigated. A steady increase in the cumulative yield was observed on increasing the temperature up to 200 °C. The saturation of the product formation curve after 4 h (at all temperatures) was attributed to the strong adsorption of O_2 produced in the CO_2 photolysis, which blocks the reaction sites. This conjecture was supported by two observations: 1) only about 25 % of the stoichiometrically produced O_2 was detected and 2) the temperature-dependent measurements indicated that the desorption of O_2 and intermediate products might be the rate-limiting step.

An increased product yield at elevated temperature was also observed in an investigation on various TiO_2 thin films. It was found that the largest methane yield was obtained at 80 °C and 45 vol % CO_2.[141] The employed photocatalytic structure was a sputtered mixed-phase film (70 % anatase, 30 % rutile) deposited at low angle. This film proved to be

superior to pure-phase or high-angle sputtered films, as well as a P-25 film prepared by dip coating. This finding was attributed to the high photocatalytic activity of the numerous rutile–anatase phase interfaces and to the enhanced absorption of visible light (up to 550 nm) associated with non-stoichiometric oxygen vacancies.

A photocatalytically active zeolite structure (TS-1) was synthesized by replacing silicon atoms in the zeolite framework with titanium.[142] The CO_2 reduction experiments were carried out in an H_2 atmosphere under UV illumination, and yielded methane. In comparison, silicate without titanium did not show the photocatalytic activity of TS-1. Interestingly, upon exposure to UV illumination, the amount of adsorbed carbon species on the catalyst increased by two orders of magnitude. These were assumed to be hydrogenized CO_2 molecules, such as $^{\bullet}CH_3$ radicals.

The use of Ti-oxide/Y-zeolite catalysts in the presence of CO_2 and gaseous H_2O was shown to strongly improve the yield of CO_2 reduction products—mostly methane, methanol, and some ethene, ethane, as well as CO—under UV illumination compared to the use of anatase TiO_2 powder.[70b,143] The largest yield of methanol was obtained with an ex-Ti-oxide/Y-zeolite (1.1 wt% TiO_2) catalyst prepared by an ion-exchange method. The absorption spectra indicate, however, that the absorption of such a catalyst was blue-shifted compared to that of imp-Ti-oxide/Y-zeolite structures prepared by impregnation techniques. This shift is attributed to a higher dispersion of Ti oxide species, which is in turn considered to be linked to the enhanced reactivity of the catalyst to form methanol. Additionally, the ex-Ti-oxide/Y-zeolite exhibited a strong photoluminescence originating from the radiative decay of a long-lived (54 μs) charge-transfer excited state to the ground state of the tetrahedrally coordinated Ti atoms. These are considered to be highly efficient photocatalytic reaction sites, which is supported by the observation that the photoluminescence is quenched by both water vapor and CO_2. The effect of loading the catalyst with Pt was also investigated and found to increase the methane yield as well as strongly decrease the methanol yield. The observed quenching of the photoluminescence was attributed to the transfer of photoexcited electrons to the metal, thus effectively separating these electrons from their concomitantly generated holes.[144] The redox half-reactions are thus spatially separated so that carbon and $^{\bullet}OH$ radicals form at different reaction sites, thus preventing them from reacting with each other to form methanol.

The microporous TS-1 zeolite was compared with titanium-containing mesoporous silicate zeolites (Ti-MCM-41, Ti-MCM-48; Figure 3).[70b,145] The product distribution was the same as found previously and all the zeolites outperformed bulk TiO_2 powder, with Ti-MCM-48 resulting in the highest rate of formation of both major products. This was again attributed to a higher dispersion of the reactive TiO_2 species. Additionally, the comparatively larger pore size (> 20 Å) within the 3D channel structure may have contributed to this result. Accordingly, the yield was further improved up to 20 times by increasing the pore size to 70 Å (Ti-SBA-15).[146]

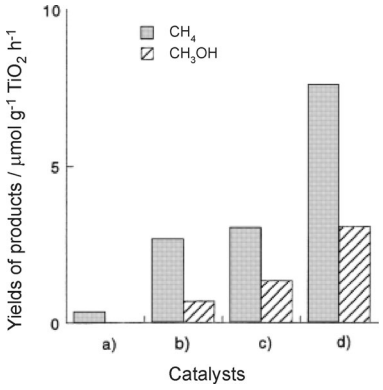

Figure 3. The formation rates of CH_4 and CH_3OH in the photocatalytic reduction of CO_2 with H_2O on a) TiO_2 powder, b) TS-1, c) Ti- MCM-41, and d) Ti-MCM-48 zeolite catalysts. Reproduced from Ref. [145] with permission.

Photoluminescence measurements of two types of Ti-β zeolites—Ti-β(OH) and Ti-β(F)—showed that the photoluminescence of the OH system was much stronger.[70a,147] While the addition of CO_2 led to a similar quenching in both zeolites, the addition of water had a much stronger effect on Ti-β(OH). This was attributed to its hydrophilic character and translated directly into its photocatalytic performance: the yield of methane and methanol was much larger for Ti-β(OH). A remarkable feature of fluorine-containing, hydrophobic, Ti-β(F), however, was a selectivity of 41% for methanol, which was unmatched by previously investigated zeolitic systems. These results were attributed to the low concentration of water molecules compared to CO_2 molecules, which underlines the importance of the adsorption affinity of H_2O on highly dispersed TiO_2 species incorporated in zeolite structures.

Analogous to photocatalysts of highly dispersed titanium species in zeolite structures, an amine-functionalized titanium metal–organic framework (NH_2-MIL-125(Ti)) was demonstrated to be able to photoreduce CO_2 to formate under irradiation with visible light, although at comparably low conversion rates.[148]

Thin, porous silica films containing titanium species increased the rate of CO_2 photoreduction twofold compared with the best zeolite powders.[69b,149] The highest quantum efficiency (0.3%) was obtained with the Ti-PS(50) catalyst, which has a hexagonally shaped pore structure. Interestingly, a thin-film photocatalyst with a cubic pore structure exhibited a high selectivity for methanol (nearly 60%). This was explained by this material having a less hydrophilic surface so that fewer water molecules were in the vicinity of the reaction sites, thus leading to preferential formation of methanol. Conversely, an anatase TiO_2 powder catalyst (JRC-TiO-4, 49 $m^2 g^{-1}$) with a large band gap and numerous surface OH^- groups deposited on the bottom of a quartz cell was shown to reduce CO_2 into methane most efficiently in the presence of water vapor. The selectivity could be tuned by loading the catalyst with Cu^+ ions, which increased the yield of methanol.[41a,150]

The effect of copper loading on methanol generation was also investigated in a custom-built reactor made of optical fibers coated with Cu-TiO_2. Methanol was the only reported reduction product from CO_2 and water vapor,[151] and its yield was better than with pure TiO_2. Such selectivity in the gas phase is possibly due to a preference of the hydrogen atoms adsorbed on copper to react with oxygen atoms of the co-adsorbed methoxy intermediate, thereby forming methanol. On the other hand, in the liquid phase, protons originate from the solution and react with the carbon atom of the methoxy group, thus producing methane.[46b]

The optimum copper loading was found to be 1.2 wt%; the lower formation rates at larger concentrations were argued to be caused by shading the TiO_2 and thus reduced light absorption. Copper(I) was identified to be the primary state of the copper, in agreement with earlier findings.[65b,152] Increased adsorption of hydroxyl radicals on the Cu surface was considered another factor that enhanced the reactivity of the system. A similar improvement in the yield of methanol was also achieved by loading with silver.[153] The addition of copper and iron to the TiO_2 fiber coating led to the photocatalytic formation of ethene and methane and trace amounts of ethane and methanol.[85] The yield of ethene was lower when either of the metals was added individually, compared to the application of both metals together. Additionally, in the latter case, the rate of ethene formation was stable over longer periods of time, whereas the systems loaded with a single metal dopant worked well for only a limited time. It was argued that the function of the iron was to improve the charge separation and the transfer of photogenerated holes from TiO_2 to H_2O via the valence band of iron oxide, to enhance the absorption of light, and to provide additional specific catalytic centers. At the same time, adding the iron apparently slowed down the rate of formation of methane. However, a mixture of TiO_2 and SiO_2 instead of pure TiO_2 as a photocatalytic substrate was more selective for methane than ethene.[154] A TiO_2 (0.5 wt% Cu, 0.5 wt% Fe) system sensitized with a ruthenium dye (N3) to extend the absorption range further improved the yield of methane under concentrated sunlight.[155]

Overall, the decoration of TiO_2 particles with copper and the use of highly dispersed TiO_2 species inside mesoporous silica structures have both proven to be successful strategies for improving the photocatalytic efficiency of the CO_2 reduction process. Therefore, the two approaches were combined in a one-pot sol–gel synthesis of a Cu/TiO_2-SiO_2 catalyst, which was then coated onto glass wool.[156] The optimal loading concentration of copper was found to be 0.5 wt% (Figure 4). In the course of the illumination of the photocatalyst, a color change from greenish white to dark gray was observed. This color change was associated with the reduction of Cu^I to Cu^0 by photogenerated electrons, which was accompanied by a decrease in the photocatalytic reactivity. The catalyst was regenerated upon exposure to air, whereby the gray color faded to white again, likely due to re-oxidation of Cu^0 to Cu^I.

Mesoporous Cu-TiO_2-SiO_2 composite particles were also synthesized by self-assembly, which allowed a more homogeneous phase to be obtained.[157] These particles supported on glass wool were demonstrated to photoreduce CO_2 to CO. The highest yields were obtained with 2 mol% TiO_2 and 0.01 mol% Cu. Hollow nanocubes of CuO-$TiO_{2-x}N_x$ were recently shown to improve the rate of formation of methane compared to pure TiO_2 P-25 particles.[158] The improved photocatalytic activity was linked to various properties of these hybrid structures. In particular, the heterojunction formed between CuO and TiO_2 was argued to allow rapid charge separation and improve catalytic performance, while the presence of nitrogen in the hybrid structure improved the absorption in the visible range (see Scheme 8b).

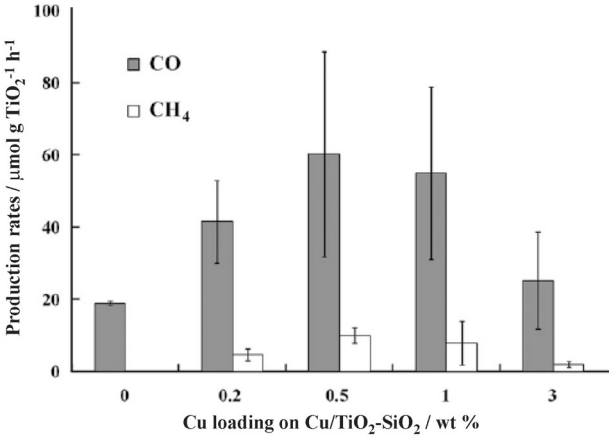

Figure 4. Influence of the copper loading concentration of a TiO_2–SiO_2 composite system on the formation rates of methane and carbon monoxide. Reproduced from Ref. [156] with permission.

Arrays of TiO_2 nanotubes (NTs) were investigated by Varghese et al. as a means for improving the generation of charge carriers and transport properties of the system.[11a,69a] They possess a large surface area, but their wall thickness is in the range of the diffusion lengths of charge carriers, thus allowing the charges to migrate to the surface where they participate in the catalytic reactions. The columnar shape of the NTs was assumed to additionally facilitate directed charge transfer. The absorption spectrum of these NTs was extended into the visible range by doping with nitrogen, while copper and platinum were sputtered onto the surfaces to provide catalytic centers. The products reported to have formed photocatalytically under natural sunlight included CO, H_2, olefins, branched paraffins, and methane. Experiments with NTs of different lengths showed that the performance of the structure increased up to a length of 25 μm, remained uncorrelated between 25 and 70 μm, and decreased for longer NTs. The latter observation was ascribed to an inhomogeneous distribution of the metal NPs. The catalytic effects of the NPs were not the same: while platinum facilitated the formation of H_2, Cu increased the formation of CO fivefold. The synergistic surface loading with Cu (52%) and Pt (48%) by sputtering resulted in an increase in the amount of produced hydrocarbons compared to individual loading. Moreover, the uniform deposition of copper NPs by a wet chemistry route led to a further increase in the hydrocarbon yield. A similar increase was observed for

uniformly distributed platinum NPs by a microwave-assisted solvothermal method.[159]

Anatase TiO_2 nanorods with dominant reactive {010} facets and decorated with 1 wt% Pt were used to photocatalytically convert CO_2 into methane at a higher rate than P-25 NPs decorated with the same amount of Pt.[160] This emphasized the role of the shape of the catalyst, as P-25 is generally considered to be a more photocatalytically active material than pure anatase.[95a] Nanostructured platinized TiO_2 films (Pt-TiO_2) were shown to be highly efficient at photoconverting CO_2 into methane.[161] The maximum rate was 1361 $\mu mol\, g^{-1} h^{-1}$, with a corresponding quantum efficiency of 2.41%.

Dye sensitization was also used for photoreduction at a solid–gas interface. To this end, TiO_2 films prepared by dip-coating glass beads were functionalized with ruthenium and perylene dyes.[162] The major product of the CO_2 photoreduction was methane; traces of CO and H_2 were also detected. These were observed through illumination with visible light only when the sensitizer was used. Importantly, an improvement in the methane yield was only found for films decorated with platinum NPs, not for impregnated ones. In fact, platinum NPs immersed in TiO_2 might be detrimental to the efficiency of the photocatalysis because of their function as electron traps.[163]

In a similar approach to utilize visible light, a TiO_2-based composite was sensitized with quantum dots (QDs), which led to an alignment of the energy band for a fast injection of electrons into TiO_2 and better charge separation.[164] The quantum dots of 2.5 nm CdSe[78] and 3–5 nm PbS[165] QDs were used in conjunction with metal co-catalyst NPs, such as Cu or Pt. The CdSe/Pt/TiO_2 composite yielded mostly methane and small amounts of methanol, CO, and H_2; however, no products were observed under illumination with visible light without the CdSe QDs. PbS/Cu/TiO_2 composites produced CO, methane, ethane, and H_2. A fivefold increase in the yield of products was noted when 4 nm PbS QDs were used under illumination with white light, compared with the Cu/TiO_2 composite alone. After prolonged illumination, the PbS QDs deactivated through photooxidation, as is typical for sulfides (see Section 4.3.1).

In another study, the sensitization of TiO_2 nanotubes with Bi_2S_3, a semiconductor with a narrow band gap (E_g = 1.28 eV), increased the rate of formation of methanol by a factor of 2.2 to 43.6 $\mu mol\, g^{-1} h^{-1}$.[166] Sensitization with rhodium was also demonstrated to have a positive effect on the photocatalytic reduction of CO_2 on TiO_2. In the liquid phase, Rh/TiO_2 increased the yield of methanol, formaldehyde, and formic acid from a CO_2-saturated aqueous suspension.[167] In the gas phase, functionalization of the TiO_2 with rhodium improved the rate of formation of CO from CO_2 and hydrogen.[168] The reduction of rhodium to a metallic state was accompanied by a decrease in activity and a shift in the product selectivity from CO to methane.

The CO_2 photoreduction was also investigated on plasmonic gold NPs deposited on anatase films.[169] Their illumination with a monochromatic light in the visible region of the spectrum (532 nm) afforded methane with a rate 24 times higher than that of bare TiO_2. This effect was attributed to the excitation of the plasmon resonance of the NPs leading to an enhancement of the local electromagnetic field, which in turn generates electron–hole pairs in the adjacent TiO_2 at a much larger rate than the incident light.[126b] In contrast, plasmon excitations on Au NPs were demonstrated to directly transfer electrons to the TiO_2 conduction band only at an excitation wavelength of 254 nm, which matches the excitation energy of d-band electrons in gold. These electrons can transfer to the lower-lying conduction band states of TiO_2. At this excitation wavelength, additional photocatalytic products were detected including methanol, ethane, and formaldehyde. Methane was the main product for the TiO_2 catalyst loaded with Ag/Au bimetallic NPs prepared by a microemulsion method.[170]

Charge recombination is often one of the limiting factors of the photocatalytic performance of TiO_2 materials. Multiwalled carbon nanotubes (MWCNTs), used as a support for TiO_2 NPs, provide a means to effectively separate the charges and reduce their recombination,[171] in a similar manner to TiO_2–graphene composites described in Section 4.2.1. However, most applications operate in an oxidative environment, for example, in the photocatalytic degradation of dyes,[172] wherein the hole stays on the TiO_2 and participates in the oxidation reaction while the electron is transported away. Nevertheless, MWCNT–TiO_2 composites have been shown to increase the efficiency of the CO_2 reduction to ethanol, methane, and formic acid.[173] Low concentrations of MWCNTs gave the best results; it was argued that higher concentrations resulted in a shading effect of the NTs, thereby limiting the absorption of light by TiO_2. It was also shown that the activity of the composite structures in repeated cycles was much higher than of pure TiO_2 structures.

4.3. Reduction of CO_2 on Other Semiconductors

Despite the great advances made in the photocatalytic reduction of CO_2 with TiO_2 and derivative materials, the efficiency of the process remains low. To a large extent this can be ascribed to its band structure, which is acceptable, but certainly not optimal for the reduction of CO_2 driven by solar energy.[82a] Firstly, the potential of its conduction band electrons is only slightly more negative than the multielectron reduction potentials of CO_2, thus providing very small overpotentials, whereas the potential of the valence band holes is much more positive than the water oxidation potential, which is thermodynamically not necessary. Secondly, the wide band gap (3.2 eV) limits the absorption of light to the UV range. The two most common methods for extending the absorption range to visible light—sensitization or doping—do not fully address the problem. Sensitizing agents (dyes or QDs) often degrade when exposed to UV light and photogenerated oxidizing holes in TiO_2. Dopant atoms, on the other hand, can become centers of charge recombination. Moreover, the additional energy states associated with foreign atoms are highly localized, in effect suppressing charge mobility.[89] Therefore, while TiO_2 remains a benchmark photocatalyst, there is a lot of interest in alternative semiconductors, such as transition or main group metal oxides, chalcogenides, nitrides, and phosphides, for the

photoreduction of CO_2. This very diverse group of materials contains both narrow and wide band gap semiconductors, yet many of them offer a more favorable band structure than TiO_2. It is noteworthy that many recent developments on relevant semiconductors originated from research on the photocatalytic splitting of water, as both processes share similar constraints on the energy bands.[19,174] Specifically, the quest for new semiconductor materials is focused on the following points:

1) raising the valence band energy to decrease the band gap;
2) moving the conduction band to more reductive potentials;
3) improving the quantum efficiency of exciton formation and reducing charge recombination; and
4) using novel nanoscale morphologies to provide a large surface area with multiple photocatalytically active sites.[89]

Examples of the non-TiO_2 photocatalytic systems are collected in Table 2 and described in detail in the following sections on sulfide, oxide, and phosphide semiconductors.

4.3.1. *Sulfides*

From a historical perspective, sulfide semiconductors initially received a lot of attention. Their valence band, made of 3p orbitals of the sulfur atoms, is shifted upwards compared with those of the oxide analogues, while the conduction band electrons are also more reductive.[174b] Many sulfides have a narrow band gap (e.g. PbS, Bi_2S_3), with the onset of absorption in the visible or even infrared region. They have hence been used as photosensitizers for TiO_2, as described in Section 4.2.2.[165,166] CdSe was also recently used as a photosensitizer for ZnO nanorods.[87c] The major disadvantage is that sulfides are generally not stable under illumination in an aqueous dispersion because of the oxidation of lattice S^{2-} ions to elemental sulfur and eventually to sulfates.[175] To prevent the photocorrosion, additional reducing agents such as sulfite (SO_3^{2-}), thiosulfate ($S_2O_3^{2-}$), or hypophosphite ($H_2PO_2^-$) anions, tertiary amines (e.g. triethylamine, TEA), or alcohols (e.g. propan-2-ol) were used to scavenge the photogenerated holes. ZnS and CdS were the most studied sulfides for CO_2 reduction. The former is a direct wide band gap semiconductor ($E_g = 3.66$ eV in the bulk), hence it absorbs only in the UV range, but it possesses a strongly reducing conduction band ($E_{CB} = -1.85$ V versus the NHE at pH 7).[176] In several reports, ZnS has been shown to preferentially reduce CO_2 to formates with high quantum yields.[59,177] Henglein et al.[177a] and Yoneyama[178] speculated that smaller ZnS NPs are more efficient due to their larger band gap, higher surface area, and greater affinity for CO_2. Loading of 3.9 nm ZnS NPs with 0.035 mol% Cd^{2+} in an aqueous dispersion at pH 5.5 in the presence of propan-2-ol increased the quantum yield at 280 nm twofold to 32.5%.[177c] A further increase in the cadmium content resulted in the formation of CO. Kanemoto et al. obtained a cumulative quantum yield of 72% with irradiation at 313 nm (75.1 μmol h^{-1} HCOOH, 86 μmol h^{-1} H_2, and 1.7 μmol h^{-1} CO) at pH 7 in the presence of NaH_2PO_2 and Na_2S.[177b] Sulfide anions are protonated to HS^- at pH 7. The role of hydrogen sulfide anions was to eliminate surface sulfur vacancies, which trap CB electrons, rather than to be sacrificial electron donors. They reportedly also shift the conduction band edge of sulfide semiconductors to more negative potentials, because of modified surface charging by the absorbed anions.[179]

Fujiwara observed the selective production of formate by ZnS NPs with a diameter of 2 nm in DMF when zinc acetate was used as a precursor of the nanocrystals; however, a mixture of HCOOH and CO was obtained with a zinc perchlorate precursor.[59] This was explained by the strong interaction of acetate anions with Zn cations, which inhibits the formation of sulfur vacancies that act as catalytic sites for the formation of CO. On the other hand, perchlorate interacts weakly with Zn^{2+} species, which remain coordinated by the solvent. Excess amounts of $Zn(OAc)_2$ additionally enhanced the rate of formation of HCOOH. ZnS NPs were also loaded on a silica matrix with a large surface area (340 $m^2 g^{-1}$) to improve the stability of the semiconductor and adsorption of CO_2.[180] The best results were obtained for silica loaded with 13% ZnS (7 mmol $g^{-1} h^{-1}$ HCOOH). Interestingly, the addition of a platinum co-catalyst resulted in further reduction steps to yield HCHO and methanol at the expense of formate.

As a consequence of the narrow band gap of 2.4 eV, the onset of absorption with CdS is at 520 nm,[164] although its conduction band electrons are less reductive ($E_{CB} = -0.9$ V at pH 7 versus the NHE)[175] than those in ZnS. Accordingly, 3–5 nm diameter CdS NPs were shown to reduce CO_2 to CO in DMF in the presence of TEA and small amounts of water (1%) under irradiation with visible light ($\lambda > 400$ nm).[181] A quantum yield of 9.8% was reported at 405 nm (8.37 μmol h^{-1} of CO). The selective formation of CO originated from the bidentate adsorption of a CO_2 molecule at Cd atoms near a sulfur vacancy and the subsequent transfer of one electron to form a bound anion radical $CO_2^{\bullet-}$. This adsorbate reacted with a second CO_2 molecule and following another electron transfer produced CO through an elimination reaction, thereby leaving a carbonate anion behind.[59] The cation–dipole interaction of the lattice Cd^{2+} with DMF led to a cationic surface by preventing the adsorption of H^+, consequently generating H_2 or formate. However, the use of solvents with a higher dielectric constant than DMF (propan-2-ol, CH_3CN, etc.) increased the ratio of formate to CO. Only formate was produced in water, because in polar solvents the radical anion is weakly bound to the surface and a proton can interact with its C atom.[62b] Tetramethylammonium cations form an aprotic layer at the surface, and therefore, in the absence of H^+, the dimerization of $CO_2^{\bullet-}$ radicals to oxalate anions was observed.[182] Further reduction products of oxalic acid, such as glyoxylic acid and glycolic acid, were also observed, thus drawing analogies to natural photosynthetic processes. A similar dimerization process was observed by Kisch and Lutz for CdS particles embedded in a silica matrix, which yielded formate, HCHO, and oxalate as products.[183] The reaction of the radicals was assumed to proceed in solution or on silica rather than on the CdS surface. CdS NPs were also anchored to a phyllosilicate clay mineral (montmorillonite) to protect the material against photooxidation in an aqueous dispersion.[184] In this setup, hydrogen, methane,

Table 2: Non-TiO_2 semiconductor-based systems for CO_2 reduction.

Semiconductor	Structure	E_g[a]	Co-catalyst	Major product	R_{max}[b]	PE[c]	Other products	Ref.
ZnS	nanoparticles	3.66	Cd^{2+}	HCOOH	10.5[d]	32.5% (280 nm)	H_2	[177c]
ZnS	nanoparticles	3.66	–	HCOOH	75.1[d]	72% (313 nm)	H_2, CO	[177b]
ZnS	nanoparticles	3.66	Zn^{2+}	HCOOH	15.4[d]	–	–	[59]
ZnS	nanoparticles in silica	3.66	–	HCOOH	7000	–	–	[180]
CdS	nanoparticles	2.4	–	CO	8.37[d]	9.8% (400 nm)	H_2	[181a]
CdS	nanoparticles	2.4	Cd^{2+}	CO	3.0[d]	–	–	[59]
CdS	nanoparticles	2.4	–	CO	0.13[d]	–	H_2,HCOOH	[62b]
CdS	nanoparticles	2.4	TMA^+[k]	oxalate	58.3[d]		glyoxylate	[182b]
CdS	nanoparticles in silica	2.4	–	HCOOH	81.5	–	HCHO,oxalic acid	[183]
CdS	nanoparticles in MMT[k]	2.63	–	CH_4	1.0	–	H_2, CO	[184]
MnS	particles	3.0	–*	HCOOH	–	4.5% (UV)	CO	[185]
Bi_2S_3/CdS	particles	1.28	–	CH_3OH	88	–	–	[186]
$Cu_xAg_yIn_zZn_kS_m$	nanoparticles	1.4	RuO_2	CH_3OH	34.3	–	–	[187]
Cu_2ZnSnS_4	photocathode	1.5	Ru complex	HCOOH	> 5[e]	-	-	[188]
WO_3	monoclinic crystals	2.79	–	CH_4	0.34	–	–	[194]
$W_{18}O_{49}$	nanowires	2.7	–	CH_4	666[f]	–	–	[195]
ZrO_2	particles	5.0	1 wt% Cu	CO	2.5[d]	–	H_2	[196]
$SrTiO_3$	particles	3.2	Pt	CH_4	–	0.01%	–	[197]
$BaTiO_3$	particles	3.2	–	HCOOH, HCHO	–	0.0021%	–	[182b, 198]
$K_2Ti_6O_{13}$	particles	> 3.0	0.3 wt% Pt	CH_4	0.2	–*	H_2,HCOOH, HCHO	[199]
$BaLa_4Ti_4O_{15}$	plate-shaped particles	3.8	Ag	CO	22[d]	–	H_2,HCOOH	[200]
$KNbO_3$	SSR particles[g]	3.1	Pt	CH_4	70[f]	–	–	[202]
$NaNbO_3$	cubic crystal nanoparticles	3.29	0.5 wt% Pt	CH_4	4.86	–	–	[203]
$NaNbO_3$	nanowires	3.4	Pt	CH_4	653[f]	–	–	[204]
HNb_3O_8	nanobelts	3.66	–	CH_4	3.58	–	–	[211]
$LiNbO_3$	particles	3.6	–	HCOOH	7700[d]	2.0%[h]	HCHO	[213]
N-Ta_2O_5	nanoparticles	2.4	Ru-dcbpy[k]	HCOOH	70	1.9% (405 nm)	H_2, CO	[58b]
N-Ta_2O_5	nanoparticles	2.4	Ru-dpbpy[k]	HCOOH	60[e]	–	CO	[215]
$BiVO_4$	monoclinic crystals	2.24	–	C_2H_5OH	406.6[d]		CH_3OH	[221]
Bi_2WO_6	nanoplates	2.75	–	CH_4	1.1	–	–	[222]
$InTaO_4$	SSR particles[g]	2.6	1 wt% NiO	CH_3OH	1.39	2.45%[i]	–	[230]
$InTaO_4$	particles	2.6	1 wt% NiO	CH_3OH	11.1	0.063%	–	[231]
N-$InTaO_4$	SSR particles[g]	2.28	3.2 wt% Ni@NiO	CH_3OH	165	–	–	[232]
$InNbO_4$	SSR particles[g]	2.5	1 wt% NiO	CH_3OH	1.58	–	–	[233]
Zn_2GeO_4	mesoporous	4.5	1 wt% Pt	CH_4	28.9[f]	0.2% (251 nm)		[237]
Zn_2GeO_4	nanobelts	4.5	Pt,RuO_2	CH_4	25	–	–	[239]
Zn_2GeO_4	nanorods	4.65	3 wt% RuO_2	CO	17.9[j]	–	CH_4	[240]
$Zn_xGe_yO_zN_k$	mesoporous	2.70	Pt	CH_4	2.7[f]	–	CO	[243]
$Zn_{1.7}GeN_{1.8}O$	sheaflike	2.6	Pt,RuO_2	CH_4	11.5	0.024% (420 nm)	–	[241]
$In_2Ge_2O_7$(En)	nanowires	3.98	Pt	CO	0.9	–	–	[244]
Zn_2SnO_4	nanoplates	3.87	Pt,RuO_2	CH_4	86.7[f]	–	–	[245]
β-Ga_2O_3	mesoporous	4.9	–	CO	1.46	3.9%	CH_4	[249]
$ZnGa_2O_4$	mesoporous	4.4	1 wt% RuO_2	CH_4	50.4[j]	–	–	[250]
$CuGaO_2$	SSR particles[g]	2.6	–	CO	9[f]	–	–	[254]
p-GaP	photocathode	2.3	pyridine	CH_3OH	–	2.6% (465 nm)	–	[17b]
p-InP	photocathode	1.35	Ru complex	HCOOH	140[d]	–	–	[17c]
p-InP	photocathode	1.35	Ru complex	HCOOH	–	0.04%[h]	–	[255]

[a] Where available, the band gap width refers to specific structure instead of bulk, expressed in eV. [b] Maximum formation rate reported for the major product(s), in $\mu mol\,g^{-1}\,h^{-1}$, unless stated otherwise. [c] Photonic efficiency, unless stated otherwise. [d] In $\mu mol\,h^{-1}$. [e] Turnover number. [f] In $ppm\,g^{-1}\,h^{-1}$. [g] Sintered particles prepared by solid-state reaction. [h] Power conversion efficiency. [i] (Internal) Quantum efficiency. [j] In $ppm\,h^{-1}$. [k] dcbpy = 4,4'-dicarboxy-2,2'-bipyridine, dpbpy = 4,4'-diphosphonate-2,2'-bipyridine , MMT = montmorillonite, TMA^+ = tetramethylammonium cation.

and CO were reported with an overall efficiency 4–8 times larger than the analogous system containing P-25 particles. Methane was considered to be a product of the hydrogenation of CO_2 by the evolving H_2, instead of the direct photoreduction of CO_2.

Other sulfides were used less often. Manganese sulfide ($E_g = 3.0$ eV) reduced bicarbonate dissolved in water (pH 7.5) to formate with a photonic efficiency of 4.2% under UV irradiation, although the semiconductor was degraded by oxidation of S^{2-} to sulfate.[185] Bi_2S_3, with a narrow band gap of 1.28 eV, absorbs in the visible range and has been shown to reduce CO_2 to methanol, especially when used in conjunction with CdS particles.[186] The highest formation rate, about 88 $\mu mol\,g^{-1}\,h^{-1}$, was obtained for 15 wt% Bi_2S_3, and was two

to three times higher than for either semiconductor alone. Methanol was also obtained with the complex sulfide $Cu_xAg_yIn_zZn_kS_m$ in the presence of sodium nitrite.[187] This sulfide is a solid solution of wide band gap ZnS with narrow band gap Cu_2S and $AgInS_2$, and has an intermediate band gap of about 1.4 eV, depending on the proportions. The highest formation rate, 34.3 μmol g^{-1} h^{-1}, was observed for $Cu_{0.12}Ag_{0.30}In_{0.38}Zn_{1.22}S_2$. Recently Arai et al. employed Cu_2ZnSnS_4, a quaternary sulfide with a narrow band gap ($E_g = 1.5$ eV) and reductive conduction band ($E_{CB} = -1.3$ V), to photoelectrochemically reduce CO_2 to formate in the presence of a metal complex electrocatalyst.[188] This semiconductor operated effectively under illumination with visible light, and its p-type character facilitated electron transfer to the catalyst, where CO_2 reduction proceeded preferentially to proton reduction. Nevertheless, it required an external bias of −0.4 V—in place of a hole scavenger—to prevent photooxidation.

4.3.2. Oxides

In contrast to sulfides, many oxides do not suffer from photooxidation under irradiation and can be used in photocatalyzed reduction and oxidation reactions. Indeed, two groups of metal oxides with closed-shell electronic configurations of the metal have been at the center of interest in regard to the photocatalytic reduction of CO_2. The first group contains octahedrally coordinated d^0 transition metal ions—Ti^{4+}, Zr^{4+}, Nb^{5+}, Ta^{5+}, V^{5+}, and W^{6+}—which have an empty d orbital. TiO_2 is the most prominent member of the group, which includes binary oxides (e.g. ZrO_2, Nb_2O_5, Ta_2O_5) and a number of more complex oxides referred to as titanates, niobates, tantalates, etc.[23,189] These often occur in a perovskite, AMO_3 (e.g. $SrTiO_3$, $NaNbO_3$), or in perovskite-related structures. The second group contains main group metal oxides in a d^{10} configuration (i.e. with a fully occupied d orbital) with a general formula M_yO_z or $A_xM_yO_z$, where M stands for Ga, Ge, In, Sn, or Sb, while A is an electropositive cation such as an alkali, alkaline earth, or rare earth metal ion.[174b,190] Many of these photocatalytically active binary and ternary oxides initially found application in the photocatalytic splitting of water, but have very recently started to also be employed for the photoreduction of CO_2.

The top of the valence band in binary d^0 and d^{10} metal oxides is primarily made of oxygen 2p orbitals. This means that a photogenerated hole in the VB has a strongly oxidizing character, which is thermodynamically capable of oxidizing water. Scaife[191] noted that their approximate potential is 2.94 V versus the NHE, while Matsumoto[192] suggested that it can be estimated as 1.23 V + E_g/2. In any case, a wide band gap is needed for the conduction band to be sufficiently reductive. The theoretical limit for the reduction of CO_2 is −0.24 V versus the NHE at pH 7 [see Eq. (6)], but in practice some overpotential is necessary and the band gap has to be larger than 3.0 eV. The conduction band of d^0 oxides has a strong d-orbital character, which originates from the antibonding interaction between transition metal t_{2g} (i.e. *d*) orbitals and oxygen.[95a,189] In simplified terms, the excitation of the electron from the VB to CB can be seen as charge transfer from the oxygen atom to the metal, for example, leading to the excited state $(Ti^{3+}\text{-}O^-)^*$, postulated for TiO_2.[71] In these oxides, the minimum of the CB and hence the band gap increases as the effective electronegativity of the transition-metal ion decreases, which can be ordered as $W^{6+} > Nb^{5+} \approx Ti^{4+} > Ta^{5+} > Zr^{4+}$.[189] Accordingly, WO_3 has the smallest band gap of 2.7 eV, and with the edge of its conduction band located at 0.0 V versus the NHE at pH 7, it cannot reduce CO_2.[27,193] However, a rectangular sheetlike monoclinic crystal of WO_3 with dominant {002} facets has been shown recently to possess a slightly larger band gap (2.79 eV) and a conduction band elevated by 0.3 V.[194] This was sufficient to enable formation of small amounts of CH_4 from CO_2 (0.34 μmol g^{-1} h^{-1}; see Table 2). Competition from proton reduction was negligible because the E_{CB} potential was still too positive for this reaction to proceed ($E_{NHE}(H^+/H_2) = -0.41$ V at pH 7). In another recent development, 0.9 nm thin and several micrometer long $W_{18}O_{49}$ nanowires were able to reduce CO_2 under illumination with visible light.[195] This was attributed to the presence of numerous oxygen vacancies or defects in the monoclinic structure of the nanowires providing reduction sites and improving the adsorption of CO_2. The photocatalytic activity was suppressed after exposure to H_2O_2, presumably by filling the vacancies. This was accompanied by a change in the color of the catalyst from deep blue to the standard yellow of WO_3.

Other oxides in the series have wider band gaps, up to 5.0 eV for ZrO_2. With its CB minimum at a strongly negative potential ($E_{CB} = -1.4$ V versus the NHE at pH 7), ZrO_2 is capable of reducing CO_2 to CO in an aqueous dispersion without a co-catalyst or a sacrificial electron donor, although the rate of concurrent water reduction was 100 times higher.[196] At the same time, the width of its band gap severely restricts the absorption of light.

Despite its weakly reductive CB, TiO_2 is the binary oxide used most extensively for CO_2 reduction (see Section 4.2). Similar results as for TiO_2 were obtained with alkaline earth metal titanates, which have band gaps of comparable energy (ca. 3.2 eV). $SrTiO_3$ was shown to photoreduce CO_2 to methane in the presence of Pt,[197] while the use of $BaTiO_3$ for the reduction of CO_2 resulted in the formation of formate and HCHO.[182b,198] The rates of the reactions were low; for example in the latter case, the photonic efficiency was 0.0021 % for illumination at 320 nm < λ < 580 nm. Interestingly, a different barium titanate, $BaTi_4O_9$, with an orthorhombic crystal structure was considered to be more photoactive because of distortions in the TiO_6 octahedral structure (Ti^{4+} ions displaced from the center of gravity of six oxygen ions). This local anisotropy is responsible for the generation of a dipole moment, which is thought to promote charge separation through an internal polarization field, a typical effect in ferroelectric materials.[190] $BaTi_4O_9$ was, however, not tested for the reduction of CO_2 but only for the splitting of water. Potassium hexatitanate, $K_2Ti_6O_{13}$, loaded with Pt was also able to reduce CO_2 to CH_4, HCOOH, and HCHO, but their combined rate of formation was still 240 times lower than that of H_2.[199] These results underline the importance of choosing an appropriate co-catalyst. For example, silver is a known electrocatalyst for the reduction of CO_2 to CO. With

this background, Iizuka et al. have recently produced CO almost selectively by using a wide band gap (3.8 eV) quaternary titanate, $BaLa_4Ti_4O_{15}$, decorated with 10 nm Ag NPs formed by the reduction of Ag^+ in solution with hypophosphite.[200] Apart from traces of HCOOH, hydrogen was generated at a lower rate than CO, while O_2 was formed at a stoichiometrically matching rate. In this way, no hole scavenger was necessary because the water functioned as an electron donor. It was claimed that the crystal structure of the material facilitated the separation of the reduction and oxidation sites, thereby preventing reoxidation of the products. The reduction sites were located at the edges of the layers of the perovskite structure, while the oxidation proceeded at the basal plane.

Niobates with a perovskite structure share many characteristics (nontoxicity, stability, indirect wide band gap) with titanates, although their conduction band is slightly more reductive. For example, the minimum of the CB of $NaNbO_3$ is located at −0.71 V versus the NHE at pH 7.[201] $NaNbO_3$ and $KNbO_3$ decorated with platinum NPs by photodeposition were both shown to reduce CO_2 to CH_4 without sacrificial electron donors.[202] Potassium niobate performed about 2.5 times better, which was attributed to a smaller band gap (3.1 eV for $KNbO_3$ versus 3.4 eV for $NaNbO_3$) and higher mobilities of the charge carriers, which were deduced from DFT calculations of the energy bands. Similar arguments of a more dispersive conduction band were used to explain the two-times higher rate of formation of CH_4 with the cubic crystal structure of $NaNbO_3$ compared to the more common orthorhombic one (4.86 versus 2.45 $\mu mol\,g^{-1}\,h^{-1}$).[203] It was also demonstrated that $NaNbO_3$ nanowires with a diameter of about 100 nm and a length of about 50 μm produced methane at a significantly higher rate than micrometer-sized particles.[204] The nanostructured material possessed a much larger surface area and its crystal lattice had fewer defects. Moreover, the high aspect ratio provided short pathways for electron and hole transport. These results conform with a trend that the photocatalytic activity of nanostructured niobates is at least tenfold higher that of their bulk counterparts.[205]

Lamellar perovskite niobates and tantalates hold great promise as active photocatalysts.[206] They are composed of thin (ca. 1 nm) sheets of edge- and/or corner-shared NbO_6 or TaO_6 octahedra, with the other cation intercalated between the layers.[23] The structure is favorable for the separation and transfer of photoexcited charges, deposition of co-catalysts, and selective intercalation of reactants.[207] In this context, layered calcium niobate $HCa_2Nb_3O_{10}$[208] or strontium niobate $Sr_2Nb_2O_7$ and tantalate $Sr_2Ta_2O_7$[209] or niobic acid HNb_3O_8[210] have proven effective for the generation of H_2. The acid in the form of 50 nm thick, 300–500 nm wide, and 5 μm long nanobelts prepared by a hydrothermal method was also employed successfully to selectively photoreduce CO_2 to CH_4.[211] The rate of formation with the acid was twice as high as that with KNb_3O_8 because of its hydrophilic nature and Brønsted acidity. It was speculated that, because of the high concentration of CO_2 at the reaction sites, the photogenerated $H^{\cdot}$ radicals were trapped by CO_2 molecules instead of combining to form H_2. Moreover, the nanobelts led to a 20 times higher yield than the same compounds prepared by a solid-state reaction and an about 10 times higher yield than P-25 particles.

A sustained dipole in ferroelectric materials causes significant band bending at the interfaces and thus effectively separates the photoinduced charges.[212] This means that the reduction and oxidation sites can be spatially separated, which slows down back reactions. Ferroelectric $LiNbO_3$, with a remnant polarization of 65 $\mu C\,cm^{-2}$ and a low electron affinity (i.e. highly reducing), photoreduced CO_2 to formic acid and HCHO with a power conversion efficiency of 2%, which is 11 times more efficiently than P-25 particles.[213] In addition, the ferroelectric surfaces might facilitate CO_2 adsorption which would lower its reduction potential.

Nitrogen doping is a typical example of band gap engineering designed to improve the absorption of light in the visible range (see Scheme 8b). This approach relies on additional intraband states originating from nitrogen 2p orbitals which have higher energies than oxygen 2p orbitals and, therefore, lie above the valence band of the oxides. Its application to TiO_2 was discussed in Section 4.2.2.[11a,69a] In the case of niobic acid, nitrogen doping reduced the band gap by 0.8 eV and red-shifted the onset of absorption by 80 nm (Scheme 12). Importantly, the lamellar structure of the acid

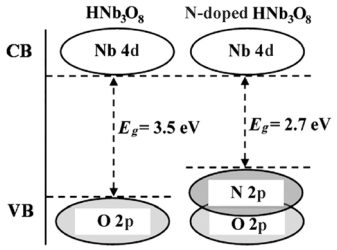

Scheme 12. Schematic band structures of HNb_3O_8 and N-doped HNb_3O_8. Reproduced from Ref. [89] with permission.

was preserved in the doping process, and hence the resulting material remained highly photocatalytically active.[210] Tantalum pentoxide Ta_2O_5 has a wide band gap of 4.0 eV, but following treatment with gaseous NH_3 the gap shrank to only 2.4–2.5 eV, thus resulting in a shift of the adsorption edge from 320 to 500 nm.[214] It lost its n-type character in the process through elimination of the oxygen vacancies and became a p-type semiconductor. This is a favorable feature for the injection of a photoexcited electron into a co-catalyst. Sato et al. employed N-Ta_2O_5 anchored with a ruthenium-based electrocatalyst $[Ru(dcbpy)_2(CO)_2]^{2+}$ to reduce CO_2 to formic acid and CO under irradiation with visible light.[58b] The quantum yield at 405 nm was estimated to be 1.9% and 1.0% at 435 nm. The maximum of the valence band was shifted upwards in N-Ta_2O_5 to about 1.1 V, and the photocatalyst was hence unable to use water as an electron donor (i.e. oxidize it). TEOA fulfilled the role of a hole scavenger and—partially—of a proton source. Chemisorption of the metal complex through phosphonic groups rather than carboxylic groups was found to increase the efficiency almost fivefold because of stronger electronic coupling

between the semiconductor and the electrocatalyst.[215] The band gap can be narrowed by further replacement of oxygen with nitrogen atoms.[174b] Oxy(nitride) TaON has a band gap of 2.4 eV, while that of the nitride Ta_2N_3 is even smaller at 2.1 eV. The position of the conduction band, composed in each case of Ta 5d orbitals, was not affected, thus offering a way to improve the absorption of light without lowering the reduction potential.

The disadvantages of doping through an increased recombination rate and decreased charge mobility can be suppressed by the formation of multi-metal oxides. The introduction of cations, such as Ag^+, Pb^{2+}, and Bi^{3+}, with fully occupied low energy d or s orbitals into the VB, contributes to the up-shift of the band. In the case of $AgTaO_3$ and $AgNbO_3$, the new valence band formed by hybridization of oxygen 2p and silver 4d orbitals effectively decreases the band gap by 0.6 eV (Scheme 13) without noticeable changes to the perovskite structure.[216] As a consequence of the higher VB, $AgNbO_3$ becomes active in the visible range (> 420 nm) and results in the generation of H_2. The recent findings regarding $CuNbO_3$ are even more promising.[217] This p-type semiconductor has a narrow band of 1.95 eV originating from the Cu 3d character of the valence band and a conduction band minimum appropriate for CO_2 reduction. Furthermore, its electronic structure permits nearly direct band gap transitions because of Cu to Nb d-d excitations, thereby facilitating the harvesting of light.[218] In related copper(I) tantalates, $Cu_5Ta_{11}O_{30}$ and $Cu_3Ta_7O_{19}$, which have band gap widths of 2.59 eV and 2.47 eV, respectively, the conduction band, composed of Ta 5d orbitals, is even more reductive at −1.53 V and −1.28 V.[219] The crystal structures of these oxides consist of pentagonal TaO_7 bipyramids instead of TaO_6 octahedra. Such a structure exhibits a stronger delocalization of the conduction band states within layers of the bipyramids, which results in a higher electron mobility. It appears that the copper(I) compounds are very good candidates for the photocatalytic reduction of CO_2 and have been discussed in such a context, but this expectation is yet to be verified experimentally.[217]

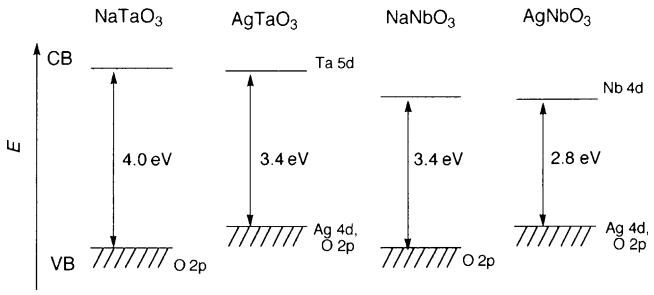

Scheme 13. Comparison of the band structures of $NaTaO_3$, $AgTaO_3$, $NaNbO_3$, and $AgNbO_3$. Reproduced from Ref. [216] with permission.

Such verification has already been performed for several d^0 metal oxides containing Bi^{3+} ions, where the valence band is shifted upwards by hybridization of occupied oxygen 2p and bismuth 6s orbitals.[220] For example, bismuth vanadate $BiVO_4$ with a monoclinic scheelite structure has a band gap of only 2.24 eV and was shown to selectively photoreduce CO_2 to ethanol, although under weaker illumination some methanol was also formed.[221] It was argued that the dimerization of intermediate C_1 species occurred as a result of their high concentration at the surface and the intensity of the irradiation producing a large number of photogenerated electrons. The rate of formation of ethanol obtained with monoclinic $BiVO_4$ was even 17 times higher than with tetragonal $BiVO_4$, possibly because of the easier adsorption of CO_2 on the former and the larger (2.56 eV) band gap of the latter. More recently, square nanoplates of Bi_2WO_6 with a thickness of about 10 nm prepared by a hydrothermal route were demonstrated to photocatalytically reduce CO_2 to methane when illuminated with visible light.[222] Their band gap of 2.75 eV was a little larger than that in the bulk material (2.69 eV),[223] but the size and shape allowed for quick electron transfers to the surface and for provision of a highly active surface with a {001} facet for CO_2 adsorption and subsequent dissociation.

The photocatalytic splitting of water by indium tantalum oxide doped with nickel, $In_{1-x}Ni_xTaO_4$ ($x = 0$–0.2), under irradiation with visible light was reported by Zou et al., and generated much interest in this group of semiconductors.[224] It was the first observation of the concurrent photocatalytic generation of both H_2 and O_2 without an applied bias and a UV light source; however, the measured optical band gaps for $InTaO_4$ ($E_g = 2.6$ eV) and $InNbO_4$ ($E_g = 2.5$ eV) caused some controversy.[225] Both ternary oxides have a wolframite structure which contains corner-shared InO_6 and TaO_6 (NbO_6) octahedra arranged in a zigzag pattern. DFT calculations have shown that both systems have wide band gaps (3.70–3.96 eV for $InTaO_4$[226] and 3.43 eV for $InNbO_4$)[90] with an indirect transition between the VB dominated by the oxygen 2p orbital and the CB dominated by the Ta 5d (Nb 4d) orbital. Clearly, the calculated band gaps were significantly larger than the experimental ones. The actual discrepancy was even larger because DFT methods tend to underestimate rather than overestimate the E_g value. Various hypotheses have been put forward to account for the activity of these oxides in visible light: 1) oxygen vacancies that create interband (gap) impurity states below the Fermi level[90,227] (Scheme 8d), 2) absorption by Frenkel excitons,[90] or 3) In_2O_3 impurities which exhibit a matching (2.62 eV) band gap.[226b,228] None of these hypotheses has as yet sufficient corroborating evidence, and the explanation remains elusive. This confusing picture is exacerbated by the fact that nickel is used for two different roles. Firstly, it serves as a dopant which further decreases the band gap of $In_{1-x}Ni_xTaO_4$ because of the distorted structure of the NiO_6 octahedra[226b] or because of the introduction of dopant states above the valence band.[227] It can also weakly contribute to the absorption of light at about 2.7 eV, which originates from internal d-d transitions; however, this excitation is photocatalytically inactive. Secondly, nickel is also a co-catalyst, often in a Ni@NiO configuration, referred to as NiO_y.

Despite this lack of understanding, $InTaO_4$ and $InNbO_4$ prepared by either a high-temperature solid-state reaction or by a sol–gel synthesis[229] have been employed in studies of CO_2 photoreduction. Pan and Chen suspended 1–2 μm $InTaO_4$ particles in an aqueous solution of $KHCO_3$ and

observed that methanol was produced at a rate of 1.39 μmol $g^{-1} h^{-1}$ under illumination from a 500 W halogen lamp.[230] According to the authors, this rate corresponded to an (internal) quantum efficiency of 2.45%. Wang et al. showed that the addition of a NiO co-catalyst, which acts as an electron trap and facilitates the formation of H· radicals that react with CO_2, increases the rate of formation of methanol in the aqueous phase almost tenfold.[231] They also achieved a rate of formation of 11.1 μmol $g^{-1} h^{-1}$ in the vapor phase in an optical fiber reactor under intense irradiation of 327 mW cm^{-2}. The (external) quantum efficiency in the aqueous- and vapor-phase experiments was 0.0045% and 0.063%, respectively.

Tsai et al. decreased the band gap of $InTaO_4$ to 2.28 eV by doping with nitrogen.[232] They inferred that the conduction band of $InTaO_4$ is not reductive enough ($E_{CB} = -0.8$ V versus the NHE at pH 0) for transferring electrons to NiO ($E_{CB} = -0.96$ V versus the NHE). Hence, they used a Ni@NiO structure to trap electrons in the nickel and to provide catalytic centers on the NiO surface. The reported rate of formation of methanol was 65 μmol $g^{-1} h^{-1}$ upon illumination with visible light (390–770 nm). It was increased twofold by nitrogen doping and threefold by the addition of the co-catalyst. In another study, Ni@NiO was found to be a more effective co-catalyst of $InNbO_4$ than Co_3O_4 NPs, although the difference was only about 5% in favor of nickel.[233] The presence of small amounts of Nb_2O_5 during preparation helped to maintain the small size of the NiO particles needed for their photocatalytic activity.

Metal oxides in which the core ion is in a d^{10} electronic configuration have attracted considerable attention in recent years because of the characteristics of their conduction band. In contrast to d^0 oxides, where the conduction band is primarily composed of d orbitals, in d^{10} oxides hybridized s and p orbitals form the lower end of the band. Such mixing of orbitals confers a large dispersion in k-space on the band and thereby a high mobility of the photogenerated electrons.[23,190] Many of the ternary d^{10} oxides also contain Zn^{2+} ions because the p-d repulsion of the occupied oxygen 2p and zinc 3d orbitals raises the valence band without affecting the level of the conduction band, and thus decreasing the gap.[234] The respective oxides are also in general stable in water under UV irradiation.

Zinc germanate, Zn_2GeO_4, has been the subject of several studies on the photocatalytic reduction of CO_2 in the last few years. As a consequence of the wide band gap of 4.5 eV, it was earlier proven to be capable of splitting water, especially when decorated with RuO_2 NPs as oxidation catalysts.[235] Its willemite crystal structure consists of GeO_4 and ZnO_4 tetrahedra. Interestingly, the GeO_4 tetrahedra are heavily distorted so that a dipole moment of 1.6 D is generated inside. The associated field is thought to promote the electron–hole separation, as was previously discussed for $BaTi_4O_9$. Recent computational studies have shown that CO_2 preferentially adsorbs on the Zn_2GeO_4 surface near or at an oxygen vacancy site.[236] In the latter case it can dissociate to CO, thereby filling the vacancy with its oxygen atom. Without a vacancy, a CO_2 molecule adsorbs through either bridged carbonate-like species or bidentate carbonates, depending on the crystal facet. The activity of zinc germanate synthesized by a solid-state reaction was low because of its small specific surface area (0.6 $m^2 g^{-1}$), but employing it in a micro/mesoporous material configuration with a much larger surface area (90.5 $m^2 g^{-1}$) improved the rate of formation of methane from 1.4 to 9.5 ppm $g^{-1} h^{-1}$.[237] Advances in solvothermal synthetic methods to prepare nanostructured Zn_2GeO_4 enabled further improvements.[238] Monocrystalline nanobelts with a thickness of 7 nm, widths of 20–50 nm, and lengths of hundreds of nanometers photoreduced CO_2 to methane at a rate of 1.5 μmol $g^{-1} h^{-1}$.[239] Deposition of RuO_2 and Pt NPs (co-catalysts of oxidation and reduction, respectively) on the nanobelts enhanced the formation rate to 25 μmol $g^{-1} h^{-1}$. In another report, monocrystalline hexagonal prism Zn_2GeO_4 nanorods (250 nm in length and 150 nm in width) were shown to produce CO at a rate of 17.9 ppm h^{-1} and methane at a rate of 3.5 ppm h^{-1}.[240] The relatively large size of the nanorods meant that the quantum confinement effects were small and the band gap rose merely to 4.65 eV. The minimum of the conduction band was estimated to be at around −0.7 V versus the NHE at pH 7, thus suggesting that thermodynamically the eight-electron reduction of CO_2 to methane is indeed possible.

Nevertheless, the wide band gap remains a significant limiting factor. This is why—similar to the Ta_2O_5 compounds—efforts have been focused on decreasing the band gap through the creation of a solid solution with nitrides. To this end, zinc germanium oxynitride $(Zn_{1.44}Ge)(N_{2.08}O_{0.38})$ has been synthesized and demonstrated to possess a suitably narrow band of about 2.7 eV.[242] The decrease in the gap width stems from the repulsion between the electrons in the zinc 3d and the electrons in the nitrogen 2p and oxygen 2p orbitals in the upper valance band, which raises the top of the valance band. Accordingly, the oxynitride was able to reduce CO_2 to methane at a rate of 2.7 ppm $g^{-1} h^{-1}$ under illumination with visible light in the presence of platinum NPs.[243] This rate was a little better than a comparable rate obtained for N-doped TiO_2 material. The percentage content of nitrogen in the compound depends on the duration of the nitridation in NH_3. A nitridation time of 10 h was found to be optimal. Methane was also obtained when sheaflike hyperbranched structures of visible-light-active $Zn_{1.7}GeN_{1.8}O$ were employed under ambient conditions.[241] The reported photonic (i.e. external quantum) yield at 420 nm was 0.024%. Figure 5

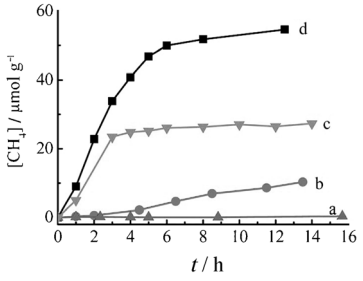

Figure 5. CH_4 generation over a) $Zn_{1.7}GeN_{1.8}O$, b) 1 wt% Pt-loaded $Zn_{1.7}GeN_{1.8}O$, c) 1 wt% RuO_2-loaded $Zn_{1.7}GeN_{1.8}O$, and d) 1 wt% RuO_2 and 1 wt% Pt co-loaded $Zn_{1.7}GeN_{1.8}O$ as a function of irradiation times with visible light. Reproduced from Ref. [241] with permission.

shows the effect of decorating the structures with RuO_2 and platinum NPs on the efficiency of the photoreduction, with the best results obtained when both types of NPs were used together. While methane was the major product of the CO_2 reduction on zinc germanate, carbon monoxide was produced almost selectively with the indium germanate $In_2Ge_2O_7(En)$ (En = ethylenediamine).[244] Ultrathin nanowires of the material, prepared in an En/water solvent and loaded with platinum NPs, were active in the UV range ($E_g = 3.98$ eV) and formed CO in the presence of water vapor at a rate of about 0.9 $\mu mol\, g^{-1} h^{-1}$ when illuminated with a Xe arc lamp. The benefits of nanostructures are further exemplified by hexagonal nanoplates of zinc stannate, Zn_2SnO_4, arranged to form micrometer-sized octahedra.[245] As a consequence of the conduction band minimum located at −1.17 V versus the NHE, this d^{10} ternary oxide is a suitable material for the photoreduction of CO_2, albeit only under UV illumination ($E_g = 3.6$ eV in the bulk and 3.87 eV for the nanoplates). The rate of formation of methane with the nanostructured sample was 20.1 $ppm\, g^{-1}$, compared to only 1.5 $ppm\, g^{-1}$ with the bulk sample. The rate increase was attributed to the high surface area, high rate of electron transfer along the nanoplates, facile electrolyte diffusion within the meshlike structure of the octahedral, and the significant light scattering by the micrometer-sized objects, which is beneficial for the absorption of light. The addition of co-catalysts, RuO_2 and Pt NPs, substantially improved the results, and led to the highest CH_4 formation rate of 86.7 $ppm\, g^{-1}$ under identical conditions.

Gallium oxide, especially the polymorph α-Ga_2O_3 with a high surface area, has a good affinity towards CO_2 through surface OH groups and the formation of various (bi)carbonate species.[246] This property has been used in studies of the photocatalytic hydrogenation of CO_2 on the surface of Ga_2O_3, that is reduction with H_2.[247] The same reductant was also used in the reduction of CO_2 to methanol on gallium oxide based zinc-copper double layered hydroxides.[248]

However, Ga_2O_3 has a high reducing potential (−1.45 V versus the NHE at pH 7) and is able to photoreduce CO_2 without the use of additional reductants and co-catalysts. Recently, Park et al. employed mesoporous β-Ga_2O_3 with a pore size of 3.9 nm and microporous channels to convert CO_2 into CO and CH_4 with formation rates of 1.46 and 0.21 $\mu mol\, g^{-1} h^{-1}$, respectively.[249] The rates were about four times higher than for the bulky β-Ga_2O_3 analogue. This improvement was attributed to the higher active surface area as well as to efficient electron-transfer properties, good penetration of light, and gas diffusion in the porous structures. Mesoporous zinc gallate, $ZnGa_2O_4$, with a spinel crystal structure and a wide band gap of 4.4 eV was also shown to induce the photocatalytic reduction of CO_2 to methane.[250] In contrast, the same compound prepared by a solid-state reaction produced only traces of methane. Similar to other d^{10} oxides, the improved separation of the electrons and holes by decoration of the semiconductor with RuO_2 NPs led to a significant, almost tenfold, increase in the rate of formation of CH_4.

Gallium zinc (oxy)nitride, $(Ga_{1-x}Zn_x)(N_{1-x}O_x)$, could alleviate the major deficiency of zinc gallate, that is the width of its band gap. This semiconductor can be construed as a solid solution of GaN and ZnO, but its activity to visible light is a little surprising because both components have wide band gaps.[251] This activity is thought to originate from the interaction of oxygen 2p with nitrogen 2p and zinc 3d orbitals which shift up the valence band.[252] It was recently shown that the band gap can be modulated between 2.2 and 2.7 eV by varying the content of GaN and ZnO.[253] With a band gap of 2.2 eV, which corresponds to an onset of absorption at 565 nm, a significant part of the solar spectrum can be covered. This semiconductor has been applied successfully to the splitting of water under illumination with visible light,[19,83a] but—to our knowledge—has not yet been used for the photoreduction of CO_2, unlike its Ge-containing counterpart.[243]

All of the methods presented here for narrowing the band gap to harvest visible light have relied on raising the energy of the valence band. The futility of modifying the conduction band level is illustrated well in a recent study on delafossite Fe-substituted $CuGaO_2$.[254] Delafossites, materials with the general formula ABO_2, contain layers of octahedrally coordinated B^{3+} ions interlaced with layers of A^+ ions. They usually only absorb UV light; however, $CuGaO_2$ has a weak absorption feature at 2.6 eV, which is associated with an indirect gap transition. This is, presumably, due to a similar effect as discussed earlier for $CuNbO_3$, of the copper 3d orbitals raising the valence band. At the same time, when some of the Ga^{3+} ions were substituted with Fe^{3+}, the resulting $CuGa_{1-x}Fe_xO_2$ ($x = 0.05$–0.20) absorbed strongly in the visible region because of a narrow band gap of 1.5 eV. $CuGaO_2$ was shown to photocatalytically reduce CO_2 to CO at a relatively low rate of about 9 $ppm\, g^{-1} h^{-1}$, but this rate was not increased with $CuGa_{1-x}Fe_xO_2$, irrespective of the iron concentration. The authors argued that the introduction of Fe^{3+} ions lowered the conduction band because of distortions in the crystal lattice so that its level was below the reduction potential of CO_2 to CO. Therefore, despite enhancing the absorption of light, the photocatalytic activity did not improve and, if anything, worsened.

4.3.3. Phosphides

Several main group metal phosphides, in particular GaP and InP, have also been studied for their ability to reduce CO_2 in photochemical or photoelectrochemical setups. GaP is a p-type semiconductor with a reasonably narrow band gap (2.3 eV) and a very favorable, highly reducing, position of the conduction band. It was shown in the seminal work by Inoue et al. to photoreduce CO_2 to methanol and smaller amounts of HCHO much more efficiently than, for example, TiO_2 or ZnO.[27] Barton et al. have also employed p-GaP as a photocathode in a photoelectrochemical cell, in which a photonic (external quantum) yield of 2.6% at 465 nm was obtained for the conversion of CO_2 into methanol with the electrode held at −0.5 V versus the saturated calomel electrode (SCE).[17b] Pyridine was added to the electrolyte to act as a co-catalyst and was thought to be responsible for the selectivity of the process towards methanol through intermediate carbamate species.

On the other hand, p-InP semiconductors tend to photoreduce CO_2 to formate, although the minimum of its conduction band is located about 0.85 V lower. Arai et al. built a photoelectrochemical cell with a zinc-doped InP photocathode ($E_g = 1.35$ eV) modified with a ruthenium coordination polymer $[Ru(L\text{-}L)(CO)_2]_n$, in which L-L is a diimine ligand.[17c] The system exhibited good selectivity for the formation of formate in an aqueous environment under irradiation with visible light ($\lambda > 400$ nm) and an applied potential of -0.6 V. Importantly, isotope analysis using $^{13}CO_2$ and D_2O has proven that the CO_2 and water acted as sources of carbon and protons, respectively. The system was further combined with a second photocatalyst based on TiO_2-Pt, which was designed to oxidize water (i.e. extract electrons) in a separate compartment.[255] The constructed system, referred to as a Z-scheme, is composed of two photocatalysts, which have similar band-gap widths but shifted band edges. It operates on the basis of a two-step excitation, where the less reductive electron recombines with the less oxidative hole, leaving the more active species to drive redox reactions. In such a scheme, InP anchored with a ruthenium electrocatalyst photoreduced CO_2 to formate without any external bias, with a power conversion efficiency of 0.03%, thus underlining the viability of the two-compartment photoelectrochemical approach.

5. Conclusions

At present, the formation rates of products of the photocatalytic reduction of CO_2 on semiconductors rarely exceed tens of $\mu mol\, g^{-1}\, h^{-1}$. This means that the efficiency of the process is generally lower than in natural photosynthesis or in the photocatalytic generation of H_2. There has been, however, a surge of interest in the field over the last few years, as reflected by the quickly growing numbers of publications. Recent developments are concentrated on new photocatalytic materials (e.g. novel oxynitrides of metals with d^0 electronic configurations or oxides of d^{10} metals) and on new nanoscale structures that offer a large surface area, improved charge separation, and directional electron transfers. The mechanism of the process is also the subject of many studies, usually based on a combination of experimental and computational methods. These studies attempt to answer the yet unresolved questions concerning the chemical pathways of CO_2 reduction which determine the selectivity of the entire reaction. Of particular interest are the approaches to overcome the barrier associated with the activation of a CO_2 molecule towards the first one-electron reduction. This step appears to be a rate-limiting one, because of the highly negative electrochemical reduction potential of CO_2 to the anion radical $CO_2^{\bullet-}$ compared to the conduction band levels of commonly employed semiconductors. Other important aspects of the mechanism which are relevant for a deeper understanding of the process include charge-carrier dynamics within the semiconductors and at their interfaces with the metal co-catalysts; the effect of the nanostructure of the photocatalyst itself and the employed co-catalyst; and the impact of the choice of the catalytic metal on the outcome of the process. As a result of the extensive body of research already devoted to TiO_2, it is considered a good model system on which these fundamental mechanistic questions can be investigated.

The lack of a single measure of efficiency which would allow for an unequivocal comparison of heterogeneous photocatalytic systems has to be considered as a serious impediment to advancing the field. The situation could be partially ameliorated by standardizing the experimental conditions as well as by publishing at least two of the popular measures, one related to the amount of the catalyst (e.g. formation rate) and one related to the strength of the illumination (e.g. photonic efficiency). An alternative would be to devise a new measure that encompasses both relationships. Both approaches would be valuable steps forward for a consistent assessment of the efficiency of any system with respect to others and thereby enable identification of the best performing ones and paths for further improvement.

Photocatalytic reactions taking place in the presence of sacrificial electron donors are inherently short-term, as they only work until the donor is used up. Thus far, virtually all the studied systems focused on the half-reactions of the CO_2 reduction. Full cycle systems, with a stronger emphasis on the oxidation half-reaction (e.g. generation of oxygen or hydrogen peroxide), will be necessary to allow for long-term studies. This could give insight into whether CO_2 photoreduction is a commercially viable approach for the production of solar fuel. A reliance solely on cheap and abundant materials will be an important aspect for the future adoption of this technology, even if small sacrifices in efficiency have to be conceded. In this context, semiconductors such as TiO_2 might have an advantage over some novel materials in terms of production costs.

One significant problem in the photocatalytic redox reactions is the separation of the two half-reactions to avoid reverse processes. The photoelectrochemical cells—hybrid systems of photovoltaic and photocatalytic devices—offer a possibility to effectively address this issue and utilize the advantages of both types of solar devices. As such, they deserve more attention in future studies.

The heterogeneous photocatalytic reduction of CO_2 on semiconductors is not yet ready to be implemented in real-life solar fuel applications. However, with the current pace of developments in the field, the emerging understanding of the mechanism, as well as novel materials should bring the promise held by this process much closer to fulfilment in the near future.

We acknowledge funding by the Federal Ministry of Education and Research (BMBF) for the "Solar2Fuel" project, part of the "Forum Organic Electronics" cluster. We thank all project partners, especially those at BASF, for fruitful discussions. J.K.S. acknowledges support of the Bavarian State Ministry of Science, Research, and Arts through the grant "Solar Technologies go Hybrid (SolTech)".

Received: September 5, 2012
Revised: December 21, 2012
Published online: June 13, 2013

[1] a) M. Fontecave, *Angew. Chem.* **2011**, *123*, 6836 – 6837; *Angew. Chem. Int. Ed.* **2011**, *50*, 6704 – 6705; b) C. Pasten, J. C. Santamarina, *Energy Policy* **2012**, *49*, 468 – 476.
[2] N. S. Lewis, D. G. Nocera, *Proc. Natl. Acad. Sci. USA* **2006**, *103*, 15729 – 15735.
[3] International Energy Agency in World Energy Outlook 2011, http://www.worldenergyoutlook.org, **2011**.
[4] G. Centi, S. Perathoner, *ChemSusChem* **2010**, *3*, 195 – 208.
[5] E. J. Maginn, *J. Phys. Chem. Lett.* **2010**, *1*, 3478 – 3479.
[6] M. Aresta, A. Dibenedetto, *Dalton Trans.* **2007**, 2975 – 2992.
[7] a) J. P. Smol, *Nature* **2012**, *483*, S12 – S15; b) Atmospheric CO_2 level for July 2012: $\delta = 394.49$ ppm, http://www.co2now.org, **2012**.
[8] P. N. Pearson, M. R. Palmer, *Nature* **2000**, *406*, 695 – 699.
[9] M. Mikkelsen, M. Jorgensen, F. C. Krebs, *Energy Environ. Sci.* **2010**, *3*, 43 – 81.
[10] a) D. M. D'Alessandro, B. Smit, J. R. Long, *Angew. Chem.* **2010**, *122*, 6194 – 6219; *Angew. Chem. Int. Ed.* **2010**, *49*, 6058 – 6082; b) K. M. K. Yu, I. Curcic, J. Gabriel, S. C. E. Tsang, *ChemSusChem* **2008**, *1*, 893 – 899.
[11] a) S. C. Roy, O. K. Varghese, M. Paulose, C. A. Grimes, *ACS Nano* **2010**, *4*, 1259 – 1278; b) N. D. McDaniel, S. Bernhard, *Dalton Trans.* **2010**, *39*, 10021 – 10030.
[12] a) G. A. Olah, G. K. S. Prakash, A. Goeppert, *J. Am. Chem. Soc.* **2011**, *133*, 12881 – 12898; b) G. A. Olah, A. Goeppert, G. K. S. Prakash, *J. Org. Chem.* **2009**, *74*, 487 – 498.
[13] a) M. Cokoja, C. Bruckmeier, B. Rieger, W. A. Herrmann, F. E. Kühn, *Angew. Chem.* **2011**, *123*, 8662 – 8690; *Angew. Chem. Int. Ed.* **2011**, *50*, 8510 – 8537; b) K. Huang, C.-L. Sun, Z.-J. Shi, *Chem. Soc. Rev.* **2011**, *40*, 2435 – 2452.
[14] C. Das Neves Gomes, O. Jacquet, C. Villiers, P. Thuéry, M. Ephritikhine, T. Cantat, *Angew. Chem.* **2012**, *124*, 191 – 194; *Angew. Chem. Int. Ed.* **2012**, *51*, 187 – 190.
[15] a) A. A. Peterson, J. K. Nørskov, *J. Phys. Chem. Lett.* **2012**, *3*, 251 – 258; b) E. E. Benson, C. P. Kubiak, A. J. Sathrum, J. M. Smieja, *Chem. Soc. Rev.* **2009**, *38*, 89 – 99.
[16] H. Li, P. H. Opgenorth, D. G. Wernick, S. Rogers, T.-Y. Wu, W. Higashide, P. Malati, Y.-X. Huo, K. M. Cho, J. C. Liao, *Science* **2012**, *335*, 1596 – 1596.
[17] a) M. Halmann, *Nature* **1978**, *275*, 115 – 116; b) E. E. Barton, D. M. Rampulla, A. B. Bocarsly, *J. Am. Chem. Soc.* **2008**, *130*, 6342 – 6344; c) T. Arai, S. Sato, K. Uemura, T. Morikawa, T. Kajino, T. Motohiro, *Chem. Commun.* **2010**, *46*, 6944 – 6946.
[18] W. Wang, S. Wang, X. Ma, J. Gong, *Chem. Soc. Rev.* **2011**, *40*, 3703 – 3727.
[19] K. Maeda, K. Domen, *J. Phys. Chem. Lett.* **2010**, *1*, 2655 – 2661.
[20] a) J. Schneider, H. Jia, J. T. Muckerman, E. Fujita, *Chem. Soc. Rev.* **2012**, *41*, 2036 – 2051; b) J. Agarwal, E. Fujita, H. F. Schaefer, J. T. Muckerman, *J. Am. Chem. Soc.* **2012**, *134*, 5180 – 5186; c) A. J. Morris, G. J. Meyer, E. Fujita, *Acc. Chem. Res.* **2009**, *42*, 1983 – 1994.
[21] a) H. Takeda, K. Koike, H. Inoue, O. Ishitani, *J. Am. Chem. Soc.* **2008**, *130*, 2023 – 2031; b) B. Gholamkhass, H. Mametsuka, K. Koike, T. Tanabe, M. Furue, O. Ishitani, *Inorg. Chem.* **2005**, *44*, 2326 – 2336.
[22] a) A. L. Linsebigler, G. Lu, J. T. Yates, *Chem. Rev.* **1995**, *95*, 735 – 758; b) M. A. Henderson, *Surf. Sci. Rep.* **2011**, *66*, 185 – 297.
[23] A. Kubacka, M. Fernández-García, G. Colón, *Chem. Rev.* **2012**, *112*, 1555 – 1614.
[24] K. J. Young, L. A. Martini, R. L. Milot, R. C. Snoeberger III, V. S. Batista, C. A. Schmuttenmaer, R. H. Crabtree, G. W. Brudvig, *Coord. Chem. Rev.* **2012**, *256*, 2503 – 2520.
[25] a) A. Fujishima, X. Zhang, D. A. Tryk, *Surf. Sci. Rep.* **2008**, *63*, 515 – 582; b) J.-M. Herrmann, *Appl. Catal. B* **2010**, *99*, 461 – 468.
[26] a) B. Ohtani, *Chem. Lett.* **2008**, *37*, 216 – 229; b) A. J. Bard, M. A. Fox, *Acc. Chem. Res.* **1995**, *28*, 141 – 145; c) S. Styring, *Faraday Discuss.* **2012**, *155*, 357 – 376.
[27] T. Inoue, A. Fujishima, S. Konishi, K. Honda, *Nature* **1979**, *277*, 637 – 638.
[28] M. R. Hoffmann, S. T. Martin, W. Choi, D. W. Bahnemann, *Chem. Rev.* **1995**, *95*, 69 – 96.
[29] P. V. Kamat, *J. Phys. Chem. Lett.* **2012**, *3*, 663 – 672.
[30] A. Furube, T. Asahi, H. Masuhara, H. Yamashita, M. Anpo, *J. Phys. Chem. B* **1999**, *103*, 3120 – 3127.
[31] S. H. Szczepankiewicz, A. J. Colussi, M. R. Hoffmann, *J. Phys. Chem. B* **2000**, *104*, 9842 – 9850.
[32] D. M. Adams, L. Brus, C. E. D. Chidsey, S. Creager, C. Creutz, C. R. Kagan, P. V. Kamat, M. Lieberman, S. Lindsay, R. A. Marcus, R. M. Metzger, M. E. Michel-Beyerle, J. R. Miller, M. D. Newton, D. R. Rolison, O. Sankey, K. S. Schanze, J. Yardley, X. Zhu, *J. Phys. Chem. B* **2003**, *107*, 6668 – 6697.
[33] a) A. Wood, M. Giersig, P. Mulvaney, *J. Phys. Chem. B* **2001**, *105*, 8810 – 8815; b) M. Jakob, H. Levanon, P. V. Kamat, *Nano Lett.* **2003**, *3*, 353 – 358.
[34] S. Kim, S.-J. Hwang, W. Choi, *J. Phys. Chem. B* **2005**, *109*, 24260 – 24267.
[35] a) V. Subramanian, E. Wolf, P. V. Kamat, *J. Phys. Chem. B* **2001**, *105*, 11439 – 11446; b) A. Furube, T. Asahi, H. Masuhara, H. Yamashita, M. Anpo, *Chem. Phys. Lett.* **2001**, *336*, 424 – 430.
[36] H. Kisch, *Angew. Chem.* **2013**, *125*, 842 – 879; *Angew. Chem. Int. Ed.* **2013**, *52*, 812 – 847.
[37] D. P. Colombo, R. M. Bowman, *J. Phys. Chem.* **1996**, *100*, 18445 – 18449.
[38] a) K. J. P. Schouten, Y. Kwon, C. J. M. van der Ham, Z. Qin, M. T. M. Koper, *Chem. Sci.* **2011**, *2*, 1902 – 1909; b) T. Yui, A. Kan, C. Saitoh, K. Koike, T. Ibusuki, O. Ishitani, *ACS Appl. Mater. Interfaces* **2011**, *3*, 2594 – 2600.
[39] A. Paul, D. Connolly, M. Schulz, M. T. Pryce, J. G. Vos, *Inorg. Chem.* **2012**, *51*, 1977 – 1979.
[40] a) J. Rasko, F. Solymosi, *J. Phys. Chem.* **1994**, *98*, 7147 – 7152; b) N. Ulagappan, H. Frei, *J. Phys. Chem. A* **2000**, *104*, 7834 – 7839; c) W. Lin, H. Frei, *J. Am. Chem. Soc.* **2005**, *127*, 1610 – 1611; d) C. C. Yang, Y. H. Yu, B. van der Linden, J. C. S. Wu, G. Mul, *J. Am. Chem. Soc.* **2010**, *132*, 8398 – 8406.
[41] a) M. Anpo, H. Yamashita, Y. Ichihashi, S. Ehara, *J. Electroanal. Chem.* **1995**, *396*, 21 – 26; b) N. M. Dimitrijevic, B. K. Vijayan, O. G. Poluektov, T. Rajh, K. A. Gray, H. Y. He, P. Zapol, *J. Am. Chem. Soc.* **2011**, *133*, 3964 – 3971; c) N. M. Dimitrijevic, I. A. Shkrob, D. J. Gosztola, T. Rajh, *J. Phys. Chem. C* **2012**, *116*, 878 – 885; d) I. A. Shkrob, N. M. Dimitrijevic, T. W. Marin, H. He, P. Zapol, *J. Phys. Chem. C* **2012**, *116*, 9461 – 9471.
[42] K. Tanaka, K. Miyahara, I. Toyoshima, *J. Phys. Chem.* **1984**, *88*, 3504 – 3508.
[43] J. Lee, D. C. Sorescu, X. Deng, *J. Am. Chem. Soc.* **2011**, *133*, 10066 – 10069.
[44] a) A. Hagfeldt, G. Boschloo, L. Sun, L. Kloo, H. Pettersson, *Chem. Rev.* **2010**, *110*, 6595 – 6663; b) D. W. Bahnemann, M. Hilgendorff, R. Memming, *J. Phys. Chem. B* **1997**, *101*, 4265 – 4275.
[45] a) S. S. Tan, L. Zou, E. Hu, *Catal. Today* **2008**, *131*, 125 – 129; b) K. Kočí, L. Obalová, O. Šolcová, *Chem. Process Eng.* **2010**, *31*, 395 – 407.
[46] a) D. T. Whipple, P. J. A. Kenis, *J. Phys. Chem. Lett.* **2010**, *1*, 3451 – 3458; b) A. A. Peterson, F. Abild-Pedersen, F. Studt, J. Rossmeisl, J. K. Norskov, *Energy Environ. Sci.* **2010**, *3*, 1311 – 1315.
[47] a) H. He, P. Zapol, L. A. Curtiss, *Energy Environ. Sci.* **2012**, *5*, 6196 – 6205; b) V. P. Indrakanti, H. H. Schobert, J. D. Kubicki, *Energy Fuels* **2009**, *23*, 5247 – 5256.

[48] P. D. Tran, L. H. Wong, J. Barber, J. S. C. Loo, *Energy Environ. Sci.* **2012**, *5*, 5902 – 5918.
[49] a) H. J. Freund, M. W. Roberts, *Surf. Sci. Rep.* **1996**, *25*, 225 – 273; b) V. P. Indrakanti, J. D. Kubicki, H. H. Schobert, *Energy Environ. Sci.* **2009**, *2*, 745 – 758.
[50] W. H. Koppenol, J. D. Rush, *J. Phys. Chem.* **1987**, *91*, 4429 – 4430.
[51] M. Gattrell, N. Gupta, A. Co, *J. Electroanal. Chem.* **2006**, *594*, 1 – 19.
[52] S. Tan, Y. Zhao, J. Zhao, Z. Wang, C. Ma, A. Zhao, B. Wang, Y. Luo, J. Yang, J. Hou, *Phys Rev. B* **2011**, *84*, 155418.
[53] K. Tanaka, J. M. White, *J. Phys. Chem.* **1982**, *86*, 3977 – 3980.
[54] G. Rothenberger, D. Fitzmaurice, M. Gratzel, *J. Phys. Chem.* **1992**, *96*, 5983 – 5986.
[55] G. Redmond, D. Fitzmaurice, *J. Phys. Chem.* **1993**, *97*, 1426 – 1430.
[56] B. Enright, D. Fitzmaurice, *J. Phys. Chem.* **1996**, *100*, 1027 – 1035.
[57] I. A. Shkrob, T. W. Marin, H. He, P. Zapol, *J. Phys. Chem. C* **2012**, *116*, 9450 – 9460.
[58] a) G. Kim, W. Choi, *Appl. Catal. B* **2010**, *100*, 77 – 83; b) S. Sato, T. Morikawa, S. Saeki, T. Kajino, T. Motohiro, *Angew. Chem.* **2010**, *122*, 5227 – 5231; *Angew. Chem. Int. Ed.* **2010**, *49*, 5101 – 5105.
[59] H. Fujiwara, H. Hosokawa, K. Murakoshi, Y. Wada, S. Yanagida, T. Okada, H. Kobayashi, *J. Phys. Chem. B* **1997**, *101*, 8270 – 8278.
[60] a) S. Qin, F. Xin, Y. Liu, X. Yin, W. Ma, *J. Colloid Interface Sci.* **2011**, *356*, 257 – 261; b) S. Kaneco, H. Kurimoto, Y. Shimizu, K. Ohta, T. Mizuno, *Energy* **1999**, *24*, 21 – 30.
[61] J. J. Murcia, M. C. Hidalgo, J. A. Navío, V. Vaiano, P. Ciambelli, D. Sannino, *Catal. Today* **2012**, *196*, 101 – 109.
[62] a) S. Kaneco, Y. Shimizu, K. Ohta, T. Mizuno, *J. Photochem. Photobiol. A* **1998**, *115*, 223 – 226; b) B.-J. Liu, T. Torimoto, H. Yoneyama, *J. Photochem. Photobiol. A* **1998**, *113*, 93 – 97.
[63] C. A. Craig, L. O. Spreer, J. W. Otvos, M. Calvin, *J. Phys. Chem.* **1990**, *94*, 7957 – 7960.
[64] S. Liu, Z. Zhao, Z. Wang, *Photochem. Photobiol. Sci.* **2007**, *6*, 695 – 700.
[65] a) I. H. Tseng, J. C. S. Wu, H.-Y. Chou, *J. Catal.* **2004**, *221*, 432 – 440; b) I. H. Tseng, W.-C. Chang, J. C. S. Wu, *Appl. Catal. B* **2002**, *37*, 37 – 48.
[66] a) R. D. Richardson, B. K. Carpenter, *J. Am. Chem. Soc.* **2008**, *130*, 3169 – 3180; b) B. K. Carpenter, *J. Phys. Chem. A* **2007**, *111*, 3719 – 3726.
[67] R. D. Richardson, E. J. Holland, B. K. Carpenter, *Nat. Chem.* **2011**, *3*, 301 – 303.
[68] a) M. Subrahmanyam, S. Kaneco, N. Alonso-Vante, *Appl. Catal. B* **1999**, *23*, 169 – 174; b) N. Sasirekha, S. J. S. Basha, K. Shanthi, *Appl. Catal. B* **2006**, *62*, 169 – 180.
[69] a) O. K. Varghese, M. Paulose, T. J. LaTempa, C. A. Grimes, *Nano Lett.* **2009**, *9*, 731 – 737; b) K. Ikeue, S. Nozaki, M. Ogawa, M. Anpo, *Catal. Today* **2002**, *74*, 241 – 248.
[70] a) K. Ikeue, H. Yamashita, M. Anpo, T. Takewaki, *J. Phys. Chem. B* **2001**, *105*, 8350 – 8355; b) H. Yamashita, Y. Fujii, Y. Ichihashi, S. G. Zhang, K. Ikeue, D. R. Park, K. Koyano, T. Tatsumi, M. Anpo, *Catal. Today* **1998**, *45*, 221 – 227.
[71] K. Mori, H. Yamashita, M. Anpo, *RSC Adv.* **2012**, *2*, 3165 – 3172.
[72] E. B. Cole, P. S. Lakkaraju, D. M. Rampulla, A. J. Morris, E. Abelev, A. B. Bocarsly, *J. Am. Chem. Soc.* **2010**, *132*, 11539 – 11551.
[73] a) G. R. Dey, A. D. Belapurkar, K. Kishore, *J. Photochem. Photobiol. A* **2004**, *163*, 503 – 508; b) G. Dey, K. Pushpa, *Res. Chem. Intermed.* **2007**, *33*, 631 – 644.
[74] a) S. Sato, *J. Phys. Chem.* **1983**, *87*, 3531 – 3537; b) M. D. Ward, J. R. White, A. J. Bard, *J. Am. Chem. Soc.* **1983**, *105*, 27 – 31; c) M. Kaise, H. Kondoh, C. Nishihara, H. Nozoye, H. Shindo, S. Nimura, O. Kikuchi, *J. Chem. Soc. Chem. Commun.* **1993**, 395 – 396.
[75] a) Y. Hori, K. Kikuchi, S. Suzuki, *Chem. Lett.* **1985**, *14*, 1695 – 1698; b) Y. Hori, H. Wakebe, T. Tsukamoto, O. Koga, *Electrochim. Acta* **1994**, *39*, 1833 – 1839.
[76] a) S. E. Braslavsky, A. M. Braun, A. E. Cassano, A. V. Emeline, M. I. Litter, L. Palmisano, V. N. Parmon, N. Serpone, *Pure Appl. Chem.* **2011**, *83*, 931 – 1014; b) N. Serpone, *J. Photochem. Photobiol. A* **1997**, *104*, 1 – 12.
[77] T. Maschmeyer, M. Che, *Angew. Chem.* **2010**, *122*, 1578 – 1582; *Angew. Chem. Int. Ed.* **2010**, *49*, 1536 – 1539.
[78] C. Wang, R. L. Thompson, J. Baltrus, C. Matranga, *J. Phys. Chem. Lett.* **2010**, *1*, 48 – 53.
[79] a) H. Kisch, *Angew. Chem.* **2010**, *122*, 9782 – 9783; *Angew. Chem. Int. Ed.* **2010**, *49*, 9588 – 9589; b) T. Maschmeyer, M. Che, *Angew. Chem.* **2010**, *122*, 9784 – 9785; *Angew. Chem. Int. Ed.* **2010**, *49*, 9590 – 9591.
[80] N. Serpone, A. Salinaro, A. Emeline, V. Ryabchuk, *J. Photochem. Photobiol. A* **2000**, *130*, 83 – 94.
[81] E. W. McFarland, J. Tang, *Nature* **2003**, *421*, 616 – 618.
[82] a) M. D. Hernández-Alonso, F. Fresno, S. Suárez, J. M. Coronado, *Energy Environ. Sci.* **2009**, *2*, 1231 – 1257; b) T. A. Kandiel, A. Feldhoff, L. Robben, R. Dillert, D. W. Bahnemann, *Chem. Mater.* **2010**, *22*, 2050 – 2060; c) Y. Ohko, K. Hashimoto, A. Fujishima, *J. Phys. Chem. A* **1997**, *101*, 8057 – 8062; d) C.-y. Wang, J. Rabani, D. W. Bahnemann, J. K. Dohrmann, *J. Photochem. Photobiol. A* **2002**, *148*, 169 – 176.
[83] a) K. Maeda, K. Teramura, D. Lu, T. Takata, N. Saito, Y. Inoue, K. Domen, *Nature* **2006**, *440*, 295; b) Y. Tamaki, K. Watanabe, K. Koike, H. Inoue, T. Morimoto, O. Ishitani, *Faraday Discuss.* **2012**, *155*, 115 – 127; c) H. Yan, J. Yang, G. Ma, G. Wu, X. Zong, Z. Lei, J. Shi, C. Li, *J. Catal.* **2009**, *266*, 165 – 168; d) C. u. Gomes Silva, R. Juárez, T. Marino, R. Molinari, H. García, *J. Am. Chem. Soc.* **2011**, *133*, 595 – 602.
[84] M. Grätzel, *Inorg. Chem.* **2005**, *44*, 6841 – 6851.
[85] T.-V. Nguyen, J. C. S. Wu, *Appl. Catal. A* **2008**, *335*, 112 – 120.
[86] M. Halmann, V. Katzir, E. Borgarello, J. Kiwi, *Sol. Energy Mater.* **1984**, *10*, 85 – 91.
[87] a) N. Serpone, E. Borgarello, M. Grätzel, *J. Chem. Soc. Chem. Commun.* **1984**, 342 – 344; b) P. A. Sant, P. V. Kamat, *Phys. Chem. Chem. Phys.* **2002**, *4*, 198 – 203; c) F. Liao, Z. Zeng, C. Eley, Q. Lu, X. Hong, S. C. E. Tsang, *Angew. Chem.* **2012**, *124*, 5934 – 5938; *Angew. Chem. Int. Ed.* **2012**, *51*, 5832 – 5836.
[88] a) H. Imahori, S. Kang, H. Hayashi, M. Haruta, H. Kurata, S. Isoda, S. E. Canton, Y. Infahsaeng, A. Kathiravan, T. Pascher, P. Chábera, A. P. Yartsev, V. Sundström, *J. Phys. Chem. A* **2011**, *115*, 3679 – 3690; b) E. Lestini, K. Nikitin, J. K. Stolarczyk, D. Fitzmaurice, *ChemPhysChem* **2012**, *13*, 797 – 810.
[89] H. Tong, S. Ouyang, Y. Bi, N. Umezawa, M. Oshikiri, J. Ye, *Adv. Mater.* **2012**, *24*, 229 – 251.
[90] G.-L. Li, Z. Yin, *Phys. Chem. Chem. Phys.* **2011**, *13*, 2824 – 2833.
[91] H. Tong, N. Umezawa, J. Ye, *Chem. Commun.* **2011**, *47*, 4219 – 4221.
[92] A. Fujishima, K. Honda, *Nature* **1972**, *238*, 37 – 38.
[93] a) B. O'Regan, M. Grätzel, *Nature* **1991**, *353*, 737 – 740; b) H. J. Snaith, L. Schmidt-Mende, *Adv. Mater.* **2007**, *19*, 3187 – 3200.
[94] D. Cummins, G. Boschloo, M. Ryan, D. Corr, S. N. Rao, D. Fitzmaurice, *J. Phys. Chem. B* **2000**, *104*, 11449 – 11459.
[95] a) X. Chen, S. S. Mao, *Chem. Rev.* **2007**, *107*, 2891 – 2959; b) U. Diebold, *Surf. Sci. Rep.* **2003**, *48*, 53 – 229; c) T. Tachikawa, M. Fujitsuka, T. Majima, *J. Phys. Chem. C* **2007**, *111*, 5259 – 5275.
[96] D. Dung, J. Ramsden, M. Grätzel, *J. Am. Chem. Soc.* **1982**, *104*, 2977 – 2985.
[97] N. Serpone, D. Lawless, R. Khairutdinov, *J. Phys. Chem.* **1995**, *99*, 16646 – 16654.

[98] M. A. Grela, A. J. Colussi, *J. Phys. Chem. B* **1999**, *103*, 2614 – 2619.
[99] I. Martini, J. H. Hodak, G. V. Hartland, *J. Phys. Chem. B* **1998**, *102*, 9508 – 9517.
[100] a) T. Miyagi, M. Kamei, T. Mitsuhashi, T. Ishigaki, A. Yamazaki, *Chem. Phys. Lett.* **2004**, *390*, 399 – 402; b) G. Li, K. A. Gray, *Chem. Phys.* **2007**, *339*, 173 – 187; c) R. Boppella, P. Basak, S. V. Manorama, *ACS Appl. Mater. Interfaces* **2012**, *4*, 1239 – 1246.
[101] a) T. Ohno, K. Sarukawa, K. Tokieda, M. Matsumura, *J. Catal.* **2001**, *203*, 82 – 86; b) D. Gumy, S. A. Giraldo, J. Rengifo, C. Pulgarin, *Appl. Catal. B* **2008**, *78*, 19 – 29; c) D. C. Hurum, A. G. Agrios, K. A. Gray, T. Rajh, M. C. Thurnauer, *J. Phys. Chem. B* **2003**, *107*, 4545 – 4549; d) D. C. Hurum, K. A. Gray, T. Rajh, M. C. Thurnauer, *J. Phys. Chem. B* **2005**, *109*, 977 – 980; e) K. Komaguchi, H. Nakano, A. Araki, Y. Harima, *Chem. Phys. Lett.* **2006**, *428*, 338 – 342; f) A. Sclafani, J. M. Herrmann, *J. Phys. Chem.* **1996**, *100*, 13655 – 13661; g) Z. Zhang, J. Lee, J. T. Yates, R. Bechstein, E. Lira, J. Ø. Hansen, S. Wendt, F. Besenbacher, *J. Phys. Chem. C* **2010**, *114*, 3059 – 3062.
[102] a) T. Kawahara, Y. Konishi, H. Tada, N. Tohge, J. Nishii, S. Ito, *Angew. Chem.* **2002**, *114*, 2935 – 2937; *Angew. Chem. Int. Ed.* **2002**, *41*, 2811 – 2813; b) J. Zhang, Q. Xu, Z. Feng, M. Li, C. Li, *Angew. Chem.* **2008**, *120*, 1790 – 1793; *Angew. Chem. Int. Ed.* **2008**, *47*, 1766 – 1769.
[103] a) L. Jing, S. Li, S. Song, L. Xue, H. Fu, *Sol. Energy Mater. Sol. Cells* **2008**, *92*, 1030 – 1036; b) B. Sun, P. G. Smirniotis, *Catal. Today* **2003**, *88*, 49 – 59.
[104] S. Leytner, J. T. Hupp, *Chem. Phys. Lett.* **2000**, *330*, 231 – 236.
[105] G. Li, L. Chen, M. E. Graham, K. A. Gray, *J. Mol. Catal. A* **2007**, *275*, 30 – 35.
[106] A. G. Thomas, K. L. Syres, *Chem. Soc. Rev.* **2012**, *41*, 4207 – 4217.
[107] T. Tachikawa, T. Majima, *Chem. Commun.* **2012**, *48*, 3300 – 3302.
[108] a) K. Drew, G. Girishkumar, K. Vinodgopal, P. V. Kamat, *J. Phys. Chem. B* **2005**, *109*, 11851 – 11857; b) A. Yamakata, T.-a. Ishibashi, H. Onishi, *J. Phys. Chem. B* **2003**, *107*, 9820 – 9823.
[109] T. Mizuno, K. Adachi, K. Ohta, A. Saji, *J. Photochem. Photobiol. A* **1996**, *98*, 87 – 90.
[110] Y. Ku, W.-H. Lee, W.-Y. Wang, *J. Mol. Catal. A* **2004**, *212*, 191 – 196.
[111] K. Kočí, L. Obalová, L. Matějová, D. Plachá, Z. Lacný, J. Jirkovský, O. Šolcová, *Appl. Catal. B* **2009**, *89*, 494 – 502.
[112] S. Kaneco, H. Kurimoto, K. Ohta, T. Mizuno, A. Saji, *J. Photochem. Photobiol. A* **1997**, *109*, 59 – 63.
[113] H. Inoue, T. Matsuyama, B.-J. Liu, T. Sakata, H. Mori, H. Yoneyama, *Chem. Lett.* **1994**, *23*, 653 – 656.
[114] B.-J. Liu, T. Torimoto, H. Matsumoto, H. Yoneyama, *J. Photochem. Photobiol. A* **1997**, *108*, 187 – 192.
[115] B.-J. Liu, T. Torimoto, H. Yoneyama, *J. Photochem. Photobiol. A* **1998**, *115*, 227 – 230.
[116] K. Kočí, V. Matějka, P. Kovář, Z. Lacný, L. Obalová, *Catal. Today* **2011**, *161*, 105 – 109.
[117] K. Hirano, K. Inoue, T. Yatsu, *J. Photochem. Photobiol. A* **1992**, *64*, 255 – 258.
[118] I. H. Tseng, J. C. S. Wu, *Catal. Today* **2004**, *97*, 113 – 119.
[119] Slamet, H. W. Nasution, E. Purnama, S. Kosela, J. Gunlazuardi, *Catal. Commun.* **2005**, *6*, 313 – 319.
[120] D. Luo, Y. Bi, W. Kan, N. Zhang, S. Hong, *J. Mol. Struct.* **2011**, *994*, 325 – 331.
[121] H.-C. Yang, H.-Y. Lin, Y.-S. Chien, J. Wu, H.-H. Wu, *Catal. Lett.* **2009**, *131*, 381 – 387.
[122] B. Srinivas, B. Shubhamangala, K. Lalitha, P. A. K. Reddy, V. D. Kumari, M. Subrahmanyam, B. R. De, *Photochem. Photobiol.* **2011**, *87*, 995 – 1001.
[123] O. Ishitani, C. Inoue, Y. Suzuki, T. Ibusuki, *J. Photochem. Photobiol. A* **1993**, *72*, 269 – 271.
[124] Z. Goren, I. Willner, A. J. Nelson, A. J. Frank, *J. Phys. Chem.* **1990**, *94*, 3784 – 3790.
[125] T.-F. Xie, D.-J. Wang, L.-J. Zhu, T.-J. Li, Y.-J. Xu, *Mater. Chem. Phys.* **2001**, *70*, 103 – 106.
[126] a) S. Gao, K. Ueno, H. Misawa, *Acc. Chem. Res.* **2011**, *44*, 251 – 260; b) Z. Liu, W. Hou, P. Pavaskar, M. Aykol, S. B. Cronin, *Nano Lett.* **2011**, *11*, 1111 – 1116; c) K. Awazu, M. Fujimaki, C. Rockstuhl, J. Tominaga, H. Murakami, Y. Ohki, N. Yoshida, T. Watanabe, *J. Am. Chem. Soc.* **2008**, *130*, 1676 – 1680.
[127] K. Kočí, K. Matějů, L. Obalová, S. Krejčíková, Z. Lacný, D. Plachá, L. Čapek, A. Hospodková, O. Šolcová, *Appl. Catal. B* **2010**, *96*, 239 – 244.
[128] S. Krejčíková, L. Matějová, K. Kočí, L. Obalová, Z. Matěj, L. Čapek, O. Šolcová, *Appl. Catal. B* **2012**, *111 – 112*, 119 – 125.
[129] a) P. Pathak, M. J. Meziani, Y. Li, L. T. Cureton, Y.-P. Sun, *Chem. Commun.* **2004**, 1234 – 1235; b) W. Kim, T. Seok, W. Choi, *Energy Environ. Sci.* **2012**, *5*, 6066 – 6070.
[130] P. Pathak, M. J. Meziani, L. Castillo, Y.-P. Sun, *Green Chem.* **2005**, *7*, 667 – 670.
[131] T. W. Woolerton, S. Sheard, E. Reisner, E. Pierce, S. W. Ragsdale, F. A. Armstrong, *J. Am. Chem. Soc.* **2010**, *132*, 2132 – 2133.
[132] T. W. Woolerton, S. Sheard, E. Pierce, S. W. Ragsdale, F. A. Armstrong, *Energy Environ. Sci.* **2011**, *4*, 2393 – 2399.
[133] T. W. Woolerton, S. Sheard, Y. S. Chaudhary, F. A. Armstrong, *Energy Environ. Sci.* **2012**, *5*, 7470 – 7490.
[134] M. A. Asi, C. He, M. Su, D. Xia, L. Lin, H. Deng, Y. Xiong, R. Qiu, X.-Z. Li, *Catal. Today* **2011**, *175*, 256 – 263.
[135] Y. T. Liang, B. K. Vijayan, K. A. Gray, M. C. Hersam, *Nano Lett.* **2011**, *11*, 2865 – 2870.
[136] a) H. Zhang, X. Lv, Y. Li, Y. Wang, J. Li, *ACS Nano* **2010**, *4*, 380 – 386; b) Y. Zhang, Z.-R. Tang, X. Fu, Y.-J. Xu, *ACS Nano* **2011**, *5*, 7426 – 7435.
[137] W. Tu, Y. Zhou, Q. Liu, Z. Tian, J. Gao, X. Chen, H. Zhang, J. Liu, Z. Zou, *Adv. Funct. Mater.* **2012**, *22*, 1215 – 1221.
[138] M. Anpo, K. Chiba, *J. Mol. Catal.* **1992**, *74*, 207 – 212.
[139] F. Saladin, L. Forss, I. Kamber, *J. Chem. Soc. Chem. Commun.* **1995**, 533 – 534.
[140] F. Saladin, I. Alxneit, *J. Chem. Soc. Faraday Trans.* **1997**, *93*, 4159 – 4163.
[141] L. Chen, M. E. Graham, G. Li, D. R. Gentner, N. M. Dimitrijevic, K. A. Gray, *Thin Solid Films* **2009**, *517*, 5641 – 5645.
[142] S. Yamagata, M. Nishijo, N. Murao, S. Ohta, I. Mizoguchi, *Zeolites* **1995**, *15*, 490 – 493.
[143] M. Anpo, H. Yamashita, Y. Ichihashi, Y. Fujii, M. Honda, *J. Phys. Chem. B* **1997**, *101*, 2632 – 2636.
[144] a) M. Anpo, M. Takeuchi, *J. Catal.* **2003**, *216*, 505 – 516; b) P. V. Kamat, *J. Phys. Chem. C* **2007**, *111*, 2834 – 2860.
[145] M. Anpo, H. Yamashita, K. Ikeue, Y. Fujii, S. G. Zhang, Y. Ichihashi, D. R. Park, Y. Suzuki, K. Koyano, T. Tatsumi, *Catal. Today* **1998**, *44*, 327 – 332.
[146] J.-S. Hwang, J.-S. Chang, S.-E. Park, K. Ikeue, M. Anpo, *Top. Catal.* **2005**, *35*, 311 – 319.
[147] a) K. Ikeue, H. Yamashita, T. Takewaki, M. E. Davis, M. Anpo, *J. Synchrotron Radiat.* **2001**, *8*, 602 – 604; b) H. Yamashita, K. Ikeue, T. Takewaki, M. Anpo, *Top. Catal.* **2002**, *18*, 95 – 100.
[148] Y. Fu, D. Sun, Y. Chen, R. Huang, Z. Ding, X. Fu, Z. Li, *Angew. Chem.* **2012**, *124*, 3420 – 3423; *Angew. Chem. Int. Ed.* **2012**, *51*, 3364 – 3367.
[149] a) K. Ikeue, S. Nozaki, M. Ogawa, M. Anpo, *Catal. Lett.* **2002**, *80*, 111 – 114; b) Y. Shioya, K. Ikeue, M. Ogawa, M. Anpo, *Appl. Catal. A* **2003**, *254*, 251 – 259.
[150] H. Yamashita, H. Nishiguchi, N. Kamada, M. Anpo, Y. Teraoka, H. Hatano, S. Ehara, K. Kikui, L. Palmisano, A. Sclafani, M. Schiavello, M. Fox, *Res. Chem. Intermed.* **1994**, *20*, 815 – 823.

[151] J. C. S. Wu, H.-M. Lin, C.-L. Lai, *Appl. Catal. A* **2005**, *296*, 194 – 200.
[152] K. Tennakone, A. H. Jayatissa, S. Punchihewa, *J. Photochem. Photobiol. A* **1989**, *49*, 369 – 375.
[153] J. Wu, T.-H. Wu, T. Chu, H. Huang, D. Tsai, *Top. Catal.* **2008**, *47*, 131 – 136.
[154] T.-V. Nguyen, J. C. S. Wu, *Sol. Energy Mater. Sol. Cells* **2008**, *92*, 864 – 872.
[155] T.-V. Nguyen, J. C. S. Wu, C.-H. Chiou, *Catal. Commun.* **2008**, *9*, 2073 – 2076.
[156] Y. Li, W.-N. Wang, Z. Zhan, M.-H. Woo, C.-Y. Wu, P. Biswas, *Appl. Catal. B* **2010**, *100*, 386 – 392.
[157] W.-N. Wang, J. Park, P. Biswas, *Catal. Sci. Technol.* **2011**, *1*, 593 – 600.
[158] S.-I. In, D. D. Vaughn, R. E. Schaak, *Angew. Chem.* **2012**, *124*, 3981 – 3984; *Angew. Chem. Int. Ed.* **2012**, *51*, 3915 – 3918.
[159] X. Feng, J. D. Sloppy, T. J. LaTempa, M. Paulose, S. Komarneni, N. Bao, C. A. Grimes, *J. Mater. Chem.* **2011**, *21*, 13429 – 13433.
[160] J. Pan, X. Wu, L. Wang, G. Liu, G. Q. Lu, H.-M. Cheng, *Chem. Commun.* **2011**, *47*, 8361 – 8363.
[161] W.-N. Wang, W.-J. An, B. Ramalingam, S. Mukherjee, D. M. Niedzwiedzki, S. Gangopadhyay, P. Biswas, *J. Am. Chem. Soc.* **2012**, *134*, 11276 – 11281.
[162] a) O. Ozcan, F. Yukruk, E. Akkaya, D. Uner, *Top. Catal.* **2007**, *44*, 523 – 528; b) O. Ozcan, F. Yukruk, E. U. Akkaya, D. Uner, *Appl. Catal. B* **2007**, *71*, 291 – 297.
[163] D. Uner, M. M. Oymak, *Catal. Today* **2012**, *181*, 82 – 88.
[164] R. Vogel, P. Hoyer, H. Weller, *J. Phys. Chem.* **1994**, *98*, 3183 – 3188.
[165] C. Wang, R. L. Thompson, P. Ohodnicki, J. Baltrus, C. Matranga, *J. Mater. Chem.* **2011**, *21*, 13452 – 13457.
[166] X. Li, H. Liu, D. Luo, J. Li, Y. Huang, H. Li, Y. Fang, Y. Xu, L. Zhu, *Chem. Eng. J.* **2012**, *180*, 151 – 158.
[167] F. Solymosi, I. Tombácz, *Catal. Lett.* **1994**, *27*, 61 – 65.
[168] a) Y. Kohno, H. Hayashi, S. Takenaka, T. Tanaka, T. Funabiki, S. Yoshida, *J. Photochem. Photobiol. A* **1999**, *126*, 117 – 123; b) Y. Kohno, T. Yamamoto, T. Tanaka, T. Funabiki, *J. Mol. Catal. A* **2001**, *175*, 173 – 178.
[169] W. Hou, W. H. Hung, P. Pavaskar, A. Goeppert, M. Aykol, S. B. Cronin, *ACS Catal.* **2011**, *1*, 929 – 936.
[170] A. Cybula, M. Klein, A. Zielińska-Jurek, M. Janczarek, A. Zaleska, *Physicochem. Probl. Miner. Process.* **2012**, *48*, 159 – 165.
[171] a) Y. Yao, G. Li, S. Ciston, R. M. Lueptow, K. A. Gray, *Environ. Sci. Technol.* **2008**, *42*, 4952 – 4957; b) H. Yu, X. Quan, S. Chen, H. Zhao, *J. Phys. Chem. C* **2007**, *111*, 12987 – 12991.
[172] Y. Xie, S. Heo, S. Yoo, G. Ali, S. Cho, *Nanoscale Res. Lett.* **2010**, *5*, 603 – 607.
[173] X.-H. Xia, Z.-J. Jia, Y. Yu, Y. Liang, Z. Wang, L.-L. Ma, *Carbon* **2007**, *45*, 717 – 721.
[174] a) X. Chen, S. Shen, L. Guo, S. S. Mao, *Chem. Rev.* **2010**, *110*, 6503 – 6570; b) K. Maeda, K. Domen, *J. Phys. Chem. C* **2007**, *111*, 7851 – 7861.
[175] D. Meissner, R. Memming, B. Kastening, *J. Phys. Chem.* **1988**, *92*, 3476 – 3483.
[176] F. R. F. Fan, P. Leempoel, A. J. Bard, *J. Electrochem. Soc.* **1983**, *130*, 1866 – 1875.
[177] a) A. Henglein, M. Gutiérrez, C. H. Fischer, *Ber. Bunsenges. Phys. Chem.* **1984**, *88*, 170 – 175; b) M. Kanemoto, T. Shiragami, C. Pac, S. Yanagida, *J. Phys. Chem.* **1992**, *96*, 3521 – 3526; c) H. Inoue, H. Moriwaki, K. Maeda, H. Yoneyama, *J. Photochem. Photobiol. A* **1995**, *86*, 191 – 196.
[178] H. Yoneyama, *Catal. Today* **1997**, *39*, 169 – 175.
[179] L. M. Peter, K. G. U. Wijayantha, D. J. Riley, J. P. Waggett, *J. Phys. Chem. B* **2003**, *107*, 8378 – 8381.
[180] P. Johne, H. Kisch, *J. Photochem. Photobiol. A* **1997**, *111*, 223 – 228.
[181] a) M. Kanemoto, K.-i. Ishihara, Y. Wada, T. Sakata, H. Mori, S. Yanagida, *Chem. Lett.* **1992**, *21*, 835 – 836; b) S. Yanagida, M. Kanemoto, K.-i. Ishihara, Y. Wada, T. Sakata, H. Mori, *Bull. Chem. Soc. Jpn.* **1997**, *70*, 2063 – 2070.
[182] a) B. R. Eggins, J. T. S. Irvine, E. P. Murphy, J. Grimshaw, *J. Chem. Soc. Chem. Commun.* **1988**, 1123 – 1124; b) B. R. Eggins, P. K. J. Robertson, E. P. Murphy, E. Woods, J. T. S. Irvine, *J. Photochem. Photobiol. A* **1998**, *118*, 31 – 40.
[183] H. Kisch, P. Lutz, *Photochem. Photobiol. Sci.* **2002**, *1*, 240 – 245.
[184] P. Praus, O. Kozák, K. Kočí, A. Panáček, R. Dvorský, *J. Colloid Interface Sci.* **2011**, *360*, 574 – 579.
[185] X. V. Zhang, S. T. Martin, C. M. Friend, M. A. A. Schoonen, H. D. Holland, *J. Am. Chem. Soc.* **2004**, *126*, 11247 – 11253.
[186] X. Li, J. Chen, H. Li, J. Li, Y. Xu, Y. Liu, J. Zhou, *J. Nat. Gas Chem.* **2011**, *20*, 413 – 417.
[187] J.-Y. Liu, B. Garg, Y.-C. Ling, *Green Chem.* **2011**, *13*, 2029 – 2031.
[188] T. Arai, S. Tajima, S. Sato, K. Uemura, T. Morikawa, T. Kajino, *Chem. Commun.* **2011**, *47*, 12664 – 12666.
[189] H. W. Eng, P. W. Barnes, B. M. Auer, P. M. Woodward, *J. Solid State Chem.* **2003**, *175*, 94 – 109.
[190] Y. Inoue, *Energy Environ. Sci.* **2009**, *2*, 364 – 386.
[191] D. E. Scaife, *Solar Energy* **1980**, *25*, 41 – 54.
[192] Y. Matsumoto, *J. Solid State Chem.* **1996**, *126*, 227 – 234.
[193] G. R. Bamwenda, H. Arakawa, *Appl. Catal. A* **2001**, *210*, 181 – 191.
[194] Y. P. Xie, G. Liu, L. Yin, H.-M. Cheng, *J. Mater. Chem.* **2012**, *22*, 6746 – 6751.
[195] G. Xi, S. Ouyang, P. Li, J. Ye, Q. Ma, N. Su, H. Bai, C. Wang, *Angew. Chem.* **2012**, *124*, 2445 – 2449; *Angew. Chem. Int. Ed.* **2012**, *51*, 2395 – 2399.
[196] K. Sayama, H. Arakawa, *J. Phys. Chem.* **1993**, *97*, 531 – 533.
[197] J. C. Hemminger, R. Carr, G. A. Somorjai, *Chem. Phys. Lett.* **1978**, *57*, 100 – 104.
[198] M. Ulman, B. Aurian-Blajeni, M. Halmann, *Isr. J. Chem.* **1982**, *22*, 177 – 179.
[199] G. Guan, T. Kida, A. Yoshida, *Appl. Catal. B* **2003**, *41*, 387 – 396.
[200] K. Iizuka, T. Wato, Y. Miseki, K. Saito, A. Kudo, *J. Am. Chem. Soc.* **2011**, *133*, 20863 – 20868.
[201] J. F. McCann, A. Khan, *Electrochim. Acta* **1982**, *27*, 89 – 94.
[202] H. Shi, Z. Zou, *J. Phys. Chem. Solids* **2012**, *73*, 788 – 792.
[203] P. Li, S. Ouyang, G. Xi, T. Kako, J. Ye, *J. Phys. Chem. C* **2012**, *116*, 7621 – 7628.
[204] H. Shi, T. Wang, J. Chen, C. Zhu, J. Ye, Z. Zou, *Catal. Lett.* **2011**, *141*, 525 – 530.
[205] E. M. Sabio, R. L. Chamousis, N. D. Browning, F. E. Osterloh, *J. Phys. Chem. C* **2012**, *116*, 3161 – 3170.
[206] a) T. Takata, Y. Furumi, K. Shinohara, A. Tanaka, M. Hara, J. N. Kondo, K. Domen, *Chem. Mater.* **1997**, *9*, 1063 – 1064; b) Y. Miseki, H. Kato, A. Kudo, *Energy Environ. Sci.* **2009**, *2*, 306 – 314.
[207] a) E. C. Carroll, O. C. Compton, D. Madsen, F. E. Osterloh, D. S. Larsen, *J. Phys. Chem. C* **2008**, *112*, 2394 – 2403; b) Y. Ebina, T. Sasaki, M. Harada, M. Watanabe, *Chem. Mater.* **2002**, *14*, 4390 – 4395.
[208] O. C. Compton, C. H. Mullet, S. Chiang, F. E. Osterloh, *J. Phys. Chem. C* **2008**, *112*, 6202 – 6208.
[209] A. Kudo, H. Kato, S. Nakagawa, *J. Phys. Chem. B* **2000**, *104*, 571 – 575.
[210] X. Li, N. Kikugawa, J. Ye, *Adv. Mater.* **2008**, *20*, 3816 – 3819.
[211] X. Li, H. Pan, W. Li, Z. Zhuang, *Appl. Catal. A* **2012**, *413 – 414*, 103 – 108.
[212] a) J. L. Giocondi, G. S. Rohrer, *J. Phys. Chem. B* **2001**, *105*, 8275 – 8277; b) P. M. Jones, D. E. Gallardo, S. Dunn, *Chem. Mater.* **2008**, *20*, 5901 – 5906.
[213] M. Stock, S. Dunn, *Ferroelectrics* **2011**, *419*, 9 – 13.

[214] T. Morikawa, S. Saeki, T. Suzuki, T. Kajino, T. Motohiro, *Appl. Phys. Lett.* **2010**, *96*, 142111 – 142113.
[215] T. M. Suzuki, H. Tanaka, T. Morikawa, M. Iwaki, S. Sato, S. Saeki, M. Inoue, T. Kajino, T. Motohiro, *Chem. Commun.* **2011**, *47*, 8673 – 8675.
[216] H. Kato, H. Kobayashi, A. Kudo, *J. Phys. Chem. B* **2002**, *106*, 12441 – 12447.
[217] U. A. Joshi, A. Palasyuk, D. Arney, P. A. Maggard, *J. Phys. Chem. Lett.* **2010**, *1*, 2719 – 2726.
[218] U. A. Joshi, A. M. Palasyuk, P. A. Maggard, *J. Phys. Chem. C* **2011**, *115*, 13534 – 13539.
[219] L. Fuoco, U. A. Joshi, P. A. Maggard, *J. Phys. Chem. C* **2012**, *116*, 10490 – 10497.
[220] a) A. Kudo, K. Omori, H. Kato, *J. Am. Chem. Soc.* **1999**, *121*, 11459 – 11467; b) A. Walsh, Y. Yan, M. N. Huda, M. M. Al-Jassim, S.-H. Wei, *Chem. Mater.* **2009**, *21*, 547 – 551.
[221] Y. Liu, B. Huang, Y. Dai, X. Zhang, X. Qin, M. Jiang, M.-H. Whangbo, *Catal. Commun.* **2009**, *11*, 210 – 213.
[222] Y. Zhou, Z. Tian, Z. Zhao, Q. Liu, J. Kou, X. Chen, J. Gao, S. Yan, Z. Zou, *ACS Appl. Mater. Interfaces* **2011**, *3*, 3594 – 3601.
[223] C. Zhang, Y. Zhu, *Chem. Mater.* **2005**, *17*, 3537 – 3545.
[224] Z. Zou, J. Ye, K. Sayama, H. Arakawa, *Nature* **2001**, *414*, 625 – 627.
[225] J. Ye, Z. Zou, H. Arakawa, M. Oshikiri, M. Shimoda, A. Matsushita, T. Shishido, *J. Photochem. Photobiol. A* **2002**, *148*, 79 – 83.
[226] a) S. Matsushima, K. Obata, H. Nakamura, M. Arai, K. Kobayashi, *J. Phys. Chem. Solids* **2003**, *64*, 2417 – 2421; b) A. C. Malingowski, P. W. Stephens, A. Huq, Q. Huang, S. Khalid, P. G. Khalifah, *Inorg. Chem.* **2012**, *51*, 6096 – 6103.
[227] H. Chang, K. Kong, Y. S. Choi, E. In, Y. Choi, J.-O. Baeg, S.-J. Moon, *Chem. Phys. Lett.* **2004**, *398*, 449 – 452.
[228] R. L. Weiher, R. P. Ley, *J. Appl. Phys.* **1966**, *37*, 299 – 302.
[229] L. Zhang, I. Djerdj, M. Cao, M. Antonietti, M. Niederberger, *Adv. Mater.* **2007**, *19*, 2083 – 2086.
[230] P.-W. Pan, Y.-W. Chen, *Catal. Commun.* **2007**, *8*, 1546 – 1549.
[231] Z.-Y. Wang, H.-C. Chou, J. C. S. Wu, D. P. Tsai, G. Mul, *Appl. Catal. A* **2010**, *380*, 172 – 177.
[232] C.-W. Tsai, H. M. Chen, R.-S. Liu, K. Asakura, T.-S. Chan, *J. Phys. Chem. C* **2011**, *115*, 10180 – 10186.
[233] D.-S. Lee, H.-J. Chen, Y.-W. Chen, *J. Phys. Chem. Solids* **2012**, *73*, 661 – 669.
[234] K. S. Suresh, D. G. Kanhere, P. Ravindra, *J. Phys.: Condens. Matter* **1999**, *11*, 3635.
[235] J. Sato, H. Kobayashi, K. Ikarashi, N. Saito, H. Nishiyama, Y. Inoue, *J. Phys. Chem. B* **2004**, *108*, 4369 – 4375.
[236] L. Liu, W. Fan, X. Zhao, H. Sun, P. Li, L. Sun, *Langmuir* **2012**, *28*, 10415 – 10424.
[237] N. Zhang, S. Ouyang, P. Li, Y. Zhang, G. Xi, T. Kako, J. Ye, *Chem. Commun.* **2011**, *47*, 2041 – 2043.
[238] V. B. R. Boppana, N. D. Hould, R. F. Lobo, *J. Solid State Chem.* **2011**, *184*, 1054 – 1062.
[239] Q. Liu, Y. Zhou, J. Kou, X. Chen, Z. Tian, J. Gao, S. Yan, Z. Zou, *J. Am. Chem. Soc.* **2010**, *132*, 14385 – 14387.
[240] S. Yan, L. Wan, Z. Li, Z. Zou, *Chem. Commun.* **2011**, *47*, 5632 – 5634.
[241] Q. Liu, Y. Zhou, Z. Tian, X. Chen, J. Gao, Z. Zou, *J. Mater. Chem.* **2012**, *22*, 2033 – 2038.
[242] Y. Lee, H. Terashima, Y. Shimodaira, K. Teramura, M. Hara, H. Kobayashi, K. Domen, M. Yashima, *J. Phys. Chem. C* **2007**, *111*, 1042 – 1048.
[243] N. Zhang, S. Ouyang, T. Kako, J. Ye, *Chem. Commun.* **2012**, *48*, 1269 – 1271.
[244] Q. Liu, Y. Zhou, Y. Ma, Z. Zou, *RSC Adv.* **2012**, *2*, 3247 – 3250.
[245] Z. Li, Y. Zhou, J. Zhang, W. Tu, Q. Liu, T. Yu, Z. Zou, *Cryst. Growth Des.* **2012**, *12*, 1476 – 1481.
[246] S. E. Collins, M. A. Baltanás, A. L. Bonivardi, *J. Phys. Chem. B* **2006**, *110*, 5498 – 5507.
[247] H. Tsuneoka, K. Teramura, T. Shishido, T. Tanaka, *J. Phys. Chem. C* **2010**, *114*, 8892 – 8898.
[248] N. Ahmed, Y. Shibata, T. Taniguchi, Y. Izumi, *J. Catal.* **2011**, *279*, 123 – 135.
[249] H.-a. Park, J. H. Choi, K. M. Choi, D. K. Lee, J. K. Kang, *J. Mater. Chem.* **2012**, *22*, 5304 – 5307.
[250] S. C. Yan, S. X. Ouyang, J. Gao, M. Yang, J. Y. Feng, X. X. Fan, L. J. Wan, Z. S. Li, J. H. Ye, Y. Zhou, Z. G. Zou, *Angew. Chem.* **2010**, *122*, 6544 – 6548; *Angew. Chem. Int. Ed.* **2010**, *49*, 6400 – 6404.
[251] K. Maeda, K. Domen, *Chem. Mater.* **2010**, *22*, 612 – 623.
[252] V. B. R. Boppana, H. Schmidt, F. Jiao, D. J. Doren, R. F. Lobo, *Chem. Eur. J.* **2011**, *17*, 12417 – 12428.
[253] K. Lee, B. M. Tienes, M. B. Wilker, K. J. Schnitzenbaumer, G. Dukovic, *Nano Lett.* **2012**, *12*, 3268 – 3272.
[254] J. W. Lekse, M. K. Underwood, J. P. Lewis, C. Matranga, *J. Phys. Chem. C* **2011**, *116*, 1865 – 1872.
[255] S. Sato, T. Arai, T. Morikawa, K. Uemura, T. M. Suzuki, H. Tanaka, T. Kajino, *J. Am. Chem. Soc.* **2011**, *133*, 15240 – 15243.
[256] C.-C. Lo, C.-H. Hung, C.-S. Yuan, J.-F. Wu, *Sol. Energy Mater. Sol. Cells* **2007**, *91*, 1765 – 1774.
[257] S. S. Tan, L. Zou, E. Hu, *Sci. Technol. Adv. Mater.* **2007**, *8*, 89 – 92.